UNIVERSITY OF THESSALY

SCHOOL OF ENGINEERING

DEPARTMENT OF MECHANICAL ENGINEERING

Diploma thesis

Recent advancements in hydrogen storage - Comparative review on methods, operating conditions and challenges

by

Vlachos Ilias & Bekris Georgios Panagiotis

Supervisor

Prof. Tsiakaras Panagiotis

Submitted in partial fulfillment of the requirements for the degree of Diploma in Mechanical Engineering at the University of Thessaly

Volos, 2025

ΠΑΝΕΠΙΣΤΗΜΙΟ ΘΕΣΣΑΛΙΑΣ
ΠΟΛΥΤΕΧΝΙΚΗ ΣΧΟΛΗ
ΤΜΗΜΑ ΜΗΧΑΝΟΛΟΓΩΝ ΜΗΧΑΝΙΚΩΝ

Διπλωματική Εργασία

Πρόσφατες εξελίξεις στην αποθήκευση υδρογόνου - Συγκριτική ανασκόπηση μεθόδων, συνθηκών λειτουργίας και προκλήσεων

υπό

Βλάχος Ηλίας & Μπεκρής Γεώργιος Παναγιώτης

Επιβλέπων

Καθηγητής Τσιακάρας Παναγιώτης

Υπεβλήθη για την εκπλήρωση μέρους των απαιτήσεων για την απόκτηση του Διπλώματος Μηχανολόγου Μηχανικού

Βόλος, 2025

Approved by the Committee on Final Examination:

Advisor Dr. Tsiakaras Panagiotis (Supervisor)
Professor of Department of Mechanical Engineering
School of Engineering
University of Thessaly

Member Dr. Charalampous Georgios
Professor of Department of Mechanical Engineering
School of Engineering
University of Thessaly

Member Dr. Brouzgou Angeliki
Assistant Professor of Department of Energy Systems
School of Technological Sciences
University of Thessaly

ΕΥΧΑΡΙΣΤΙΕΣ

Με την ολοκλήρωση της παρούσας διπλωματικής εργασίας, καταφέραμε να κλείσουμε τον κύκλο των σπουδών μας. Θα θέλαμε να ευχαριστήσουμε θερμά τον καθηγητή και επόπτη μας κύριο Παναγιώτη Τσιακάρα για την πολύτιμη βοήθεια, γνώση, υπομονή και τις συμβουλές που μας προσέφερε καθ' όλη την διάρκεια της διαδικασίας συγγραφής της εργασίας μας καθώς και για την άμεση ανταπόκριση που μας παρείχε σε κάθε στάδιο.

Επιπλέον θα θέλαμε να ευχαριστήσουμε τα μέλη της εξεταστικής επιτροπής Δρ. Αγγελική Μπρούζγου και Δρ. Γεώργιο Χαραλάμπους για το χρόνο που αφιερώνουν για τη μελέτη και αξιολόγηση της εργασίας μας.

Τέλος, για την αγάπη, τη συναισθηματική, ηθική και οικονομική υποστήριξη σε όλη τη διάρκεια των σπουδών μας, αφενός ο Ηλίας Βλάχος θα ήθελε να ευχαριστήσει τους γονείς του Ευάγγελο και Σπυριδούλα, και αφετέρου ο Γεώργιος Μπεκρής θα ήθελε επίσης να ευχαριστήσει τους γονείς του Αντώνιο και Σωτηρία.

Acknowledgments

With the completion of this thesis, we have successfully concluded our academic journey. We would like to express our sincere gratitude to our professor and supervisor, Mr. Panagiotis Tsiakaras, for his invaluable assistance, knowledge, patience, and guidance throughout the entire process of writing this thesis, as well as for his prompt responses at every stage.

Furthermore, we would like to extend our thanks to the members of the examination committee, Dr. Angeliki Brouzgou and Dr. Georgios Charalambous, for their time and effort in reviewing and evaluating our work.

Finally, for their love, emotional, moral, and financial support throughout our studies, Ilias Vlachos would like to thank his parents, Evangelos and Spyridoula, while Georgios Bekris would also like to thank his parents, Antonios and Sotiria.

Abstract

This thesis focuses on recent advancements in hydrogen storage, providing a comparative overview of methods, operating conditions, and challenges in the field. It begins by analyzing hydrogen's role as a clean, safe, and cost-effective energy carrier, which can be produced from various sources, such as water, biomass, and fossil fuels, without emitting pollutants or greenhouse gases. Additionally, it examines hydrogen's interaction with renewable energy sources, emphasizing its importance in long-term energy storage.

A significant portion of the study is dedicated to hydrogen production through different methods, including electrolysis, direct solar water splitting, and biological approaches. The environmental impacts of hydrogen, particularly its potential contribution to global warming due to emissions, are also explored.

Hydrogen storage is identified as the central challenge for its energy applications. The thesis provides a detailed analysis of physical (e.g., compression, liquefaction) and chemical storage methods (e.g., metal hydrides, liquid organic hydrogen carriers). Chemical storage methods are highlighted as more efficient compared to physical ones, though they face challenges regarding reversibility and stability. The study further evaluates the materials used in hydrogen storage, emphasizing the need for materials with high storage density, economic feasibility, and safety.

The thesis concludes with recommendations for further research and development in hydrogen storage technologies, highlighting the importance of improving economic viability and scaling these technologies for widespread future use.

ΠΕΡΙΛΗΨΗ

Η συγκεκριμένη διπλωματική εργασία εστιάζει στις πρόσφατες εξελίξεις στον τομέα της αποθήκευσης υδρογόνου, περιγράφοντας συγκριτικά τις μεθόδους, τις συνθήκες λειτουργίας και τις προκλήσεις που αντιμετωπίζει ο τομέας. Αρχικά, αναλύεται ο ρόλος του υδρογόνου ως καθαρού, ασφαλούς και οικονομικού ενεργειακού φορέα που μπορεί να παραχθεί από διάφορες πηγές, όπως το νερό, η βιομάζα και τα ορυκτά καύσιμα, χωρίς την άμεση εκπομπή ρύπων ή αερίων θερμοκηπίου. Επιπλέον, η εργασία εξετάζει την αλληλεπίδραση του υδρογόνου με τις ανανεώσιμες πηγές ενέργειας, τονίζοντας τη σημασία του στην αποθήκευση ενέργειας μεγάλης διάρκειας.

Ένα σημαντικό τμήμα της μελέτης αφιερώνεται στην παραγωγή υδρογόνου μέσω διαφορετικών μεθόδων, όπως η ηλεκτρόλυση, η άμεση διάσπαση νερού με ηλιακή ενέργεια και οι βιολογικές μέθοδοι. Εξετάζονται επίσης οι περιβαλλοντικές επιπτώσεις του υδρογόνου, ιδιαίτερα σε σχέση με την κλιματική αλλαγή, όπως η δυνητική συμβολή του στην υπερθέρμανση του πλανήτη λόγω των εκπομπών του.

Η αποθήκευση του υδρογόνου αποτελεί το κεντρικό ζήτημα της εργασίας, με λεπτομερή ανάλυση φυσικών (π.χ. συμπίεση, υγροποίηση) και χημικών μεθόδων αποθήκευσης (π.χ. μεταλλικά υδρίδια, υγρά οργανικά φορείς υδρογόνου). Οι χημικές μέθοδοι αποθήκευσης επισημαίνονται ως πιο αποδοτικές σε σχέση με τις φυσικές, αλλά παρουσιάζουν προκλήσεις ως προς την αντιστρεψιμότητα και τη σταθερότητα. Τέλος, η εργασία αξιολογεί τα υλικά που χρησιμοποιούνται στην αποθήκευση υδρογόνου, τονίζοντας την ανάγκη για ανάπτυξη υλικών με υψηλή πυκνότητα αποθήκευσης, οικονομική αποδοτικότητα και ασφάλεια.

Η διπλωματική εργασία καταλήγει με προτάσεις για την περαιτέρω έρευνα και ανάπτυξη τεχνολογιών αποθήκευσης υδρογόνου, τονίζοντας τη σημασία της βελτίωσης της οικονομικής βιωσιμότητας και της κλιμάκωσης αυτών των τεχνολογιών για την ευρεία χρήση τους στο μέλλον.

Contents

Table of figures

Chapter 1

Introduction

In its most common form, hydrogen (^{1}H, protium), which has a proton, an electron, and no neutrons, is the smallest and most abundant element. Light, energy dense and storable, hydrogen can be produced from water, biomass, fossil fuels or a combination of these. The use of hydrogen energy does not directly produce pollutants or emit greenhouse gases, making hydrogen one of the cleanest energy sources. Hydrogen is seen as a clean, safe and inexpensive energy source of the future and makes a significant contribution to achieving zero carbon emissions [1].

Moreover, hydrogen can facilitate the expansion and advancement of renewable energy sources such as wind and solar power, which are not always capable of maintaining equilibrium with demand. Hydrogen represents the most cost-effective solution for long-term electricity storage and is one of the most promising options for the transfer and storage of renewable energy. Moreover, the technologies utilized for the production and storage of hydrogen can be optimized, expanded, and scaled up to facilitate its extensive utilization in the future [2].

A variety of techniques, including the electrolysis of water with clean energy from solar and wind sources, can be employed to create hydrogen, a versatile energy carrier. A variety of water electrolysis technologies can be employed to split water into hydrogen and oxygen. These include solid oxide water electrolysis, AEM water electrolysis, PEM water electrolysis, and alkaline water electrolysis. The objective of all technologies is the production of hydrogen without the emission of greenhouse gases, although the half-cell reactions and operational mechanisms vary. Nevertheless, the cost of electricity remains too high for this process to be economically viable at this time, which restricts its widespread use, particularly in fuel cell applications such as PEM cells [3].

Alternative CO_2-free hydrogen production techniques are therefore required in order to make it economically competitive with other fuels available on the market. Apart from gasification (blue hydrogen) and steam methane reforming (grey hydrogen), which both have some emissions depending on the feedstock used, there are other methods of producing hydrogen. Therefore, overall technological advancement and a reduction in the cost of accessing power supply services are necessary to fully realize the potential of water electrolysis as an environmentally friendly and sustainable method for producing hydrogen [3]

The following are the steps involved in producing H_2 from fossil fuels. Natural gas steam reforming, natural gas thermal cracking, partial oxidation of hydrocarbons heavier than naphtha, and coal gasification are some examples. Hydrogen can be produced from biomass using the following methods: Gasification or pyrolysis (which produces a mixture of gases, including H_2,

CH_4, H_2, and N_2), electrolysis, photolysis, thermochemical reactions, thermolysis or direct thermal breakdown, and biological output are the methods used to produce hydrogen [3] [4].

The storage of hydrogen remains a significant challenge in the context of its utilization for energy purposes. The development of hydrogen storage materials, in addition to the advancement of technologies for the compression and liquefaction of hydrogen, is of paramount importance for the promotion of extensive utilizations within the hydrogen sector. The utilization of storage materials enables the safe storage of hydrogen at higher densities in comparison to the methods of compression and liquefaction. Consequently, systems that employ these materials can be operated in a multitude of ways. Moreover, storage materials are most effective for stationary and onboard applications [5]

The two principal types of hydrogen storage material, namely chemisorption and physisorption, each possess a number of advantages and disadvantages. It is reasonable to posit that materials for storing hydrogen must exhibit high gravimetric and volumetric densities of hydrogen, be abundant, safe, inexpensive, have rapid kinetics, be easy to handle, and have appropriate thermodynamic properties (reversible hydrogen absorption and desorption) [2]

The classification of materials employed for the storage of hydrogen is illustrated in **Figure 1**. Chemical storage materials, particularly those that utilise liquid-based systems and infrastructure comparable to that employed in modern gas refuelling stations, have the potential to exhibit high energy densities and to be user-friendly. Nevertheless, a number of irreversible chemical material storage methods render the dehydrogenation process rather challenging [6]

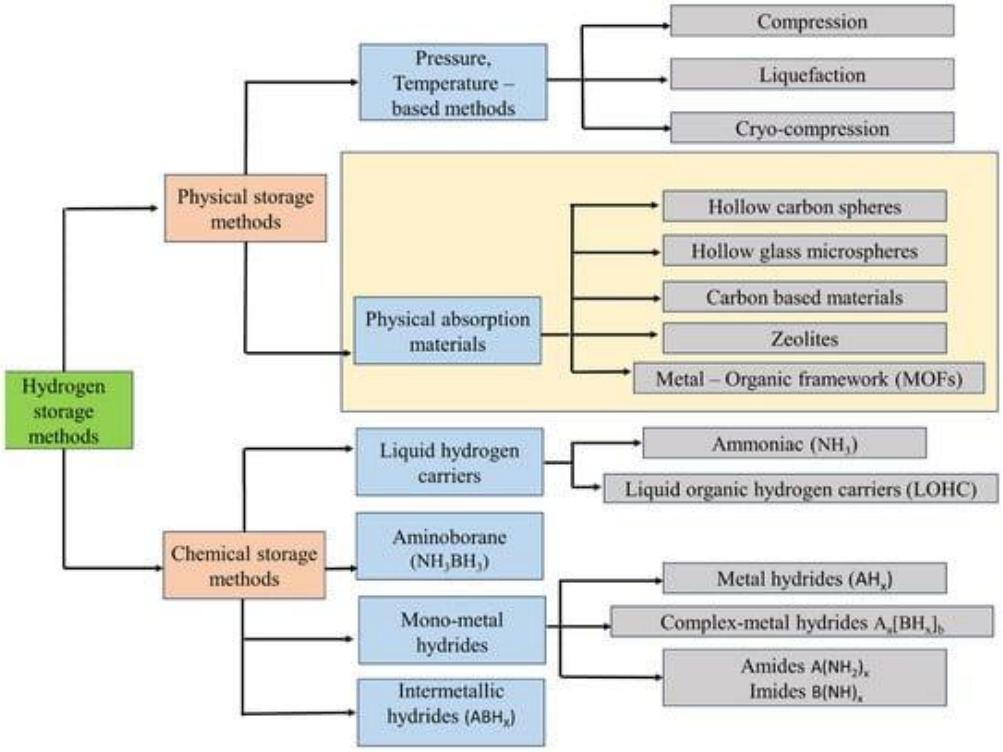

Figure 1 Classification of hydrogen storage materials [2].

Given that it generates gaseous pollutants such as carbon and nitrogen oxides, its use with ammonia and other storage compounds is inadvisable. Furthermore, despite exhibiting superior volumetric energy density and the capacity to operate at low pressure and room temperature, metal hydride storage materials display suboptimal kinetics and inadequate thermodynamic stability. In contrast, physical storage systems can be divided into two main categories: the selection of suitable absorbents and the control of the storage conditions (in terms of temperature and pressure). Examples of developed pressure or temperature-controlled storage systems for hydrogen gas include high-pressure compression technologies and cryogenic liquefaction. However, these systems are constrained by limitations in storage capacity, high costs, and safety concerns. The use of innovative porous materials as a high-throughput hydrogen absorbent in physical hydrogen storage techniques demonstrates the advantages of high storage densities, quick charging and discharging kinetics, and low costs [2].

In light of the environmental concerns and the finite nature of fossil fuels, electrochemical energy conversion and storage have emerged as the most significant and challenging technologies in the world. As long as they are developed in a way that is both economically and ecologically friendly, energy storage and conversion systems that have the ability to generate energy electrochemically have been considered as potential alternative power sources. These systems, which have found widespread application in electronic devices, electric cars, and the smart grid, include batteries, fuel cells, and electrochemical capacitors (supercapacitors) [7].

The aforementioned three types of energy storage and conversion devices exhibit disparate mechanisms, yet they share common electrochemical characteristics. At the interface between the electrolyte and electrode, where electron and ion transport are separated to enable the storage and release of energy through the charge and discharge processes, the electrochemical reactions occur. A multitude of battery technologies are currently available or in development, including primary batteries, rechargeable batteries, and solar cells. Supercapacitors are distinguished by their processing mechanism, which is either Faradaic or non-Faradaic. They include electrochemical double-layer capacitors (EDLCs) and pseudocapacitors. With regard to electrolyte characteristics, fuel cells can be classified into a number of categories. There are three specific device types: rechargeable lithium-ion batteries, pseudocapacitors, and solid oxide fuel cells (SOFC) [8] [9] [10]. Despite their differences, these devices are composed of the same fundamental components: a cathode, anode, and electrolyte, with two electrodes in contact with the electrolyte solution [7].

In the environmental sector, it is crucial to assess the climate effects of hydrogen emissions across all timescales using data that has already been published. This includes determining the potency of hydrogen as a climate factor, calculating the net warming effects of substituting clean hydrogen technologies for fossil fuels, and estimating temperature responses to anticipated levels of hydrogen demand [11]

Chapter 2

Electrochemical devices for energy conversion and storage

2.1 Fuel cells

2.1.1. Basic principles of fuel cells

Three main components comprise the fuel cell: an electrolyte, a negative electrode, and a positive electrode. On both sides of the electrolyte diaphragm, hydrogen oxidation and oxygen reduction reactions take place, respectively, according to the principle. In order to generate electricity through the hydrogen and oxidation reactions, the fuel travels to the anode and the oxidized gas is sent to the cathode [12]. Entering the battery through the anode, hydrogen undergoes a catalyst reaction that releases electrons into positively charged hydrogen ions, which then move through the electrolyte to the cathode. After entering the circuit, electrons create a current that generates electricity. Water is the sole byproduct of the chemical reaction occurring in the cell, which is caused by hydrogen ions combining with oxygen in the air through a catalyst in the cathode [13]. Fuel cell efficiency (FCE) is one of the most critical parameters for the fuel choice [14]. In some cases of fuel cells, using ethanol as fuel has the advantage of the storage and transportation of ethanol, which is much easier than fuels such as hydrogen. Parasitic current, caused by ethanol crossover through the polymer electrolyte membrane (PEM), significantly increases cathode activation overpotential, hindering fuel cell efficiency. This effect is more pronounced at low current densities due to higher ethanol crossover rates [15].

PEMFC and direct methanol fuel cells (DMFC) have garnered global attention, spurring further advancements in the field. Currently, the fuel cell technology sector is experiencing significant research efforts, driving technological improvements that pave the way for widespread commercialization. Solid electrolytes have the capability to function as ion donors or acceptors, thereby regulating the work function of metal catalysts and significantly altering their catalytic activity and selectivity in a reversible manner. This effect is especially notable with platinum, although it is not confined to any specific metal or solid electrolyte [16].

Researchers discovered that incorporating novel synthesis methods, combining Pt with metal oxides, creating core-shell structures, and applying surface modifications significantly enhanced the CO tolerance and stability of anode electrocatalysts. Despite these advancements, the researchers identified that achieving a highly CO-tolerant practical anode electrocatalyst remains a challenge. They emphasized the potential of advanced carbonaceous materials and metal oxides as alternative

supports to improve performance. The study highlighted the need for ongoing optimization efforts to make these electrocatalysts commercially viable for H_2-PEMFC applications [17].

2.1.2. Fuel cell systems

The hydrogen fuel cell has a rather complicated composition. It comprises subsystems for fuel supply, electricity management, hydrothermal management, and control in addition to the reactor. The primary system components include a hydrogen bottle, air compressor, and other parts that, when combined with the reactor, make up the fuel cell's power generation system. This article decides to present the fuel cell's component section [13].

2.1.2.1. Membrane electrode assembly.

As the central component of the hydrogen fuel cell system, the membrane electrode (MEA) is where electrochemical reactions occur, and proton and electron transfer materials are carried out. It is typically made up of the anode catalyst layer, anode gas diffusion layer, electrolyte membrane, and cathode diffusion and catalyst layers. China has produced mature research findings on both the first generation (GDE) and the second generation (CCM) at this time. Hot pressing is the first generation of technology, while the second generation of CCM, which offers the benefits of high platinum utilization and durability, is widely used. A popular area of research right now is the use of catalysts, and the ordered membrane electrode technology can make MEA have the maximum reactive area and pore connectivity [13].

2.1.2.2. Proton exchange membrane (PEM).

The main part of the proton exchange membrane fuel cell is the proton exchange membrane, which is a type of solid polymer membrane. Its functions include conducting protons, isolating electrons, and isolating reactants at various electrodes. Its primary varieties are separated into three categories: fluorine-free, partially fluorinated, and perfluoro sulfonic acid proton exchange membranes [13].

Polytetrafluoroethylene serves as the primary chain in the carbon-fluorine structure of the perfluoro sulfonic acid proton exchange membrane. A protective layer around the carbon-carbon bond can be produced by fluorine atoms with a large radius. The carbon-fluorine bond's comparatively high bond energy accounts for the proton exchange membrane's good mechanical strength and chemical stability. In addition, the sulfonic acid base group can easily form a proton-conducting channel to increase the proton conductivity of PEM because it is easy to assemble in ion-rich regions [13].

In order to create partially fluorinated proton exchange membranes, partially substituted fluoride is used rather than perfluorosulfonic acid resin or fluoride mixed with inorganic materials. The oxidation environment has a significant impact on the membrane's characteristics, so the sulfonic

acid group should be used as the proton exchange group and the perfluorinated main chain with good stability [13].

A polymer membrane made of carbon and hydrogen that exhibits high conductivity, low cost, and stable performance is known as a fluorine-free proton exchange membrane. Fluorine-free proton exchange membranes are primarily composed of aromatic polymers with benzene rings that undergo sulfonation to produce a sulfonic acid group. Examples of these include sulfonated polyaromatic ether sulfone (SPES), sulfonated polyimide (SPI), and others [13].

Researchers discovered that incorporating novel synthesis methods, combining Pt with metal oxides, creating core-shell structures, and applying surface modifications significantly enhanced the CO tolerance and stability of anode electrocatalysts. Despite these advancements, the researchers identified that achieving a highly CO-tolerant practical anode electrocatalyst remains a challenge. They emphasized the potential of advanced carbonaceous materials and metal oxides as alternative supports to improve performance. The study highlighted the need for ongoing optimization efforts to make these electrocatalysts commercially viable for H_2-PEMFC applications [17].

2.1.2.3 Solid Oxide Fuel Cell (SOFC)

Solid oxide fuel cells (SOFCs) differ significantly from their counterparts since they are solid state devices without any moving components and have distinguishing characteristics such as combustion free operation, low emissions, inherently high conversion efficiencies and very high operational temperatures (in the range of 800-1000 ◦C). Efforts have been made to introduce new electrode materials to improve their thermal stability, electrical conductivity, catalytic activity, chemical compatibility and cost-effectiveness especially with the drop in operational temperature from 400 ◦C to 700 ◦C [8].

Selection of suitable anode materials is a key to maintain superior performance of SOFCs, since anode materials accounts for nearly 95% of the overall percentage of material in anode supported cell (Shah et al., 2021). Most commonly used anode material in SOFCs is Ni-YSZ due to its high stability and excellent conductivity however, the materials is susceptible to carbon deposition when comes in contact with hydrocarbon fuels [18]. The sintering additives enhance the material's performance as an electrolyte in solid oxide fuel cells (SOFCs) [19].

The cathode is another fundamental component of a SOFC system and has different selection criteria when compared to the anode since the cathode in a SOFC requires distinctive operational properties such as high level of porosity and stability in oxygen environment. Also due to their elevated operating temperatures, SOFCs use more cost-effective and widely available transition metal oxides such as Cu, Co, Ce, Sr and Ni as an alternative to costlier metals such as Pt as cathode

since high temperature operations of the cell result in sufficiently improved kinetics and thermodynamics of the chemical reactions underpinning fuel cell operation [19]. Moreover, SOFCs can be used as a substitute for electrochemical batteries due to their high efficiencies even in reverse mode as solid oxide electrolysis cells (SOEC) in which steam is electrolyzed into hydrogen by feeding water and electric current into the cell to produce hydrogen and oxygen. Owing to these excellent properties and their modularity, fuel adaptability, diverse scale of application (small, medium and large scale) and vibration free, quiet operation, SOFC are promising candidates for use in the field of energy storage and conversion in the future [20].

Electrons are generated at the anode through oxidation and are accepted at the cathode for oxygen reduction, resulting in circuit completion with the production of electricity due to the flow of electrons from anode to cathode through an external circuit [21] [22].

A study on nitrogen-doped carbon materials with a hierarchically mesoporous structure, synthesized via the pyrolysis of an interpenetrated non-porous metal-organic framework (MOF), highlights several key findings. The synthesized MOF, specifically SCUT-11, displayed high purity and an interwoven structure rich in Zn cations, which facilitated the creation of mesopores in the final carbon. Characterizations revealed that the resulting carbon possessed a high specific surface area and a bimodal mesopore size distribution, aiding oxygen mass transfer and accessibility to catalytically active sites. Electrochemical tests demonstrated superior oxygen reduction reaction (ORR) activity for the carbon, with onset and half-wave potentials up to 1.0 and 0.88 V. Furthermore, the carbon catalyst showed remarkable anion insensitivity compared to the Pt counterpart, making it a promising candidate for various fuel cell applications [21].

In a study, the authors conducted an energy-exergy analysis to determine the optimal operating conditions for an ethanol-fuelled SOFC power plant. The plant configuration included an external steam reformer, an afterburner, a mixer and two heat exchangers (preheaters), and the study aimed to maximise the overall efficiency of the system by identifying the best combination of operating parameters and component configurations. The results indicated that optimisation of these parameters could significantly improve the performance and sustainability of ethanol-fuelled SOFC systems [23].

SOFC technology has the potential to transform the overall electrical energy generation landscape with insignificant environmental impact if it is more extensively commercialized. Their commercialization has nonetheless been limited by several disadvantages such as high material costs, the requirement of high operating temperatures (800-1000 ◦C), safety issues and the complex stack and cell assembly. Furthermore, high operating temperatures have added issues including catalyst poisoning, electrode sintering, electrode/electrolyte interfacial diffusion and

thermal/mechanical stability. These issues, and particularly the need for high operating temperatures, have forced research towards low temperature SOFC technology. The benefits of lowering operating temperatures include widening the area of application and improving the life span of the SOFCs, technical improvements (i.e., reducing the likelihood of cermet anode's redox degradation) and economic advantages (i.e., using more cost-effective cell components) [14].

2.1.2.4 Methanol Fuel Cell (DMFC)

Direct methanol fuel cells are considered as a subcategory of proton exchange membrane (PEM) fuel cells and can also be considered as low operating temperature PEM, where methanol is used as fuel. DMFCs work on the principle of directly converting the chemical energy of high energy density liquid methanol fuel to electric power via electrochemical processes with carbon dioxide and water as by products [24]. The potential for adoption of DMFCs as a key energy conversion device is predominately a result of the high specific energy of pure methanol (up to 6000 Wh kg-1) [25].

Methanol is a fuel with excellent conversion efficiency, reaching around 96.5 % which is much higher than internal combustion engine, the latter being restricted by Carnot cycle. The maximum achievable theoretical operating voltage in a methanol-air cell is ~ 1.21 V, although this cannot be attained in practical operation due to sluggish reaction kinetics and ohmic losses in the electrolyte.

One of the benefits of using methanol as fuel in DMFC is the storage and transportation of methanol, which is much easier than fuels such as hydrogen. Moreover, there is the added benefit of the high energy density of methanol, which is three orders of magnitude higher than hydrogen. Direct methanol fuel cell technology is considered promising due to characteristics such as high-power density, low operating temperatures and easy start up [15].

2.1.2.5 Ethanol Fuel Cell (EFC)

In recent years, polymer electrolyte membrane fuel cells (PEMFCs) powered directly by ethanol have attracted increasing attention due to their advantages. Ethanol is a promising fuel because it is non-toxic, renewable and can be produced in large quantities through the fermentation of sugary feedstocks. Its high theoretical mass energy density makes it a viable candidate for proton exchange membrane fuel cells. In addition, ethanol can be used in a full cycle with zero greenhouse gas emissions. However, challenges such as high anode overpotentials and fuel crossover from the anode to the cathode across the electrolyte membrane need to be addressed. The permeated ethanol and its oxidation intermediates can poison the cathode catalyst. While numerous experimental and some theoretical studies have focused on the direct use of ethanol in fuel cells (DEFC), mathematical modelling remains crucial to fuel cell development. Fundamental equations help to

simulate the processes within the fuel cell and provide a better understanding of the key parameters that affect its operation [26].

In a study, parasitic or leakage current caused by ethanol passing through the polymer electrolyte membrane (PEM) has a significant impact on fuel cell performance. This current increases the cathode activation overpotential, which is a major impediment to efficient operation1. The research used a mathematical model, validated by experimental data, which showed a direct correlation between ethanol crossover rate and parasitic current formation. The study concluded that parasitic current is more pronounced at low current densities due to higher ethanol crossover [27].

Increasing the thickness of the catalyst layer and enhancing its proton conductivity can help lower the anode overpotential. However, an optimal thickness of 10 μm is ideal for balancing performance and cost. Additionally, the ethanol feed concentration, operating temperature, and current density are key factors influencing the rate at which ethanol crosses over from the anode to the cathode through the electrolyte membrane [28]

2.1.2.6 Direct Glucose Fuel Cells (DGFCs)

Glucose has been attracting much interest due to its importance as fuel for Direct Glucose Fuel Cells (DGFCs) and their applications as implantable human devices as well as due to its high energy density (4430 W h kg^{-1}). However, further research is necessary since glucose is very stable and consequently hardly oxidized molecules. It is worth noting that to date glucose oxidation has gone through a process generating only two electrons [29].

According to literature, glucose-fed alkaline membrane fuel cells exhibit superior performance compared to proton conducting membrane fuel cells. More precisely, when the electrolyte is changed from acidic to alkaline the kinetics of the glucose electro-oxidation reaction (GER) and oxygen reduction reaction (ORR) in alkaline media are enhanced compared with those in acid media. Moreover, in an anion exchanged membrane direct glucose fuel cell (AEM-DGFC) the electro-osmotic drag is directed from the cathode to the anode, which can reduce the fuel's crossover rate from the anode to cathode and thus improve fuel cell performance. In addition, the cost of AEMs is lower than that of PEMs (mostly Nafion®) [29].

Many attempts have been made to develop efficient and stable electrocatalysts for glucose electro-oxidation, mostly in alkaline media. Many of them have been focused on Pt and Au or on their bi-metallic catalysts, Pt–Bi, Pt–Pd, Pt–Ru, Pt–Au, Ag–Au and tri-metallic catalysts, while Pd-based electrocatalysts have not been studied extensively [29].

It has been proved that in alkaline environment Pd-based electrocatalysts perform much better activity than Pt-based ones due to the quicker oxidation kinetics of various alcohols

electrooxidation. Additionally, the use of palladium instead of platinum automatically reduces the cost of a fuel cell [29].

In the acidic environment among the reported electrocatalysts, PtSn-based ones have been proved to be most appropriate for ethanol electrooxidation which is also a hardly oxidized molecule. On the other hand, Pd-based electrocatalysts have received much research attention because of their higher activity in alcohol electrooxidation in alkaline media, compared to Pt-based ones [29].

Consequently, based on the two above-mentioned facts and taking into consideration that glucose like ethanol is a hardly oxidizable molecule, Pd-based electrocatalysts could be good candidates for glucose electrooxidation. In the present work, Pd_xSn_y/C electrocatalysts have been prepared, characterized and tested for the first time as future anodes for direct glucose fuel cells with the cyclic voltammetry and chronoamperometric techniques [29].

In a study, PdxSny/C binary catalysts were produced using a modified pulse microwave-assisted polyol technique and assessed for their performance in the glucose electrooxidation reaction. These catalysts were compared to Pd/C, which was synthesized using the same method. Among them, Pd3Sn2/C demonstrated the most favorable activity for glucose electrooxidation. However, chronoamperometric analysis revealed that it became poisoned more rapidly in comparison to both PdSn/C and Pd/C electrocatalysts. Physico-chemical characterization of the electrocatalysts was carried out using transmission electron microscopy (TEM) and X-ray diffraction (XRD). Their electrocatalytic activity towards glucose electrooxidation was examined by cyclic voltammetry (CV), while their stability and poisoning rate by chronoamperometric measurements. Moreover, the effects of temperature, concentration of glucose and electrolyte were also investigated [29].

2.1.2.7. Gaseous diffusion layer.

In a fuel cell reactor, the gas diffusion layer's primary functions are to support the catalyst and offer channels for gas, proton, electron, and water reactions during electrode reactions. It has excellent thermal stability, chemical stability, and electrical conductivity. High mechanical strength, flexibility, surface smoothness, and the proper pore structure are also desirable. These characteristics, which are the embodiment of GDL structure and material properties, are essential to the electrocatalytic activity of the catalyst layer and the reactor energy conversion. [30] [13].

2.1.2.8. Bipolar plate.

The bipolar plate is the reactor's main structural element. Its function is to improve the uniformity of gas distribution and can accomplish conduction, heat conduction, and drainage. The bipolar plate is a crucial component, and the way it flows has a big influence on how quickly reactive materials are used and how well batteries work. Hard carbon, composite, and metal bipolar plates are the

most widely used materials for bipolar plates. Due to the high cost and challenging application conditions of graphite BPs, which are widely used for their exceptional performance, low-cost and user-friendly metal BPs have emerged as a development hotspot [13].

2.1.2.9. Catalyst

The catalyst, one of the components at the center of the fuel cell, lowers the activation energy of the reaction and encourages the redox process at the electrode. At the moment, platinum, low platinum, and non-platinum catalysts are the three most widely used types. Pt/C, a supported catalyst made of Pt nanoparticles scattered on a carbon powder carrier, is the most significant commercial catalyst. Currently, the template method, displacement reaction method, and template-free method are used to prepare noble metal hollow catalysts for direct alcohol fuel cells that are based on platinum and palladium [13]

Research has demonstrated the high catalytic activity, stability, and heat of a Pt catalyst with a unique shape. It has the potential to be an electrocatalyst in a variety of applications, including material preparation, activity characterization, and mechanism investigation. In addition to Pt/C, other binary alloys can catalyze cathode materials. With a high rate of precious metal utilization and oxygen reduction catalytic activity, core-shell catalysts use the transition metal element as the core and the catalyst's active component as the shell [13]

The combination of single noble atom catalysts (SNA) with two-dimensional materials (2DMs) is proving to be highly effective in a range of catalytic applications, including electrocatalysis, photocatalysis, and traditional thermocatalysis. These newly developed materials excel in catalysis due to the synergistic interplay between the 2D materials and single-atom catalysts (SACs). The 2D materials serve as support, providing a large surface area to anchor the noble metal atoms and enhancing the overall performance of the catalysts [26].

Nanocarbon as catalyst support

Compared to commercial Pt/C catalysts, nanocarbon catalyst supports, like carbon nanotubes (CNTs), improve catalyst activity and stability, leading to better fuel cell performance with higher current density and greater durability. Through increased Pt dispersion, enhanced electrical conductivity, and decreased corrosion, these supports allow for a lower Pt catalyst content [31]. Furthermore, lowering the overpotential can enable smaller fuel cell stacks and boost power density. Numerous factors, such as electroosmotic anode dehydration, mass transport overpotential, ohmic resistance, and ORR at the cathode, contribute to activation overpotential. Interestingly, 20–50% of the total mass transfer overpotential is contributed by the mass transfer in the catalyst layer.

Using innovative materials and/or fabrication techniques can improve mass transport in the catalyst layer [32].

The characteristics of an ideal carbon support include [32].

a) High surface area for fine dispersion of catalytic metal.

$$C + 2H_2O \rightarrow CO_2 + 4H^+ + 4e^- \quad (1)$$

b) Mesopores to reduce mass transportation resistance and avoid Pt poisoning by $-SO_3H$ of the ionomer [33].

c) High graphitization to resist electrochemical corrosion and oxidation reactions.

d) High conductivity to enable efficient electron pathways.

e) Doped heteroatoms to provide Pt anchoring sites.

f) Water handling capability to remove water produced due to cathodic reactions

These properties facilitate the creation of pores and channels for electron transfer, mass transport, and product release in MEA and guarantee the dispersion of active Pt nanoparticles without agglomeration [34]. Graphene, CNTs, carbon nanocoils, aerogels, carbon nanohorns, carbon nanocages, and mesoporous CB are examples of common carbon-based catalyst supports. However, it can be difficult to simultaneously achieve all of a carbon support's ideal qualities. For example, graphitized CB has lower Pt catalytic activity because of a smaller specific surface area, whereas commercialized CB is more susceptible to carbon corrosion because of its amorphous structure [33].

Due mainly to its large-scale production through chemical vapor deposition (CVD), CNF is a one-dimensional nanocarbon material that is well-known for being economically viable as an electrocatalyst support. CNFs can be made in a variety of shapes, such as ribbon, herringbone, and platelet. Even with a low Pt loading of 5 wt, this is remarkable. Pt/CNFs demonstrated similar electrocatalytic activity for the ORR in Direct Methanol Fuel Cells (DMFC) as Pt/CB, despite having a significantly higher Pt loading of 30 wt. per cent. This discovery emphasizes how CNFs can boost catalytic activity and efficiently support Pt nanoparticles while using less precious metal. Additionally, Li et al. showed how to raise the electrode's Nafon content from 30 to 50 percent using CNF-based chemicals. Because CNFs prevented the disruption of ion conduction pathways, they provided continuous electric conduction paths, which were responsible for this increase [35].

This finding emphasizes how CNFs can be used to improve the composition of the electrode and the support characteristics of the electrocatalyst, which will improve fuel cell performance overall [36].

Doped nanocarbon

Common techniques for creating doped nanocarbon materials, particularly those based on graphene, include CVD and wet chemical reduction of graphene oxide (GO). These materials frequently lack the meso- and macropores required for effective mass transfer in the fuel cell's catalyst layer, despite having a large specific surface area. Heteroatoms like nitrogen can be substituted into carbon nanotubes (CNTs) to improve their electrocatalytic capabilities and speed up electron transport pathways. Furthermore, transition metal catalyst loading (e.g. A. enhances fuel cell activity even more when Ag, Fe, Ni, and Co are applied to CNTs [35].

Doping introduces heteroatoms that increase reactivity by creating a significant number of active sites, mostly on the graphene's basal plane. There are two primary techniques for doping graphene-based materials: surface adsorption of dopants and substitutional doping. By substituting heteroatoms for carbon atoms in the graphene lattice, substitutional doping produces comparatively stable structures because of the covalent bonds that hold the atoms together. Nitrogen (N), phosphorus (P), sulfur (S), and boron (B) are common dopants that improve graphene's electrochemical characteristics. These dopants are essential for modifying the surface chemistry and electronic structure of graphene-based nanomaterials, which makes them attractive options for enhancing catalytic activity and electron transport to boost fuel cell performance [35].

Dopant-free nanocarbon electrocatalyst

In order to improve ORR performance in fuel cells, scientists are looking into ways to cause carbon atoms to become charged polarized without using heteroatom doping. The charge polarization of carbon atoms can be changed by heteroatoms to significantly improve ORR performance, but dopant-free methods are also being researched. Shen et al. (2014) have shown that because edge carbon atoms are charged polarized, graphite's edges are significantly more active for ORR than the basal plane. A direct technique to identify the active sites in carbon materials for ORR was developed through the use of an air-saturated electrolyte solution droplet that was deposited on specific edges or on the basal plane of highly oriented pyrolytic graphite. CNTs and graphite that have been ball-milled, which reveal more edge sites, also demonstrated noticeably higher ORR activity [37].

The role of structural flaws in carbon-based nanomaterials and how they affect the ORR were also examined [38]. They emphasized how defects like dislocations, vacancies, and grain boundaries change the material's electron distribution, which in turn affects catalytic activity. Their results demonstrated that flaws, particularly at graphene edges and cracks, encourage charge transfer and enhance ORR performance. Specifically, graphene edges demonstrated a quicker rate of charge

transfer than the basal plane, which resulted in increased capacitance and enhanced electrocatalytic activity. The study also found that ORR efficiency was increased by topological defects such as pentagons and heptagons, which further improved electron redistribution [38].

Tao along with partners Tao et al. [39] have effectively created graphene that is dopant-free and edge-rich, which is a very effective ORR electrocatalyst. Regarding fuel selectivity and long-term stability, this material performed better than Pt/C electrodes that are sold commercially. Using a four-electron, one-step process and careful temperature and treatment time control during Ar-plasma etching, the superior performance was attained. This technique significantly raised the graphene surface's basal plane's edge site count, which improved the material's catalytic activity. The higher charge density and the greater number of catalytically active sites are responsible for the enhanced activity at the carbon edges [39].

Pt-containing alloys as catalyst

For the direct reduction of H_2O_2 in fuel cells, MWCNTs act as efficient support for a variety of catalysts in the anode and cathode. Pd catalysts pair with MWCNTs in the anode, while catalysts in the cathode include rhodium (Rh), ruthenium (Ru), platinum (Pt), gold (Au), silver (Ag), palladium (Pd), nickel (Ni), and copper (Cu) [40]. Furthermore, PdPtPt/Au-CNT, PtPdPd/Au-CNT, and PtPdPt/Au-CNT have demonstrated strong catalytic activity in a variety of conditions. When methanol is oxidized in direct methanol fuel cells (DMFCs), H_2 and CO groups are produced, which can contaminate Pt catalysts. This is lessened by adding a second metal, like Ru, which offers more active sites for the oxidation of CO that has been adsorbed [40].

CMK-3-NiO catalysts are made from mesoporous carbon (CMK-3) and ferrocene nickel. These catalysts are then used to produce MWCNTs through CVD. CMK-3–CNT–20Pt catalysts are produced by employing the conventional wet impregnation method to disperse Pt catalysts. It should be mentioned that the crystalline nature and greater degree of graphitization of MWCNTs also affect the electrical conductivity and stability of MEAs; Pt size and surface area are not the only factors influencing higher electrocatalytic active surface area. CNTs as catalyst supports, however, are more stable and have a higher peak power density than vulcan carbon [31].

The integration of Pt alloy and cobalt-nitrogen-carbon (Co–N–C) hybrid catalyst support, specifically designated as PtCo@CoNC/NCNT/rGO (PtCo@CoNC/NTG), has been studied by Lei Huang and his group. This novel method effectively increases the ORR's efficiency by constructing a continuous network and hierarchical architecture. The addition of this hybrid catalyst support creates more active sites and facilitates strong interactions, which works in concert to increase the stability and activity of Pt-based catalysts. Huang and his colleagues' research provide important

insights into the creation of sophisticated catalyst materials for enhancing fuel cell and other electrochemical application performance [33].

Non-Pt catalyst

When compared to Pt nanoparticles, MWCNTs with Cu/Cu_xO support have been found to have greater catalytic activity. Furthermore, the electrocatalytic activity of MO_2C/CNTs (with 16.7 wt. percent Mo) is determined to be comparable to a Pt catalyst (with 20 wt percent), but it has a higher overvoltage, so more research is necessary. Moreover, MWCNTs and tin dioxide (SnO_2) nanocomposite exhibits a higher maximum power density, which makes it an attractive anode material for microbial fuel cells (MFCs). Furthermore, it has been noted that iron-based cathodic catalysts can perform on par with Pt-based catalyst cathodes in terms of current density. These results demonstrate how non-Pt catalysts can be used in a variety of electrochemical processes and stress the significance of investigating substitute materials for improved fuel cell and associated technology performance [35].

Pt Nanoparticles

A variety of techniques, including electrodeposition, chemical reduction of metal salts, and metal vapor deposition, can be used to deposit platinum nanoparticles (NPs), which have a high surface-to-volume ratio, onto carbon nanotubes (CNTs). Since stabilizing ligands can affect catalytic properties and introduce impurities, electrodeposition in particular is preferred. For instance, CVD was used to grow NPs/SWNTs over an insulating silicon/silicon dioxide (Si/H_2) surface, and for quick analysis, the microcapillary electrochemical method (MCEM) was used. It was discovered that highly loaded structures are more effective for the methanol oxidation reaction (MOR) in direct methanol fuel cells (DMFCs), whereas low-loaded, well-separated NPs are appropriate for the ORR [41].

Additionally, to avoid CNT bundling, aligned CNTs (ACNTs) are made using both dry and wet techniques, like CVD. CVD, colloidal impregnation, and heat treatment at 300 °C can be used to create Pt nanoparticles on ACNTs (PtACNTs). In PEMFCs with lower Pt loading, Pt-ACNTs show enhanced cathodic catalyst activity and endurance. Furthermore, ACNTs are hydrophobic, just like CNTs, which aids in preventing water at the cathode [32]. These techniques and discoveries aid in the creation of catalyst materials that are more robust and effective for a range of fuel cell applications. The vertically aligned structure improves water drainage, gas diffusivity, and Pt utilization, as seen in **Figure 2** [32].

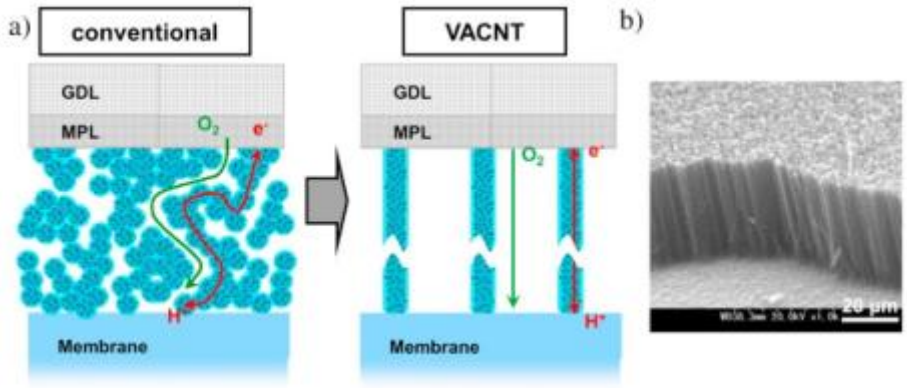

Figure 2 a. Concept of VACNT electrodes, b. SEM Image of VACNTs [32]

To ensure the long-term durability and performance of fuel cells, nanocarbon materials are essential for improving the corrosion protection of the bipolar plates. In the highly acidic environment of fuel cells, amorphous carbon film coatings made by CVD have been demonstrated to greatly increase corrosion resistance, albeit at a higher cost. Meanwhile, adding conductive polymers to aluminum bipolar plates, such as CNTs containing polyaniline, improves their conductive qualities and effectively reduces corrosion in PEMFCs (Deyab, 2014). Coating stainless-steel bipolar plates with composite films of carbon nanotubes and PTFE is another efficient method. In addition to lowering contact resistance between the bipolar plate and the MEA, this composite film significantly boosts fuel cell output power. The reliability and durability of bipolar plates in fuel cell applications could be guaranteed by these developments in nanocarbon-based corrosion protection technologies [31].

The cost-effectiveness of nanocarbon materials in comparison to conventional catalyst supports like Pt can have a substantial impact on the overall economics of fuel cell production, it is crucial to keep in mind when discussing the economic aspects of using nanocarbon in fuel cells. Although they are initially costly to produce, nanocarbon materials such as graphene and carbon nanotubes (CNTs) have benefits in terms of performance, stability, and durability that may eventually offset their higher initial costs. Furthermore, a key factor in the economic feasibility of nanocarbon production techniques is their scalability. In order to achieve economies of scale and lower production costs, nanocarbon material synthesis processes need to be optimized for large-scale production [35]

Technological developments in manufacturing, like roll-to-roll production methods, can reduce costs and streamline production processes. Furthermore, the longevity and robustness of fuel cells that use nanocarbon materials may have a big impact on the economy. The overall cost-effectiveness of fuel cell systems can be increased if nanocarbon-based catalysts help fuel cells become more durable and last longer. This will eventually lead to lower maintenance and replacement costs. Nanocarbon materials' capacity to raise fuel cell efficiency, performance, and energy density can also result in lower operating costs and increased system efficiency. More

energy output per unit of fuel consumed results from higher efficiency, which may lower fuel consumption and related expenses over the fuel cell system's lifetime [42].

2.2 Metal-air batteries

Due to their relatively benign chemistry and potential for high gravimetric capacity, metal-air batteries have been the focus of extensive research. Studies have been conducted on metal-air batteries with anodes made of Li, Na, Mg, Al, Si, K, Ca, V, Fe, Zn, Ge, and Sn. These batteries use a variety of electrolytes, including solid, polymer, ionic liquid, aqueous, and non-aqueous. Only the Zn-air battery has been commercialized to date in secondary (rechargeable) form; many of these battery chemistries have only been realized in non-rechargeable format. Rightfully, metal-air batteries are still being studied today to satisfy the demand for non-flammable, rechargeable, high-capacity, non-toxic batteries manufactured from abundant materials found on Earth [43]

The metal-air batteries with Li, Na, Si, K, Ca, Ge, and Sn anodes—among all those mentioned above—need nonaqueous electrolytes and, in the case of Sn, high temperatures of 800 C. In order to be rechargeable, magnesium-air batteries need a hybrid organic/aqueous electrolyte, which has been prepared with a neutral NaCl electrolyte in non-rechargeable form. Similar to this, primary Al-air batteries can use aqueous alkaline electrolytes; however, a NaCl electrolyte has only been shown to provide limited recharging. For Aleair secondary batteries to operate more effectively, non-aqueous electrolytes are required [43].

Both Zn-air and Fe-air batteries can be used as secondary batteries and are compatible with aqueous electrolytes. In addition to being inexpensive, easily recyclable, and free of dendrites that could harm the anode during cycling, the Fe-air battery is also environmentally friendly. Fe-air commercialization is hindered by a number of factors, including hydrogen evolution, passivation of the anode by iron-oxide films, limited cyclability, significant capacity fading, and slow oxygen reduction reaction (ORR) and oxygen evolution reaction (OER) kinetics. The Zn-air battery has been the most researched secondary metal-air battery for a long time and has been commercialized as a primary battery. This battery, which uses an aqueous alkaline electrolyte, has several benefits, such as being inexpensive, having a large capacity, being made of earthly materials, and being recyclable [43].

Nevertheless, it has slow oxygen kinetics, restricted cyclability, and dendritic growth. Although it is still in its infancy, the use of a neutral electrolyte shows promise in resolving some of these bottlenecks. The Metal-air redox flow battery is another intriguing metal-air battery format. Metal anodes made of Li, Na, V, Fe, and Zn have been the subject of extensive research; Li and Na require hybrid or non-aqueous electrolytes. The issues of hydrogen evolution, dendritic growth,

cathode clogging, restricted oxygen access, and precipitation of insoluble byproducts may be resolved by metal-air redox flow batteries [43]

Metal-air batteries, polymer electrolyte fuel cells, and electrolyzers all have similarities that are clearly visible in the Metal-air redox flow battery format. Introducing gaseous reactions is essential to all of these technologies (e.g. A. and CO_2) to the surface of the catalyst. Numerous studies on improved gas transport, gas flow field tortuosity, and catalyst durability can be directly applied to metal-air batteries. However, the metal-air battery needs catalysts that can efficiently carry out both oxygen reduction and oxygen evolution reactions, unlike electrolyzers and fuel cells. In this review, we concentrate on aqueous Metal-air secondary batteries, discussing electrolytes, OER/ORR catalysts, and reaction metrics [43]

2.2.1Types of Ion/metal – air batteries

2.2.1.1 Lithium-Ion Batteries

The "Li-ion battery," which was created by substituting carbon for Li metal as the anode, represented a significant advancement in the field of Li-based batteries. In 1991, a Li-ion battery with petroleum coke as the anode and $LiCoO_2$ as the cathode went on sale. Li-ion batteries have since taken the lead in the portable electric device market. A Li-ion cell (**Figure 3**) normally has an anode and cathode made of intercalation compounds and electrolytes based on organic solvents. [7].

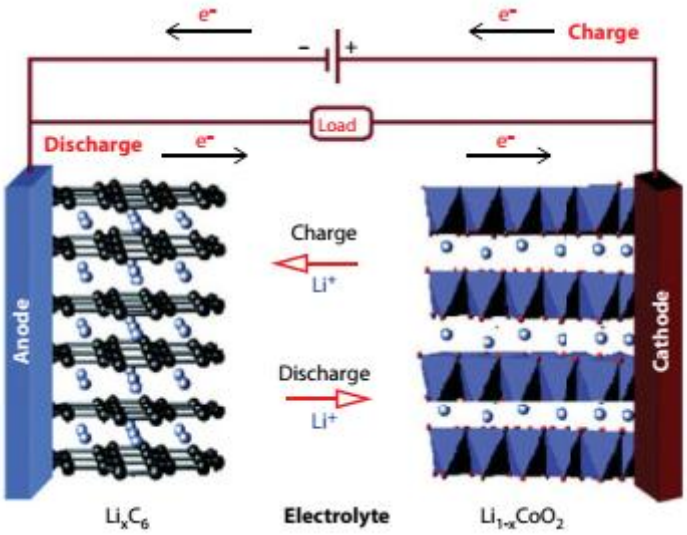

Figure 3 Schematic of Li-ion cell [7]

The intercalation compound must have high electronic conductivity, stability (both chemical and thermal), and the proper lithium chemical potential in order to function as an electrode material. A Li-ion cell with a graphite anode and a $LiCoO_2$ cathode works on the following principle [7].

$$\text{At cathode, } x\,Li^{-} + Li_{1-x}CoO_2 + xe^{-} \underset{Charge}{\overset{Discharge}{\rightleftharpoons}} LiCoO_2 \quad (2)$$

$$\text{At anode, } LiC_6 \underset{Charge}{\overset{Discharge}{\rightleftharpoons}} Li_{1-x}C_6 + xLi^{+} + xe^{-} \quad (3)$$

$$\text{Overall cell reaction, } LiC_6 + Li_{1-x}CoO_2 \underset{Charge}{\overset{Discharge}{\rightleftharpoons}} Li_{1-x}C_6 + LiCoO_2 \quad (4)$$

The majority of cathode materials are transition metal compounds. The transition metal ions undergo higher oxidation states while maintaining their crystal structure when the Li+ ion is removed. Goodenough et al. demonstrated that $LiCoO_2$ is a layered material. in 1980. Its rock salt structure is -$NaFeO_2$, with Li^+ and Co^{3+} ions occupying alternating layers. It is possible to extract up to 0.5 mol of Li from $LiCoO_2$ without causing structural instability. The presence of Co makes the material costly, and as the charging voltage rises, it experiences structural instability. Another problem is the dissolution of Co into the electrolyte. [7].

Because Ni is displaced into the Li layer during cycling and influences the lithiation/de-lithiation process, $LiNiO_2$ is less costly and has a higher energy density than $LiCoO_2$, but it has poor stability. Another layered substance with a monoclinic crystal structure is $LiMnO_2$. Capacity decay is caused by the formation of spinel $LiMn_2O_4$ as a result of delithiation. Although $LiMn_2O_4$ has been investigated as a low-cost material, the Jahn–Teller effect of Mn3+ causes poor cycle life when lithium is inserted or de-inserted at 3V. Isostructural to $LiCoO_2$, LiNi1/3Mn1/3Co1/3O_2 or $NCm^3$33 is where Ni, Co, and Mn play their respective roles in providing high capacity, cycle stability, and thermal stability. An $NCm^3$33-based cell operating between 2.5 and 4.2 V has demonstrated a stable capacity of 150 mAh g-1. Goodenough et al. published the first report on olivine LiFePO4. which was inexpensive, had a large capacity, and was thermally stable. Sadly, the material has poor lithium diffusivity and low electrical conductivity (10-9 S cm-1). To address these problems, efforts have been made to reduce the particle's size and coat it with a conducting layer [7].

Because of its high capacity, lithium metal is the best option for the anode. However, Li metal-based cells have problems like dendritic formation, electrolyte reaction, and low stability. For Li-ion batteries, graphite is a commonly used anode material. Lithium alloys containing Al, Si, Sn, etc. have been investigated as potential anode materials. In these alloy-based cells, volume expansion during lithiation causes cracks to form and active material to be lost. As an anode material, amorphous silicon has demonstrated encouraging outcomes. The most widely used electrolyte for Li-ion batteries is $LiPF_6$ in a blend of carbonate-based solvents. The development of a stable solid electrolyte interface (SEI) is significantly influenced by the solvent, and the impact of electrolyte additives has been investigated to enhance SEI characteristics. There are numerous review articles on Li-on batteries that offer advancements and a deeper comprehension of the system. [7].

As new materials (anode, cathode, and electrolyte) are introduced and battery technology advances (stock design, reduced self-discharge, and weight), lithium-ion battery performance metrics like energy/power densities, safety, stability, and cyclability continue to improve. The high cost of Li-ion batteries, which stem from the limited availability and irregular geographic distribution of elemental lithium reserves, is one of the main areas where they still lag behind their counterparts, such as lead acid or sodium ion batteries, despite their exceptional qualities. Furthermore, Li-ion batteries' capacity retention and cyclability over an extended period of time significantly decline at temperatures above 30 °C. Since additional protection circuits are needed to limit circuit currents and voltages for their safe operation to avoid overloading, operational safety is another significant concern surrounding Liion batteries [44]

2.2.1.2 Lead-acid batteries

The first rechargeable battery was created in 1859 by French physicist Raymond Gaston Plante and was called a lead-acid battery. Lead plates that have been spirally wound and submerged in a diluted sulfuric acid solution make up the battery system. Later in 1881, Faure and associates presented a novel technique using pasted plates made on lead alloy grids by combining lead oxides and sulfuric acid. It was discovered that this produced much faster and more efficient results. Even after 150 years, the basic electrochemistry of lead-acid batteries has not changed, despite a number of design modifications made intermittently to enable the battery to meet emerging performance challenges. **Figure 4** illustrates the fundamental parts and construction of a lead-acid battery. The attractive features in real-world applications, such as low cost, maximum recyclability (>98%), and operational safety, outweigh the drawbacks of lead-acid batteries, such as low specific energy and power characteristics when compared to other rechargeable batteries [44]

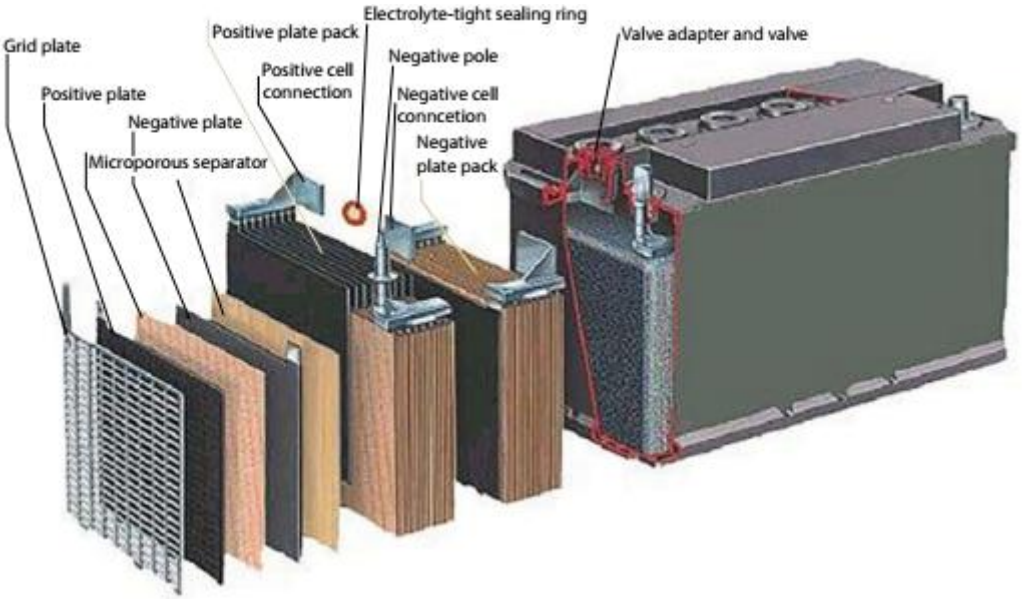

Figure 4 The components and construction of a lead-acid battery [44]

The use of aqueous electrolyte and nonflammable electrode materials in lead-acid batteries ensure operational safety. Compared to other batteries, like lithium-ion batteries, the risk of battery cases catching fire is minimal. Furthermore, compared to other battery chemistries that require significant improvement in the recycling process, the lead-acid battery's cost-effective and well-established recycling process complies with environmental regulations, making it more appealing for future applications.

Lead-acid batteries are further separated into two categories: sealed and valve-regulated. While sealed leadacid batteries with new and improved technology, called Valve Regulated Lead Acid (VRLA) based battery cells, were introduced between 196 and 1975 and are fully sealed, valve-regulated batteries have valves installed to release excess pressure generated at the positive electrode during the oxygen reduction reaction [45].

Because VRLA-based battery systems are smaller than valve-regulated cells, they are better suited for small-scale uses like portable electronics. On the other hand, valve-operated battery systems are easily expandable, which leads to increased storage capacity and a wider range of applications, including emergency lighting, UPSs, and power telecommunications. The energy/power densities of Pb-A based battery systems were not enhanced by VRLA technology, but it did lead to other advantages because of the reduced electrolyte content, such as reduced maintenance, increased dependability, and—most importantly—an easier time complying with air freight and transportation regulations. Fast response times, low daily self-discharge rates (< 0.3 percent), relatively high cycle efficiencies (~ 63-90 percent), and low capital costs are some of the additional advantages of Pb-A batteries. Lead-acid batteries also have cost-effectiveness, exceptional rate capability, exceptional charge retention, and good performance across a wide temperature range, all of which contribute to their commercial appeal [46]

Notwithstanding these advantageous characteristics, lead-acid batteries have a short lifespan (300–500 cycles), are environmentally hazardous, have a low energy density (40 Wh kg-1), and experience acid stratification. The overall cost of a battery system is increased by the need for temperature-controlled voltage management systems to address the "dry out" problems and poor performance of VRLA-based Pb-A batteries at low temperatures [47]. RandD on Pb-A batteries is currently focused on the following areas to address the performance and operational issues of lead acid batteries: (a) material innovation for improving battery performance, such as cyclability and deep discharge capability; (b) response time reduction; and (c) battery technology optimization for commercialization in a variety of applications, such as the transportation sector and photovoltaic power integration.

2.2.1.3 Nickel-Cadmium Batteries (Ni-Cd)

In 1899, Swedish engineer Waldemar Jungner received the first patent for the nickel-cadmium battery system [48]. Together with an aqueous alkali solution, such as potassium hydroxide (KOH), as an electrolyte that doesn't change much while in use, metallic cadmium and nickel hydroxide are utilized as the anode and cathode, respectively. A three-layer porous polymeric separator, typically composed of layers of nylon, polypropylene, and nylon, separates the anode and cathode and aids in electrolyte diffusion [49]. During the discharge cycle of a Ni Cd cell, cadmium (Cd) is oxidized ($Cd \rightarrow Cd(OH)_2$) at the anode and Ni is reduced ($NiOOH \rightarrow Ni(OH)_2$) at the cathode. The opposite reactions occur when charging. However, the positive and negative electrodes produce hydrogen and oxygen during the discharge cycle, respectively, necessitating venting and the addition of water [50].

Although nickel-cadmium batteries have two unique designs—one with a completely sealed cell and the other with a vent to release gases (hydrogen and oxygen)—they function on the same basic idea as other electrochemical battery systems. While vented Ni-Cd batteries are used in aircraft and diesel engine starters, where high energy per weight and volume are crucial, sealed cells are used in daily life. Fast charge and discharge as well as a long cycle life (up to 3000 cycles) are two benefits of the Ni-Cd battery system. Compared to other battery systems, like lead acid batteries, they have good size flexibility (ranging from small portable devices to large, vented cells) and can withstand deep discharge rates without any capacity loss. Before losing market share to others, better rechargeable battery systems like LIBs, Ni-Cd batteries were widely used and held the largest market share until the 1990s in applications like portable and standby power sources [51]. The Ni-Cd system's drawbacks, which include environmental issues brought on by cadmium toxicity and their high manufacturing costs (nearly ten times higher than those of lead-acid batteries), restrict their wider application. Another disadvantage of Ni-Cd batteries is that they have "memory" problems that reduce their capacity if they are not fully discharged before charging or are left unused for long periods of time [52].

2.2.1.4 Nickel-Metal Hybrid Batteries (Ni-MH)

The main goal of nickel metal hydride (Ni-MH) battery technology, which is an advancement of nickel-cadmium batteries, is to solve two major problems: the high cost of cadmium and environmental concerns. Given their similar designs and use of the same cathode and electrolyte material, Ni-MH batteries can be thought of as an enhanced version of NiCd batteries. The main distinction is that an alloy that absorbs hydrogen is used in place of the anode in Ni-MH. Furthermore, both battery systems have the same cell voltages and charge/discharge curves. In the overall cell reaction of a Ni-MH battery, hydrogen moves from one electrode to the other, much like in lithium-ion batteries, where Li ions move between the electrodes while the battery is operating.

The long cycle life (~ 500 cycles) and fast kinetics (high power densities, typically ≥ 1000 W kg-1/2) of Ni-MH batteries are based on their very simple electrochemical reactions. Although they are not as good as Li-ion cells, they have some important features that make them a better option than Ni-Cd technology, especially for use in portable electronic devices [53].

Ni-MH batteries find extensive use in electric/hybrid electric vehicles (EVs/HEVs), including the Toyota Prius. The nickel-metal hydride cell's chemistry, which provides tolerance to both overcharge and over-discharge through gas recombination reactions, determines the applications of Ni-MH batteries. Because there is no pressure build up even inside a completely sealed battery cell, this leads to a maintenance-free battery cell. Compared to other high energy density systems like sodium-sulfur and lithium-ion systems, the Ni-MH cell's exceptional capability eliminates the need for cell voltage monitoring, simplifying battery management systems (BMS) [54].

The development of other effective battery technologies (like lithium-ion batteries) and the shortcomings of Ni-MH battery systems have combined to cause a gradual decline in the applications of Ni-MH batteries. The main disadvantage of Ni-MH cells is their extremely high rate of self-discharge, which can cause a NiMH battery to lose up to a third of its charge in a month even when it is not being used. This rate is up to three times that of Ni-Cd batteries and even higher when compared to other rechargeable battery systems like lead-acid or lithium-ion. Because EVs and HEVs are used frequently, the battery's self-discharge problem is less obvious in these applications; however, it becomes more noticeable in portable electronic devices that are used infrequently. Additional drawbacks include a high cost of materials, which reduces their long-term competitiveness with other rechargeable batteries like lithium-ion [55].

2.2.1.5 Lithium-ion (Li-ion) batteries

Lithium batteries offer a high storage efficiency of 83% and are the power sources of choice for sustainable transport. Li-ion batteries are ideal for small-scale electronics and are extensively applied in renewable energy and micro-grid systems. The advantages of Li-ion batteries include sealed cells that require no maintenance, long cycle life, wide temperature range of operation, rapid charging, high charge/discharge efficiency, high energy density, and ample design flexibility. Flexibility of design involves selection of salts used as the electrolyte. Conventionally, Li-ion batteries use lithium hexafluorophosphate ($LiPF_6$) [53].

However, these batteries are limited by thermal stability, sensitivity to moisture, and the production of toxic chemicals during breakdown. Consequently, alternative salts are being investigated to mitigate these drawbacks. The implementation of solid-state electrolytes can enhance the effectiveness of Li-ion batteries due to their thermal and chemical stability. Nevertheless, solid-state

electrolytes are currently considered expensive, though advancements are being made to enhance their commercial viability [53]

Li-ion batteries have several drawbacks, such as a high initial cost, a high degree of charge/discharge randomness, a need for frequent charging, and a short cycle life. Size, application, and cathode type are some of the variables that affect the materials and percentages of each in Li-ion batteries. For instance, according to data gathered from multiple battery recycling companies, the materials and percentages used in a typical Li-ion portable battery are as follows: lithium cobalt oxide (27.5 percent), steel (20.2 percent), graphite (16 percent), polymer (14 percent), copper (9 percent), aluminum (5.5 percent), nickel (4.3 percent), and electrolyte (3.5 percent) [53]

2.2.1.6 Lithium-sulphur (Li-S) batteries

Lithium-sulphur batteries are regarded as a potentially viable solution for energy storage due to their high theoretical capacity and low cost, attributable to the abundance of sulphur. Despite theoretical projections indicating energy densities up to five times higher than that of Li-ion batteries, the practical implementation of these cells remains in its infancy. Notable limitations include capacity loss and low coulombic efficiency due to polysulfide shuttling, low volumetric density, high internal resistance, self-discharge, and rapid capacity fading. The innovative design of the cells is a potential solution to these challenges, and as such, they are receiving significant attention from researchers [53]

2.2.1.7 Nickel-cadmium (Ni-Cd) batteries

Nickel-cadmium batteries find application in a variety of devices, including phones, toys and hand tools. Nickel and cadmium are used as electrodes, with the cadmium electrode exhibiting a higher capacity. The advantages of Ni-Cd batteries include a long cycle life, durability, good charge retention, excellent long-term storage, low maintenance, and flat discharge. However, these batteries are associated with several significant drawbacks, including their low energy density, high cost relative to Pb-A batteries, and the presence of strong memory effects. Cadmium is a highly toxic metal that must be disposed of properly, and the Cd levels in municipal solid waste largely come from discarded Ni-Cd batteries. [53]

2.2.1.8 Nickel-zinc (Ni-Zn) batteries

Nickel-zinc (Ni-Zn) batteries are typically used for providing small-scale, portable power at a high rate of discharge. They are produced at a relatively low cost when compared to lithium-ion batteries and have the potential to replace both nickel-cadmium (Ni-Cd) and nickel-metal hydride (NiMH) batteries for the majority of applications. The effectiveness of Ni-Zn batteries is attributed to their high specific power, high efficiency, low cost and minimal environmental impact. However, this

configuration is not without its drawbacks, including the fact that zinc is a self-corrosive material, Ni-Zn batteries are prone to drying out, and evidence of low discharge after a number of cycles. [53]

2.2.2 Thermodynamics of OER and ORR

It is fairly well known how oxygen electrochemistry works on the cathode. Because non-noble metals are less stable in acidic environments, metal-air batteries typically use neutral or alkaline electrolytes. The performance of metal-air batteries is significantly limited by the more sluggish kinetics of neutral electrolytes, despite the fact that the same reaction pathways for oxygen redox processes have been proposed in both neutral and alkaline media [43]

Air and oxygen diffuse to the cathode catalyst upon discharge. ORR is a multi-step process that involves reactant adsorption and desorption as well as proton-coupled electron transfer. ORR takes place in the air cathode's three-phase region, where water and oxygen and electrons combine to form OH. The two-electron pathway is less advantageous because peroxide eventually forms, which damages battery components and lowers ORR efficiency. As a result, the battery life is shortened. By totally reducing O_2 to OH, the four-electron pathway prevents the production of HO_2^- and boosts reaction efficiency. [43]

Catalysts which are highly selective for the four-electron pathway are preferred. The details of the complex ORR reaction on a specific catalyst surface, however, are still not well understood and are challenging to study with current instrumentation. [43]

The oxygen reduction pathway at the active site on the catalyst surface can either be direct or associative. In the direct process, typical for Pt-based catalysts, oxygen adsorbed on the catalyst undergoes immediate O-O bond breaking resulting in Oad which is reduced to OHad and desorbed. In the associative process, the adsorbed oxygen is initially reduced to OOH_{ad} by protonation followed by O-O bond breaking. However, if the O-O bond is not immediately broken, the 2-electron reaction produces H_2O_2. [43]

Typically, two mechanisms for the oxygen evolution reaction (OER) are highlighted in academic discussions: the adsorbate evolution mechanism (AER) and the lattice oxygen mediated mechanism (LOM). While the catalytic process for OER is primarily regarded as following the AER pathway, which is essentially the reverse of the oxygen reduction reaction (ORR) described earlier, the LOM pathway is considered significant for metal oxides like perovskites. [43]

2.2.3 General classes of catalysts for OER/ORR reactions

A range of catalyst formulations has been suggested for the oxygen reduction reaction (ORR) and oxygen evolution reaction (OER) occurring at the air cathode, which can be grouped into several categories: noble metal catalysts, transition metal oxide catalysts, phosphides and sulfides, metal

phosphates and borates, carbon-based materials, and organometallic compounds. Since the two reactions involve distinct mechanisms during charging and discharging, some catalysts are designed specifically for either the ORR or OER, while others are aimed at achieving a bifunctional catalytic performance. [43]

2.2.3.1 Noble metal catalysts

Noble metal catalysts have long been recognized and thoroughly examined as traditional catalysts for oxygen electrochemistry. Platinum and its alloys exhibit strong oxygen reduction reaction (ORR) activity yet exhibit weak oxygen evolution reaction (OER) activity. In contrast, Ruthenium Dioxide (RuO_2) and Iridium Dioxide (IrO_2) possess high OER activity but show poor ORR performance. Researchers are focusing on optimizing material compositions for dual-function effectiveness, enhancing resistance to surface contamination from environmental oxygen species, and decreasing the reliance on precious metals by creating composites, nanoparticles, and thin films. Despite the high catalytic efficiency of noble metals in oxygen-related reactions and their remarkable stability across various acidic and alkaline electrolytes, their limited availability and high costs render them impractical for large-scale applications and widespread use. Nonetheless, employing (Pd/C, Pd/C, and RuO_2) as reference points to assess the performance of new catalyst materials is fully warranted [43]

2.2.3.2 Transition of metal oxides

Transition metal oxides are straightforward to synthesize and fairly cost-effective, demonstrating encouraging performance as non-noble catalysts for oxygen reactions. In the context of oxygen reduction reaction (ORR) catalysis, metal oxides primarily facilitate the conversion of HO_2 into H_2O and O_2. Various forms of manganese oxide have displayed activity for both oxygen evolution reaction (OER) and ORR. Due to the poor electrical conductivity of MnO_2 and its tendency to amorphize over time, researchers have investigated the combination of MnO_2 with other metals like Fe and Cu to enhance its conductivity, stability, and effectiveness in both ORR and OER processes. The findings indicate a performance level similar to that of commercial Pt/C catalysts. The catalytic process for the oxygen evolution reaction (OER) on MnO_2 begins with the reduction of Mn^{4+} to Mn^{3+}, which is then followed by a disproportionation reaction that produces Mn^{4+} and dissolved Mn^{2+}. This process subsequently deprotonates to form Mn^{3+}eOH and leads to the generation of oxygen. In conditions of low acidity, the step that limits the reaction rate is the disproportionation of Mn^{3+} occurring on the surface of the catalyst. [43]

Rock salt, spinel, and perovskite structures like Co3O4, FexNiyO_2, CoxFeyO_2, MnxFeyO_2, CoxFeyNizO_2, and La1.5Sr0.5NiMn0.5Ru0.5O6 are other transition metal oxides that have been

reported to have good OER catalytic activity. In these cases, the LOM OER mechanism is crucial for the enhanced adsorption of oxygen-containing active species like HO* by the Co sites at the catalyst interface, followed by redox reactions that produce OOH ads species and speed up the OER process.

Transition metal phosphates ($Co_3(PO_4)_2$), NiCoFe phosphate/oxyhydroxides $NaCoPO_4$, $Na_2CoP_2O_7$, Li2CoP2O7, and $LiCoPO_4$ have also been investigated as ORR/OER catalysts, motivated by photosynthesis. Corner-shared or edge-share metaleoxygen polyhedra are the main structural components of these catalysts, and they are capable of efficiently lowering the OER free energy. The phosphate groups' adaptable coordination capabilities can stabilize transition metal intermediate states and guarantee efficient OER. Additionally, phosphate groups could aid transition metals in assuming greater. There have been some reports of borate OER catalysts (Co, Bi, Ni), however their catalytic performance is lower than that of phosphates, most likely because the metal core is not as well stabilized. Although metal phosphates' ORR catalytic activity is rarely documented, it can be presumed that metal oxides at high OER potentials are inevitably generated, slowly degrading the catalytic activity of phosphates [43]

Metal sulfides

In addition to having higher electrical conductivity than metal oxides, metal sulfides (NiSx, CoSx, MoSx $FeNi_2S_4$, NiS2(1x)-Se2x) have also been proposed as ORR/OER catalysts. CoPx, CuPx, and FePx phosphates have also been proposed as ORR/OER catalysts, usually in composite structures. The outcomes vary greatly and cannot be linked to a person's composition. [43]

carbon-based catalysts

For ORR/OER, non-metallic carbon-based catalysts are also taken into account. Although Pt is a great ORR catalyst for Zn-air batteries, its low OER performance and high cost and scarcity prevents its widespread application. Investigating alternate earth-abundant, inexpensive, and extremely efficient electrocatalysts is therefore essential. Because of their exceptional ORR and OER performance, low cost, great corrosion resistance, and high earth abundance, carbon-based metal-free catalysts have gained popularity for use in Zn-air batteries.

[56]

A significant challenge for Zn-air batteries is to enhance the efficiency of oxygen reduction and evolution. This necessitates the creation of stable and effective ORR/OER bifunctional electrocatalysts that are inexpensive and stable. In response to this requirement, Dai and colleagues developed the first highly efficient Zn-air batteries (both primary and secondary) utilising carbon air electrodes based on N, P-doped bifunctional carbon-foam catalysts for both ORR and OER [56]

The presence of abundant active sites and a high concentration of O species on catalysts can also facilitate oxygen adsorption and promote catalytic activities towards ORR and OER. In this context, Li et al. [57] prepared two-dimensional (2D) microporous carbon sheets with a high oxygen content, which produced a small voltage gap (0.85 V) and demonstrated long-term cycling stability (up to 160 h). These properties were superior to those of Pt/C-based Zn-air batteries [57] The utilisation of N-doped ORR/OER bifunctional catalysts has the potential to enhance battery performance. Subsequent studies have demonstrated that quaternary N, which provides n-type doping, is responsible for ORR, while pyridinic N, which provides p-type doping, can serve as active sites for OER. (**Fig. 5a**) [58]

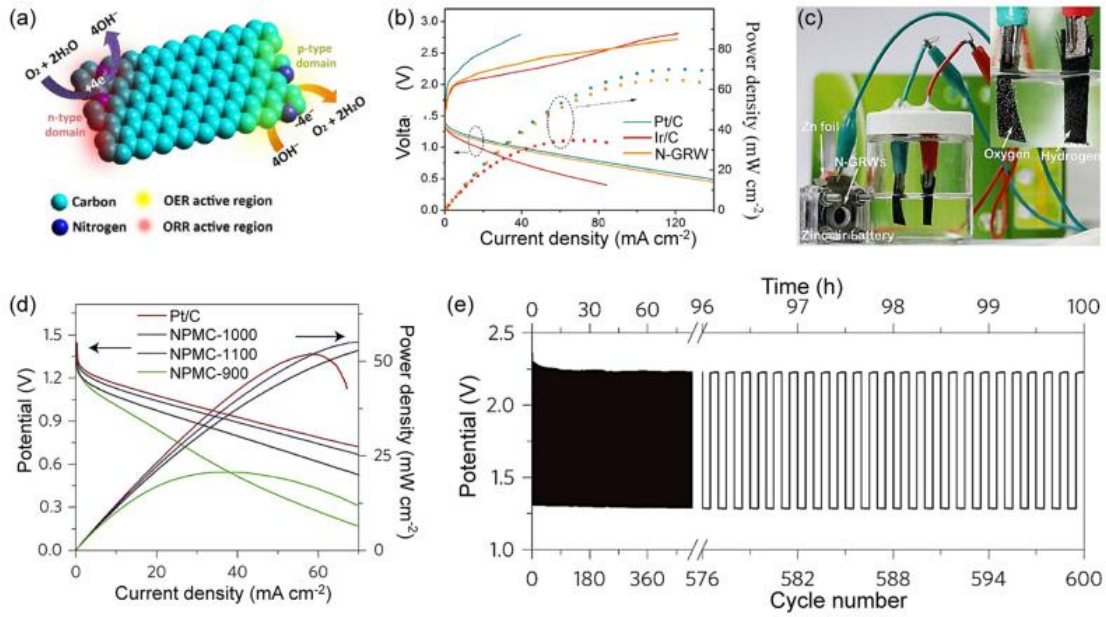

Figure 5 a. Schematic illustration of diferent active sites for ORR and OER in N-doped 3D graphene nanoribbons. b. Discharge–charge profles and power density plots of zinc-air batteries constructed with N-doped graphene nanoribbon networks, Pt/C, Ir/C, and mixed Pt/C + Ir/C. c. Application of N-doped graphene nanoribbons-based Zn-air battery in powering water splitting. Reprinted with permission from Ref. [93], Copyright 2016, AAAS. d. Polarization curves and corresponding power density plots of primary Zn-air batteries using Pt/C, N, P-doped mesoporous carbon catalysts (NPMC-900, NPMC-1000, NPMC-1100) as ORR catalysts. e. Cycling performance of a three-electrode NPMC 1000-based Zn-air battery at 2 mA cm^{-2} [58]

It was demonstrated that Zn-air batteries constructed using bifunctional N-doped 3D grapheme nanoribbon air electrodes were capable of producing a peak power density of 65 mW cm-2 (Fig. 5b). Furthermore, these batteries have been used to power splitting water units (Fig. 5c), indicating their potential for practical applications. In 2016, the non-aqueous lithium air system (NLAS) garnered significant attention following the inaugural demonstration of a lithium air system with a non-aqueous electrolyte. This was due to the high gravimetric (3458 Wh kg-1) and volumetric (3445 Wh L-1) energy density exhibited by the NLAS, which surpassed that of conventional lithium-ion batteries. [59]

The potential of ordered mesoporous carbon (OMC) synthesised with a silica template, as an electrocatalyst in NLAS has been identified as a promising avenue for further investigation. The high specific surface area, excellent electrical conductivity and fast mass transport properties of this material suggest that it could offer significant advantages in this application. For example, Sun et al. (2013) demonstrated the electrocatalytic performance of the OMC in NLAS and compared the results with those of a commercial carbon catalyst, namely super P. As anticipated, the OMC exhibited a high specific capacity and a low over potential in comparison to that of the super P cathode.

A number of other reports in the literature address the cathode performance of OMC, which has been synthesised using a variety of templates [61]**.** Recently, single-walled and multiwalled carbon nanotubes have been investigated as air cathodes for NLAS due to their appealing features, including high chemical and thermal stability, high elasticity, and high tensile strength [7].

Functional carbon materials, including graphene, mesoporous carbon, carbon nanotubes (CNTs), carbon nanofibers (CNFs), and carbon microfibers, are recognized for their efficacy as electrocatalysts in lithium-air systems, attributed to their distinctive structures and increased number of defects or vacancies. Graphene, specifically, has been investigated as an electrocatalyst and demonstrates an exceptionally high specific capacity when compared to commercial carbon-based materials. The superior electrochemical performance of graphene-based materials, in terms of cycle life and round-trip efficiency, can be attributed to their unique 3D three-phase electrochemical area and the diffusion channels that facilitate electrolyte access and oxygen diffusion, in addition to their structural advantages [7].

Although carbon-based catalysts exhibit good oxygen reduction reaction (ORR) activity, carbon corrosion at high oxygen evolution reaction (OER) potentials compromises the catalyst structure, resulting in gas film formation on the surface and subsequent battery performance degradation. Heteroatom doping (N, P, B, Si, S, F, etc.) in carbon materials significantly enhances catalytic activity by introducing more defects as active sites for oxygen reduction and facilitating the conjugation between the lone pair electrons of the doped heteroatom and the delocalized π-bonds of the carbon material. Nitrogen doping, in particular, can produce pyridinic nitrogen, pyrrolic nitrogen, and graphitic nitrogen, with the first two exhibiting positive catalytic effects on ORR. Additionally, the morphology of carbon materials influences uniformity and the amount of heteroatom doping. [43]

Thus, heteroatom-doped carbon catalysts with strategically designed pores are highly promising for advanced Li-air batteries. The variability in carbon structure and morphology allows for potential optimizations in gas and electrolyte diffusion as well as electron transport. For instance, nitrogen

doping has been shown to increase catalytic activation sites for the formation of Li_2O_2 at carbon cathodes, thereby reducing charge overpotentials in Li-O_2 batteries.

The incorporation of nitrogen species into onion-like carbons can alter electron distributions to enhance oxygen chemisorption, leading to improved ORR and OER kinetics, energy output, and recharging characteristics of Li-O_2 batteries. Nitrogen doping in graphene has also been found to facilitate the nucleation of Li_2O_2 clusters, thereby enhancing electrochemical performance. Li-air batteries utilizing N-doped CNTs with uniform nitrogen species distribution ensure a high number of nucleation sites and well-dispersed discharge products, thereby increasing discharge capacities. [56].

Li et al [62] has demonstrated the use of N-doped grapheme nano sheet (GNS) as air cathode for the first time and realized a specific capacity of 11660, 6640 and 3960 mAh gcarbon-1 at 75, 150 and 300 mA gcarbon-1 respectively. In addition, Higgins al (2013) reported that 20 wt.% N-doped graphene can deliver a specific capacity of 11746 mAh gcarbon-1 at a current density of 70 mA gcarbon-1, which is higher than commercial carbon electrodes [62].

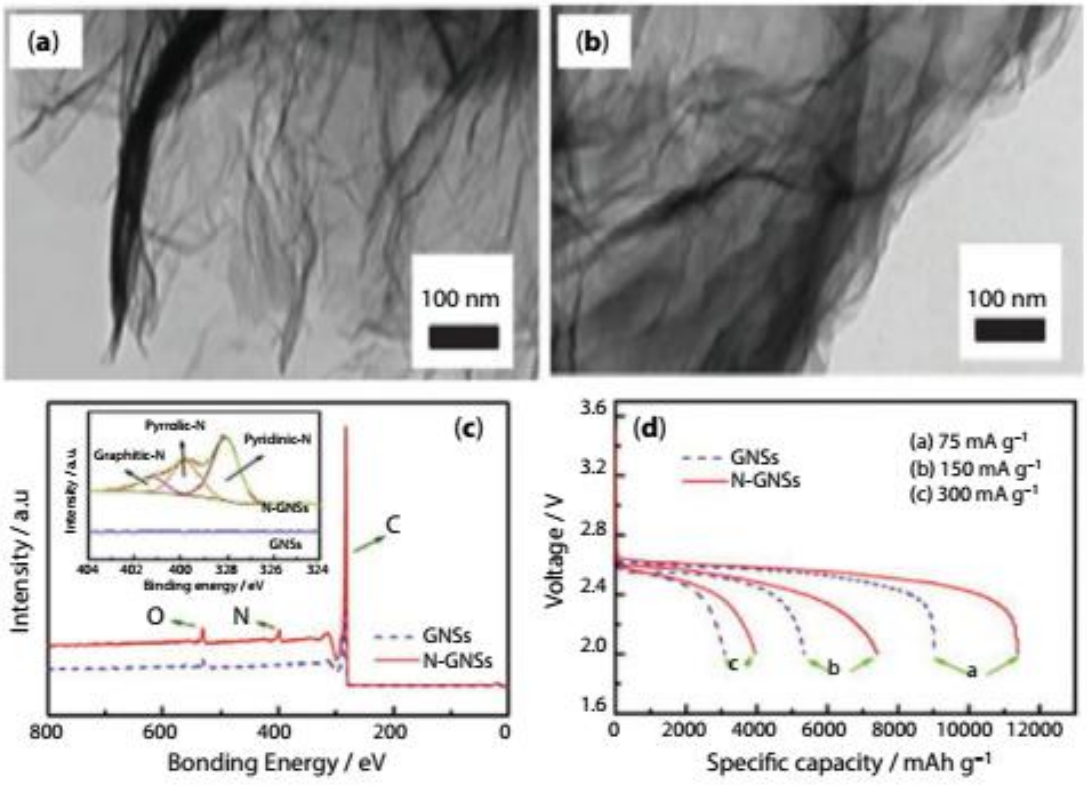

Figure 6 TEM images of GNSs (a) and N-doped GNSs (b); XPS spectra of GNSs and N-doped GNSs, the inset is N 1s spectra of two samples (c); voltage profle of GNSs and N-doped GNSs electrodes at various current densities (d) [7].

In addition to nitrogen doping, other types of heteroatoms doping or codoping have also been shown to significantly enhance catalytic activity and cell performance. Specifically, nitrogen doping has been demonstrated to increase discharge capacities, while sulfur doping has been confirmed to

support stable cycling behaviors in graphene-based Li-O_2 batteries. According to first-principles thermodynamics, Ren et al. [63] predicted that boron-doped graphene can enhance the charge rates of Li-air batteries and lower the O_2 evolution barriers by approximately 0.4 eV. Indeed, boron-doped graphene has been found to exhibit stronger adsorption for Li_2O_2 compared to pristine graphene. Consequently, the incorporation of boron into graphene structures can activate Li-O bonds and oxidize O_2^{-2} to O_2 [63].

The incorporation of transition metals (Fe, Co, Ni, Mn, etc.) or noble metals (Pt, Ir, etc.) into carbon materials (MeNeC) with nitrogen can markedly enhance their oxygen catalytic performance. This improvement can be attributed to the introduction of MeNx moieties, which serve as single-atom catalysts (SACs) characterised by high atomic efficiency, well-defined structure, and high intrinsic activity. Despite the high catalytic activity of single-atom catalysts, MeNeC catalysts are subject to a number of challenges, including carbon corrosion, low single-atom loading, and severe atom aggregation. The carbon framework derived from MOF materials, with its three-dimensional network structure, high specific surface area, and tunable porous structure, has demonstrated substantial potential for enhancing the activity of ORR/OER processes [56]

Organometallic compounds

It has been proposed that transition metal units may be effective in catalysing ORR/OER processes. In contrast to the direct and associative reaction pathways previously discussed, organometallic compounds predominantly follow stepwise reaction pathways. It is widely accepted that high valence state metal centres play a pivotal role in the formation and breaking of oxygen O-O bonds. Consequently, their stable presence is essential for enhancing the activity and durability of the catalysts. Although the current catalytic performance is not yet satisfactory, the frequent occurrence of ORR/OER in nature points to the potential of organometallic catalysts [56]. In addition to catalyst composition, factors such as morphology, crystallinity, and preparation methods are also crucial for performance. High surface area, surface defects, and the combination of multiple catalytic species on the surface facilitate reactions [56].

The activity of the oxygen evolution reaction (OER) was enhanced by increasing surface area through particle size reduction or altering morphology. Additionally, core-shell La0.7Sr0.3MnO3@MnO_2 particles have demonstrated excellent bifunctional catalytic activity for ORR/OER in secondary Zn-air batteries [56].

Doping Mg^{2+} into NiFe hydroxide has been found to improve OER performance and lower overpotential by facilitating water adsorption on the catalyst surface, thereby decreasing the distance between the oxygen in water and the metal redox centers. To optimize the OER activity of

metal sulfides, strategies such as heteroatom doping, component modulation, structural optimization, and interfacial design have been proposed. These strategies work by adjusting the binding energy of the adsorbed species, thereby reducing the overpotential of the OER process [56].

Enhancements in this category of catalysts can be achieved by improving both electron transfer and mass transfer of reactants. Carbon materials and binders are employed in the fabrication of air cathodes, serving as current collectors or conductive additives for electron transfer. In highly alkaline environments, carbon corrosion results in the formation of carboxylic acids, eventually leading to electrolyte degradation and damage to components [56].

To address this issue, self-supporting catalysts, which are directly grown on current collectors such as nickel foam or carbon cloth through electrodeposition, hydrothermal/solvothermal reaction, and vapor deposition, have been proposed. These methods eliminate the need for binders and conductive agents [56].

2.3 Supercapacitors

2.3.1 General

The rapid charge and discharge capability, high power density, and long-term stability of supercapacitors have garnered significant attention in this regard. On the basis of the charge storage mechanism, supercapacitors can be classified into two categories. One category is designated as an electrical double layer capacitor (EDLC), whereby the accumulation of electrostatic charge at the electrode-electrolyte interface is the source of the capacitance. [7]

The surface area of the electrode materials and the pathway for electrolyte ion diffusion are of critical importance with regard to EDLC capacitance [64]. A further category of supercapacitor employs a reversible faradic reaction, known as a pseudocapacitor, to store charge. Nevertheless, the simultaneous functioning of both EDLC and pseudocapacitance can be achieved through the hybridization of diverse electrode materials, which represent a primary focus of supercapacitor technology [65].

The charge storage capability of conventional capacitors is limited by two factors: the low surface areas and the geometric constraints related to the distance of separation between the two charged plates. The high specific capacitance of EDLC is a consequence of the extensive surface area of the interface and the atomic-range separation of the positive and negative charges. Carbon-based materials, including activated carbons (ACs), carbon nanotubes (CNTs) and graphene, are the most extensively utilised electrodes for supercapacitors due to their favourable physical and chemical properties. The versatility of carbonaceous materials is further exemplified by their availability in a multitude of forms, including powders, aerogels, fibres, sheets, composites, tubes, and so forth,

which constitute a significant advantage for supercapacitor applications. Moreover, the advancement of supercapacitors necessitates precise regulation of the electrical conductivity, surface area, and pore size of electrode materials. The high electrical conductivity and large specific surface area of carbonaceous materials ensure low solution resistance and facilitate electrolyte diffusion. The specific surface area and pore size of ACs can be controlled by employing a variety of activation techniques. Additionally, CNTs are regarded as a highly effective EDLC material, attributed to their elevated electrical conductivity and distinctive porous structure, which facilitates rapid ion transportation. Graphene represents a novel class of two-dimensional (2D) materials, exhibiting the most promising characteristics among carbonaceous electrodes due to its exceptionally high surface area and electrical conductivity. [7]

To achieve high energy density, it is crucial to hybridize redox electro-active species with EDLC materials. Pseudocapacitive materials, such as metal oxides/hydroxides and conducting polymers, face limitations in specific surface area, electrical conductivity, and capacitance retention. Therefore, the main objective in developing supercapacitor electrodes is to increase energy density while preserving the high-power capability of the supercapacitor. Additionally, carbonaceous materials have been used as both positive and negative electrodes in asymmetric supercapacitor applications. The unique mechanical and electronic surface properties of carbonaceous materials have also been utilized in the creation of flexible supercapacitor devices. [7]

2.3.2Nanostructured Carbonaceous Materials

Carbon-based materials are frequently employed as active electrodes in supercapacitors due to their numerous advantageous properties, including low cost, long-term stability, and ready availability. Carbonaceous materials have attracted considerable attention due to their exceptional chemical performance and physical properties. The physical characteristics pertinent to electric double-layer capacitors (EDLC) are contingent upon the potential-dependent accumulation of interfacial electrostatic charge. Energy is stored at the interface between the electrode materials and the electrolyte as a consequence of the separation of positive and negative charges, which gives rise to the formation of a double layer. This mechanism entails both surface dissociation and ion adsorption from the electrolyte, in addition to the presence of crystal lattice defects. The capacitance formed due to the charge separation i.e. the EDLC can be expressed as $C = \frac{A\varepsilon}{4\pi d}$.

In this context, A represents the surface area of the electrode, ε denotes the dielectric constant of the electrolyte, and d signifies the thickness of the double layer. Nevertheless, the modification or improvement of the surface of EDLC materials with porous structures represents a primary area of focus for many researchers. An enlarged surface area can facilitate the formation of a charged

transport path. It is therefore important to pursue further improvements in the ion transport rate within carbon electrodes while ensuring that the charge storage performance remains unaffected. [7]

The adsorption of ions in an electric double-layer capacitor (EDLC) under the application of an electric field can be explained by the adsorption isotherm. The adsorption isotherm provides an explanation of the surface coverage of ions (at a constant temperature) as a function of concentration and applied voltage. However, in contrast to the behaviour observed in gas adsorption, the dependence of ion adsorption on temperature is relatively weak. The equilibrium concentration of ions is determined by the balance between the entropy and enthalpy changes within the system. Furthermore, the concentration of ions on the electrode surface serves to minimise the total Gibbs energy free energy of the system. The electrochemical behaviour of the electrode–electrolyte system is significantly influenced by the distribution of ions in terms of enthalpy. In the event of a broad distribution of enthalpy at the adsorption sites, a linear relation with applied voltage is observed across a wide range of concentrations. Nevertheless, the divergence of enthalpy (in regard to ion electrode interactions) from the mean value gives rise to a pronounced peak at a specific voltage, exhibiting pseudocapacitive characteristics rather than those associated with EDLC. [7]

A supercapacitor is composed of two electrodes, designated as positive and negative, respectively. The energy density (EEDLC) of the symmetric EDLC cell (**Figure 7a**) is dependent upon the capacitance of the positive (C^+) and negative (C^-) electrodes, as well as the maximum potential window (VEDLC). In order to achieve a high energy density for the EDLC, it is necessary to maximise both the volumetric capacitance and the maximum working potential. The maximum potential window is once more contingent upon the stability window for a selected electrolyte. In an ideal EDLC (**Figure 7b**), the stability window is defined as the difference between the lowest stable potential (VSL) and the highest stable potential (VSH). However, the stability window is also contingent upon the presence of defects, such as impurities and functional groups, on the surface of EDLC materials. Such defects have the potential to elevate the VSL and diminish the VSH, due to their capacity to catalyse electrolyte decomposition. The potential of the electrodes undergoes a linear change over time during the course of a galvanostatic charge-discharge (CD) process. In an ideal EDLC, both the negative and positive electrodes simultaneously reach the VSL and VSH [7]

In the case of ideal EDLC, $V_{EDLC} = V_{SH} - V_{SL}$, reaches to the maximumelectrolyte stability (Figure 7b). However, the approaching time of the negative and positive electrode to VSL and VSH are different for non-ideal cases (**Figure 7c**). One of the electrodes reaches the boundary value faster than the other electrode. On that condition, the maximum value of VEDLC will be lower than the

maximum value of $V_{Electrolyte}$. On the other hand, the presence of impurity or doping also changes the VEDLC. In this case, VEDLC can counterbalance the V Electrolyte (**Figure 7d**) [7]

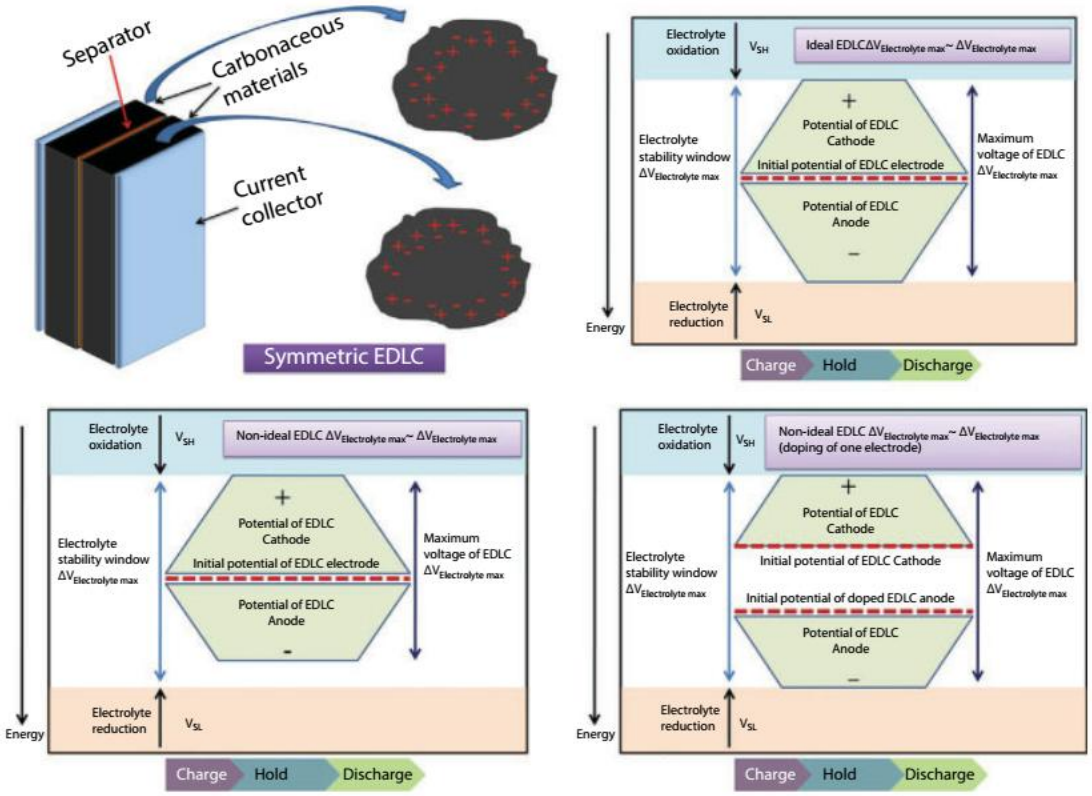

Figure 6 Schematic of (a) Construction of supercapacitor cell, Stability window of EDLC (b) ideal, (c) non-ideal and (d) in the presence of presence of impurity or doping [7].

2.3.2.1Activated carbons

There are numerous potential sources for the synthesis of ACs, including wood, corn grain, nutshells, natural fibres, leaves, coffee grounds, sugar cane, lignite, coal, pitch, and petroleum coke, among others. Furthermore, the majority of organic materials are rich in carbon and can be employed as the precursor for activated carbon. A highly porous activated carbon with reproducible properties was synthesised from a variety of synthetic polymers, including polyvinylidene chloride (PVDC), polyacrylonitrile (PAN), polyvinyl chloride (PVC), polyfurfuryl alcohol (PFA), polypyrrole (PPy), and polyaniline (PANI) [66].

In 2014, Zhi et al. [66] synthesised waste tyre-derived AC by pyrolysis and activation processes, with the activation being carried out using H_3PO_4. The pyrolysis of waste tyres in an N_2 atmosphere resulted in the production of char. Subsequently, a series of waste tire-derived ACs (WTAC1-WTAC16) were prepared using a variety of mass ratios (H_3PO_4/Char), activation temperatures, and activation times. The physical properties of the ACs, including specific surface area, total pore volume, mesopore volume, and micropore volume, are robustly influenced by the activation parameters. It was determined that the specific capacitance is predominantly influenced by the

micropore volume of the ACs, rather than the mesopore volume. Nevertheless, the rate capability was not found to be dependent on any single parameter, including micropore volume, total pore volume, and specific surface area. Instead, it is the ratio of mesopore to micropore volume that exerts the controlling influence. [66].

The advancement of efficient supercapacitors based on these characteristics is contingent upon the type of electrode material employed. Porous carbon possesses a number of advantageous electrical properties, including a high surface area, improved surface properties, good stability, a long cycle life, and excellent power output. As a result, they are the most preferred electrode material for EDLCs. A review of recent literature reveals that a number of nanocarbon materials, including graphene, carbon nanotubes and template carbons, have demonstrated exceptional capacitive behaviour. However, the utilisation of these materials in the production of supercapacitors is currently restricted. This is due to the fact that the mass production of these materials requires a complex and costly process. Biomass waste can be employed as a useful precursor in the preparation of porous carbon materials. Due to their low cost, abundance, and environmentally friendly nature. A substantial body of research has been conducted on supercapacitor electrodes developed from biomass-based porous carbons. [66].

Inal and Aktas [67] prepared a waste tea-based activated carbon by chemical activation using ZnCl2 as an activation agent and they found electrode-specific capacitance as 140 F/g at 0.1 A/g current density. In another study, nitrogen-doped porous carbon (NDC) was synthesized using a facile two-step process by using pea skin as a carbon precursor, and electrode-specific capacitance was found as a 141.1 F/g at 1.3 A/g current density [68].

Activated carbons derived from orange peels were synthesized through hydrolysis and chemical activation, utilizing potassium hydroxide, phosphoric acid, and zinc chloride as activators. Among them, the AC-H_3PO_4 electrode demonstrated the highest capacitance, achieving 240 F/g at 0.5 A/g. The electrochemical performance of these carbon materials as supercapacitor electrodes depends on the biomass type used and the specific production methods and conditions applied [68]

In this context, a supercapacitor cell was fabricated using the PP-H_3PO_4-Pd catalyst as the electrode material in a two-electrode system. In the study by [68], the PP-H_3PO_4-Pd catalyst was synthesised by treating PP with 5 M H_3PO_4 and a $PdCl_2$ solution. Furthermore, the catalytic activity of PP-H_3PO_4-Pd in methanolysis reactions was evaluated by examining the effects of varying burning temperatures and times. The performance of the catalyst, sodium borohydride ($NaBH_4$), was evaluated in order to ascertain its efficacy in the generation of hydrogen in the context of the methanolysis reaction. In experiments, the performance of the PP-H_3PO_4-Pd catalyst was tested at different $NaBH_4$ amounts, different catalyst amounts and different temperatures. Secondly, a supercapacitor cell was prepared

using PP-H_3PO_4-Pd catalyst as the electrode material by a two-electrode system. The capacity and resistance of the developed supercapacitor were analyzed by electrochemical characterizations. At the current density of 1 A/g, the gravimetric capacitance of the prepared electrode was found to be 84 F/g. This study has shown that a highly efficient PP-H_3PO_4-Pd catalyst developed from pomagranate peel for hydrogen generation can also be used as a supercapacitor electrode active material. Performance of this material is promising and needs further research to develop [68].

2.3.2.2 Graphene as Supercapacitor Electrode

The principal disadvantage of graphene as an electrode material is the tendency for the graphene sheets to agglomerate or restack. The restacking process has been observed to result in a notable reduction in the specific surface area and effective area, which in turn affects the formation of the double layer with electrolyte ions. The restacking process can be prevented by the introduction of foreign species, including different functional groups, metal oxide/hydroxide/sulfide nanoparticles. Furthermore, the charge storage mechanism is also affected by this kind of surface treatment. In addition to a purely electric double-layer capacitance (EDLC) charge storage mechanism, the functional groups may contribute to the capacitive properties through pseudocapacitance. Furthermore, doping of the pristine graphene represents an effective method of enhancing the surface area and overall charge storage capacity of the electrode materials. [7]

Surface modification is a widely employed technique for enhancing the efficacy of graphene or RGO in supercapacitor applications. Two distinct surface modification processes have been employed extensively by researchers in the field of supercapacitor applications. These are the two main categories of surface modification: Two principal categories of surface modification may be distinguished: (i) covalent modification and (ii) non-covalent modification.

The thickness of the electrode and the effective surface area of the functionalised rGO are of great consequence in determining the performance of the supercapacitor. In a study, a one-step co-deposition technique was employed to prepare a PPy/rGO film. The surface area and thickness of the deposited films are dependent on the applied charge density used for the polymerisation reaction. Additionally, the film thickness was found to be a determining factor in the optimisation of the surface area of the supercapacitor electrode. Moreover, following functionalisation, the incorporation of rGO serves to mitigate the swelling and shrinking of the Ppy components.[7]

The noncovalent functionalisation of graphene or rGO is characterised by the presence of weak interactions. Consequently, the basal structure of the graphene surface and its surface electronic properties remain unaltered. In general, the interaction between two non-polar aromatic rings with overlapping π orbitals serves as the foundation for non-covalent functionalisation. In a study

published in 2015, Jana and colleagues [69] described a single-step method for conducting the reduction, functionalisation and electrode preparation processes via an electrochemical process. The adsorption of sulfanilic acid azocromotrop on the surface of rGO is attributed to π–π interactions during anodic deposition. The high specific capacitance of 1090 F g-1 of the functionalised rGO is attributed to the pseudocapacitance contribution of the presence of -SO_3H functionalities.[69].

Another effective technique for modifying electrical conductivity and charge storage capacity of graphene is doping. In a notable contribution to the field, Han et al. [70] reported the large-scale production of B-doped rGO by one-pot synthesis (BH_3)-tetrahydrofuran (THF adduct under reflux). The introduction of boron atoms into the graphene structure resulted in a modification of the electronic properties, which in turn led to an improvement in the supercapacitor performance. The B-doped graphene exhibited enhanced accessibility to electrolyte ions, even in the presence of agglomeration. The electrolyte ions were observed to diffuse through the interstices of the agglomerated B-doped rGO. Furthermore, the interstitial network resulted in a less tortuous diffusion path in comparison to conventional high-surface-area porous electrodes. Consequently, the B-doped rGO exhibited a high specific capacitance (200 F/g) and stability.[70].

2.3.2.3Carbon Nanotube (CNT) Supercapacitor

A number of physical techniques may be employed for the synthesis of CNTs, including arc-discharge, laser vaporisation, and chemical vapor deposition (CVD). To date, there have been no reports of chemical synthesis of CNTs. CNTs were utilised as supercapacitor electrodes due to their distinctive surface electronic properties and structure [71].

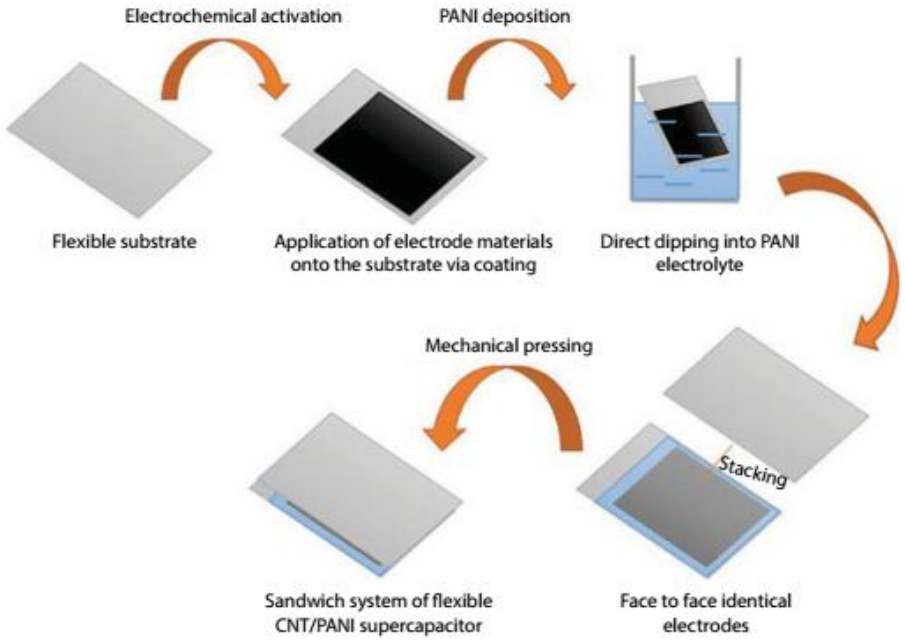

Figure 7 Schematic representation of the general strategy for the preparation of flexible CNT electrode [7]

2.3.3 Nanostructured Carbon-Based Supercapacitor Device

The fabrication of a supercapacitor device or cell entails the combination of two electrodes and a separator. Furthermore, a current collector and an outer insulation envelope are employed for packaging purposes. In accordance with the charge storage mechanism, two principal categories of supercapacitor cells have been identified: (1) symmetric (SC) and (2) asymmetric supercapacitor (ASC) [7]

In SC, identical electrodes are used as both cathode and anode, resulting in an almost similar working potential of the SC device to that of the individual electrode (tested in a three-electrode configuration). On occasion, it was observed that the operational potential of the device was less than that of the potential window of the individual electrode. The reduction in working potential observed during device formation can be attributed to the IR drop of the individual electrode. Subsequently, an ASC configuration was implemented with the objective of enhancing the device's energy density. The energy density of the device is contingent upon the working potential (V). [7]

In an ASC configuration, two distinct electrodes, each with a different potential window, are employed as the cathode and anode, respectively, within a three-electrode setup. Consequently, the ASC device exhibits a superior working potential in comparison to the symmetric supercapacitor. **Figure 9** illustrates the schematic representation of the working principle of the ASC. Another advantage of the ASC is that it is able to utilise the benefits of both the EDLC and the redox mechanism [7]

In general, an EDLC electrode is used as either a cathode or an anode, with the other side being a redox electrode. Carbonaceous materials, including AC, rGO, and CNT, are employed in SC devices in either composite or pure forms. However, in the ASC, these materials serve a dual role, functioning both as a positive electrode and a negative electrode. In general, redox materials are employed as the positive electrode, while EDLC materials are used as the negative electrode [7].

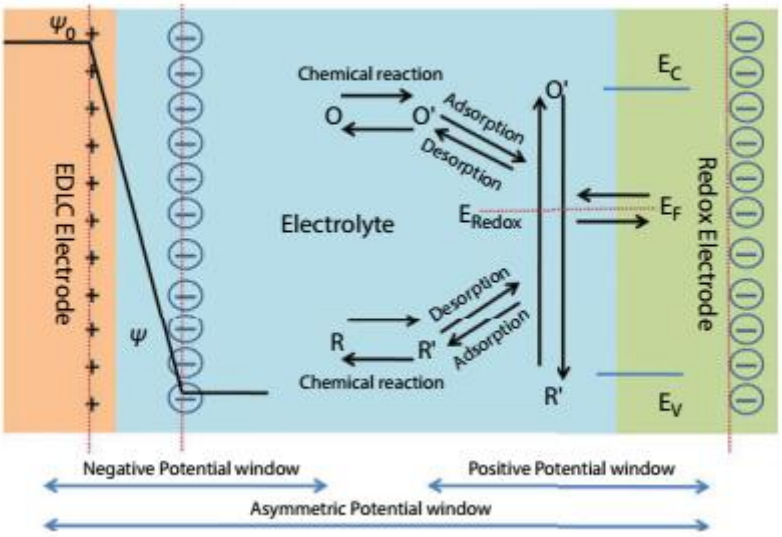

Figure 8 Schematic representation of the working principle of asymmetric supercapacitor [7].

TRGO can be employed as a negative electrode to counterbalance the iron oxide/nickel oxide positive electrode (redox). Iron oxide/nickel oxide composite exhibits high specific capacitance of ~1123 F/g in the potential range of -0.2 to 0.7V. While the fabricated ASC shows higher working potential of ~1.6 V. Te ASC is able to deliver energy and power density of 91 $Whkg^{-1}$ and 7200 W kg^{-1}, respectively. Further, the ASC shows a low relaxation time constant of ~1.3 ms along with long stability (83% after 10,000 CD cycles due to the facile EDLC of negative electrode material [72].

A variety of nano-structured carbon materials, including AC, rGO and CNT, were employed in the development of a supercapacitor electrode. The carbonaceous electrode exhibits electric double-layer capacitance (EDLC) characteristics, enabling rapid charge and discharge as well as high power density. Conversely, doping and surface modification of the carbonaceous materials were conducted with the objective of achieving high specific capacitance or large energy density. The surface electronic properties of the carbonaceous materials were modified through the use of covalent and non-covalent functionalisation techniques. Moreover, it was discovered that the band gap energy of carbonaceous materials can be regulated through doping [7].

2.4 Electrochemical sensors

A chemical sensor, as defined by IUPAC, is a device that converts chemical data, from single component concentration to complete composition analysis, into a usable analytical signal. Typically, a chemical sensor consists of two key components: a receptor and a physicochemical transducer [73]. Receptors can vary from activated or doped surfaces to complex (macro)molecules that interact specifically with the analyte. When the receptor is of biological origin, such as DNA, antibodies, or enzymes, the device is termed a biosensor. The receptor's role is to interact with the analyte and convert this recognition event into a specific output signal. Sensors must maintain high specificity for the target analyte to avoid false positives from interfering substances [74] [75].

Another essential component of sensors is the transducer, which converts the signal produced by the receptor-analyte interaction into a readable value [76]. As a result, both chemical and biosensors are categorized as either catalytic or affinity-based devices. Catalytic sensors generate the signal through catalytic activity, such as enzymatic, DNAzyme, or functionalized surfaces capable of redox reactions under specific conditions. Affinity-based devices, on the other hand, depend on highly specific interactions between the receptor and analyte, utilizing the affinity of nucleic acids (e.g., ssDNA and aptamers), antibodies-antigens, or host-guest interactions. The monitoring of these recognition events can be carried out using various methods, such as optical, gravimetric, or electrochemical techniques, depending on the type of transducer employed [77].

Electrochemical sensors, the market leaders, are the most widely used type of sensor due to their advantages such as low detection limits (down to picomoles), rapid response and low-cost instrumentation. They are available in a variety of form factors, from benchtop to fully integrated portable devices. Their primary function is to provide accurate, real-time information about the chemical composition of their surroundings. Ideally, such sensors should respond continuously and reversibly, without interfering with the sample [78]. In these devices, a biological or chemical identification layer is applied to a transduction element. The analytical information in electrochemical sensors is derived from the electrical signal generated by the interaction between the target analyte and the recognition layer [79]. Electrochemical devices for environmental monitoring vary according to the nature of the analyte, the character of the sample matrix and the required sensitivity or selectivity [80] [81] [82]. These devices mainly include amperometric and potentiometric sensors, with amperometric sensors detecting electroactive species involved in chemical or biological identification [83] [84].

Electrochemical sensors can be categorized into several types, including amperometric, potentiometric, impedimetric, photoelectrochemical, and electrogenerated chemiluminescence [85]. Potentiometric sensors establish a local Nernstian equilibrium at the sensor interface due to specific sensor-analyte interactions, providing information about the analyte's concentration when no current flows through the system. Amperometric sensors, on the other hand, apply a voltage between reference and working electrodes to trigger electrochemical oxidation or reduction and measure the resulting current as a quantitative indicator of the analyte's concentration [86].

Chapter 3

Hydrogen production and impacts on climate change

3.1 Hydrogen Production

H_2 production is crucial for achieving a sustainable low-carbon future, and it requires the implementation of advanced methods and technologies [87]. **Figure 10** illustrates the various H_2 production methods.

Figure 9 Illustration of various routes for H_2 production [88]

3.1.1. Thermochemical Routes

Thermal processes generate H_2 using energy from a variety of sources, including coal, natural gas, and biomass. As an alternative, the heat generated by closed chemical cycles aids in the production of H_2 from the feedstock, H_2O. H_2 has been produced by thermochemical methods like solar

thermochemical H_2 (STCH), natural gas reforming (steam CH_4 reforming; SMR), biomass gasification, and biomass-derived liquid reforming. In the industrial sector, up to 74% of H_2 was produced using the SMR process [89].

Biomass gasification has drawn a lot of interest as a method of producing energy in recent years. Biomass materials, like wood chips or agricultural waste, are transformed into syngas ($CO + H_2$), a flammable gas mixture, in this process. Syngas is utilized as fuel for various industrial operations, including the production of electricity. When compared to energy production based on fossil fuels, biomass gasification dramatically lowers greenhouse gas (GHG) emissions [90].

It has been suggested that biomass gasification can improve H_2 production by (i) reducing tar/car formations with KCl as a catalyst, (ii) adjusting the temperature to improve the composition of syngas, and (iii) increasing H_2 efficiency by up to 80% by utilizing calcium oxide to capture CO_2. Using pinewood sawdust and polyethylene co-gasification, the thermally decomposed spent $LiNixCoyMn1\text{-}x\text{-}yO_2$ batteries-derived novel Ni/Co/Mn-loaded mesoporous Al_2O_3 catalyst demonstrated significantly higher H_2 productivity 151 percent from a temperature of 600 to 800 ◦C compared to control catalysts (17.2 mmol/g) in order to achieve the zero-waste strategy [89].

Furthermore, the efficiency and feasibility of biomass gasification could be further increased by creating cutting-edge gasification technologies and combining it with other renewable energy sources like solar or wind power. By turning organic waste into useful energy, biomass gasification can also be utilized for waste management. Moreover, negative emissions could arise from combining carbon capture and storage technologies with biomass gasification. Because of this, gasification can be a helpful strategy in the fight against climate change. A feasible levelized cost of electricity of $0.16/kWh and an energy efficiency of 64.5 percent were attained by the integrated systems of biomass gasification, solar collection, SOEC, steam power, gas turbines, and multi-source heat and power [91].

Through a reforming process, H_2 could be produced from the liquids derived from biomass, such as ethanol, bio-oils, and other liquid biofuels. These liquids are easier to move over long distances for H_2 production and distribution at fueling stations than biomass. This is a three-step process: (i) reformate gas (H_2, CO, and CO_2) is produced when liquid fuels and steam react at high temperatures with catalysts; (ii) an H_2O–gas shift reaction produces additional H_2 and CO_2 from the reaction of CO and steam at high temperatures; and (iii) H_2 separation and purification [92].

At 800 ◦C, steam reforming biomass-derived levulinic acid with $15Ni/NiAl_2O_4$ catalysts demonstrated high concentrations of 67.9, 92.8, and 96.3 percent, respectively, as well as high carbon conversion and H_2 yield. Because large-scale biomass-based liquids can be produced at facilities close to the sources (biomass feedstocks), this process is a mid-term technology. It is also cost-effective because it lowers

the cost of transporting H_2 to reforming sites. A few significant obstacles to this process are the problematic reforming of larger molecules (liquid fuels have more carbon atoms than natural gas (CH_4)) and the requirement for effective catalysts to improve yield and selectivity. Furthermore, more research is required to determine how to lower the expenses of biomass-based liquids, machinery, operation, and maintenance while improving overall process efficiency [88]

Synthetic gas is produced by natural gas reforming gasification. Methanol, ammonia, and H_2 are frequently produced using this method. Based on liquified cold natural gas, the steam CH_4 reforming H_2 liquefaction and waste heat recovery system demonstrated specific energy consumption, coefficient of performance, and exergy efficiency of 5.93 kWh/kg of liquid H_2, 0.22 percent, and 53.24 percent, respectively, under ideal conditions to produce 10 tons of liquid H_2/day [88]

The feasibility of hydrogen production from ethanol steam reforming has been theoretically established. Additionally, recent experimental studies have focused on catalytic processes, examining the decomposition of ethanol into COx and H2 over noble and metal oxide catalysts supported on Al_2O_3, SiO_2, TiO_2, and MgO. Rh/Al_2O_3 catalysts produced hydrogen-rich gas mixtures free from ethylene and other undesirable products, making them suitable for molten carbonate fuel cell applications. Under steam reforming conditions, extensive encapsulated carbon formation was observed, while adding oxygen improved catalyst stability and reduced coke formation. Ethanol dehydrogenation produces acetaldehyde, which decarbonylates into CH_4 and CO, while ethylene undergoes fast steam reforming to C1 [93].

Cu/Ni/K/γ-Al2O3 catalysts at 300 °C and atmospheric pressure demonstrated acceptable activity, stability, and hydrogen selectivity. Copper acts as an active agent, nickel promotes C-C bond rupture, and potassium neutralizes acidic sites, enhancing catalyst performance. Ni catalysts supported on La_2O_3, Al2O3, YSZ, and MgO showed high activity and long-term stability for hydrogen production. Among supported noble metal catalysts (Rh, Ru, Pt, Pd), Rh exhibited the highest activity and selectivity for hydrogen formation, especially in low-loaded catalysts. Catalysts with cobalt particles significantly improved performance in ethanol steam reforming. Carbon deposits' extent and ordering depend on the material and reaction temperature [93].

A study on biomass-derived ethanol steam reforming over a commercial alumina-supported palladium catalyst investigated the effects of reaction temperature, H_2O/EtOH molar ratio, and contact time on catalytic activity and selectivity. Hydrogen selectivity was proportional to the H2O/EtOH molar ratio, with complete ethanol conversion even at low temperatures. Hydrogen selectivities up to 95% were achieved near 650 °C. Carbon monoxide concentration exhibited a minimum around 450 °C due to thermodynamic reasons. Carbon formation was negligible at stoichiometric H_2O/EtOH ratios but increased below stoichiometric ratios, leading to catalyst deactivation [93].

High energy consumption, the requirement for catalysts, and controlling CO_2 emissions are some of the difficulties with the natural gas reforming gasification process. Notwithstanding these obstacles, gasification of natural gas reforming has a bright future. Natural gas reforming gasification has become a potentially essential method of lowering carbon emissions and making the switch to clean energy due to technological advancements and a greater emphasis on sustainable energy solutions. Its sustainability and contribution to the creation of a circular economy would be further improved by incorporating carbon sequestration plans and utilizing renewable energy sources. [88]

Natural gas reforming is a sophisticated and established production method that expands on the infrastructure already in place for natural gas pipeline delivery. Natural gas reforming in large central plants produces about 95% of the H_2 produced in the United States, making it a crucial technological pathway for near-term H_2 production. In a study, researchers assessed SMR, surface coal gasification, and underground coal gasification with and without carbon capture as frameworks for estimating the cost of producing H_2. When new production tax credits are taken into account, the H_2 produced by SMR with 99 percent carbon capture is profitable. The costs of producing H_2 from natural gas using steam CH_4 reforming, autothermal reforming, and pyrolysis, with and without carbon capture, utilization, and sequestration, ranged from 1.48 to 2.55 and 1.22 to 2.12$/kg of H_2, respectively, with a H_2-footprint of 1.84 to 11.4 kg of CO_2/kg of H_2 and a production of 0.22 to 0.35 kg of H_2/kg of fuel [88]

Solar thermochemical processes split H_2O and produce H_2 by using concentrated solar energy to create high temperatures for thermochemical reactions. When compared to the thermochemical process (115 mmol/h/g), the solar-thermochemical process was found to increase H_2 production by 30 to 8% at 600 ˚C. In order to reach the target of $2/kg H_2 production, the Department of Energy Office of Energy Efficiency and Renewable Energy (EERE, USA) launched the STCH project in 2003. The utilization of renewable solar energy and the possibility of producing H_2 on a large scale are two benefits of this approach. [88]

However, there are obstacles to overcome in the development and application of solar thermochemical H_2 processes, including finding appropriate, effective, and long-lasting reactor materials, enhancing conversion efficiency and reaction kinetics, and creating affordable systems that can be expanded for industrial production. Moreover, there are logistical difficulties in incorporating solar thermochemical H_2 processes into current energy infrastructures and systems. The solar thermochemical H_2 process has enormous potential for a sustainable clean energy future in spite of these obstacles. Therefore, by utilizing concentrated solar energy, the solar thermochemical process provides a feasible route for producing H_2 on a large scale. The efficiency,

robustness, and scalability of this technology may be enhanced if the difficulties related to solar thermochemical H_2 processes are resolved through continued research and development [87].

All things considered, thermochemical H_2 production methods are a proven and developed technology, but they still have drawbacks in that they use non-renewable resources and produce greenhouse gases. Furthermore, to achieve high H_2 production efficiency and a better environmental footprint, these systems can be advanced by integrating carbon capture and storage technologies and using renewable feedstock. The following reactions are involved in the thermochemical reforming process that produces H_2. (Equations (5)– (9)) [88]:

Steam-CH_4 reforming: $CH_4 + H_2O + \text{heat} \rightarrow 3H_2 + CO$ (5)

H_2O-gas shift: $CO + H_2O \rightarrow H_2 + CO_2 + \text{heat}$ (6)

CH_4 partial oxidation: $CH_4 + ½O_2 \rightarrow 2H_2 + CO + \text{heat}$ (7)

Ethanol steam reforming: $C_2H_5OH + H_2O + \text{heat} \rightarrow 4H_2 + 2CO$ (8)

Biomass gasification: $C_6H_{12}O_6 + O_2 + H_2O \rightarrow H_2 + CO + CO_2 + \text{others}$ (9)

3.1.2. Electrolytic Routes

Due to its potential as a sustainable and clean energy source, electrolytic H_2 production has attracted a lot of attention lately. One method of producing H_2 without releasing greenhouse gases is electrolysis, which uses electricity to split H_2O into H_2 and O_2. As a result, this approach may help lower carbon emissions and solve the worldwide issues surrounding sustainable clean energy. Additionally, electrolysis offers flexibility to use a variety of electricity sources, including renewable energy sources like wind and solar power. The resulting green H_2 can be utilized in a number of fields, such as industry, power generation, and transportation [88].

Electrolysis systems like alkaline, PEM, SOEC, anion exchange membrane (AEM), bipolar membrane, and microbial electrolysis cells (MECs) are examples of electrochemical H_2 production processes. In an electrolyzer system made up of anode and cathode electrodes separated by an electrolyte, H_2O electrolysis—a critical process in electrochemical H_2 generation technologies—involves electric current flowing through H_2O to convert it into H_2 and O_2. O_2 and protons (H^+) in the PEM, OH^- in alkaline, or O_2^- in SOEC processes are the products of the anode's oxidation of the H_2O. These generated ions are reduced to H_2 gas as they move through the electrolyte to the cathode [88].

Electrochemical water splitting, which includes the cathodic hydrogen evolution reaction (HER) and anodic oxygen evolution reaction (OER), is an effective method to produce high-purity hydrogen [94][95][96]. Currently, the leading HER and OER electrocatalysts are made from Pt and

Ir/Ru based materials. However, their high cost and limited availability hinder large-scale application. Consequently, there is a critical need for developing low-cost and highly active alternatives to noble metals. In recent years, various cost-effective and efficient bifunctional electrocatalysts (e.g CoP@CoOOH/CP), such as transition-metal carbides or borides as Mo_2NiB_2, sulfides, phosphides (cobalt phosphides), nitrides, and oxides, have been developed for overall water splitting [97][98][99][100]. Most of these bifunctional electrocatalysts perform well in acidic or alkaline media, which pose environmental and corrosion issues. Conversely, electrolyzers operating in neutral or near-neutral pH electrolytes can use ocean, lake, or river water directly without expensive membranes or separators, being environmentally friendly and cost-effective. However, catalysts that efficiently catalyze both HER and OER at low overpotentials in neutral or near-neutral pH electrolytes are rare. Initial efforts to enhance water splitting kinetics in neutral or near-neutral pH using bifunctional catalysts are still in early stages. High cell voltage remains a challenge for water electrolysis under neutral conditions due to high OER overpotential [101].

Semiconducting materials are highly regarded as excellent electrocatalysts for electrochemical water splitting, but there remains a gap in the design and understanding of semiconducting composite electrodes. A successfully developed monolithic electrode consisting of etched copper foam and a p-n heterojunction (with a p-type Cu_2O layer and n-type TiO_2 nanodots exhibiting excellent hydrophilicity). This design reduces electron transfer resistance, optimizes water and hydrogen adsorption on the catalyst surface, and creates a space-charge region at the phase interface, enhancing the local electron density of Cu2O. These effects were confirmed through experimental results and density functional theory (DFT). Due to the accelerated Volmer-Heyrovsky pathway, the heterojunction electrode demonstrated low onset potential (18 mV), high electrocatalytic activity (114 mV at 10 mA cm^{-2}), and long-term stability for the hydrogen evolution reaction in alkaline media, comparable to platinum, enabling large-scale fabrication [102].

In another stuy, a three-dimensional metal network electrocatalyst featuring a worm-like sulfur-doped RhNi alloy (S-RhNi) has been developed to enhance hydrogen evolution reaction (HER) performance. Experimental results show that S-RhNi demonstrates Pt-like HER activity, with an onset potential near 0 mV and a Tafel slope of 24.61 mV dec−1 in a 0.5 M H2SO4 aqueous solution. Additionally, it exhibits good stability [103].

Recently, transition metal phosphides (TMPs) have been extensively studied as effective bifunctional catalysts for water splitting in basic solutions because of their natural abundance, simple synthesis, and excellent catalytic activity. However, TMPs are seldom reported as bifunctional electrocatalysts for neutral-pH water splitting, primarily due to their inherently low electronic conductivity. Essentially, the activity and conductivity of TMPs are determined by their

electronic structure. Various strategies have been developed to enhance electron transport and catalytic performance, with doping engineering shown to effectively regulate the catalyst's electronic structure, thereby significantly increasing catalytic activity [101]. Platinum-based materials are known to be the most efficient catalysts for hydrogen evolution in acidic electrolytes; however, their high cost and rarity limit widespread use [104][105]**.** Although only a few noble metal-based catalysts have surpassed the HER activity of commercial Pt/C catalysts in acidic electrolytes, the search for highly active and stable catalysts continues. As a result, earth-abundant non-Pt catalysts, such as those based on Fe, Co, Ni, Cu, Mo, and W, have been widely explored. Nevertheless, their catalytic performance still falls short compared to Pt, making the development of effective HER catalysts challenging [106].

Hydrogen evolution is known to proceed via a pathway similar to that of hydrogenation processes, where the reversible adsorption/desorption of hydrogen on the catalyst is critical for fast kinetics. Recent research by Pu et al. demonstrated that a hydrogenation catalyst, RuP2, exhibited remarkable HER performance. Rhodium (Rh) has also been reported to possess excellent properties, including chemical inertness towards mineral acids and good catalytic activity for hydrogenation reactions and ethanol oxidation. Although many non-noble metal-based materials have shown better catalytic activity than Rh/C catalysts, Rh-based materials still hold promise as candidates for HER [106].

Studies have shown that introducing heteroatom elements, such as nitrogen, phosphorus, and boron, can improve HER catalytic activity by regulating the electronic structure of carbon skeletons. Recent reports have confirmed that boron-containing materials can enhance catalytic activity for hydrogen evolution. For example, Zhang et al. found that Co@BCN material for HER displayed improved performance due to the neighboring of boron with carbon atoms [101].

A study reports a one-pot synthesis method for B-doped RhFe alloys with enhanced catalytic performance for hydrogen evolution. The as-prepared material is stable in acidic conditions and exhibits good HER activity in 0.5 M H_2SO_4 electrolyte. Samples with different Rh to Fe ratios were synthesized and reduced at various temperatures, with physicochemical and electrochemical characterizations thoroughly discussed. The results indicate that the B-doped RhFe alloy catalysts possess high catalytic activity and stability for hydrogen evolution, outperforming some of the best proposed materials [106].

3.1.2.1Alkaline Electrolyzers

Pure water is first transformed into a highly concentrated aqueous solution of an alkaline electrolyte (usually KOH or, less frequently, NaOH) in alkaline electrolyzers. Equation (10) states that

hydrogen evolves from the cathode under a direct current, while Equation (11) states that hydroxide anions migrate across the separator (or diaphragm) to the anode, where they recombine to oxygen and water [107]

$$4H^+ + 4e^- \rightarrow 2H_2 \text{ (cathode)} \quad (10)$$

$$4OH^- \rightarrow O_2 + 2H_2O + 4e \text{ (anode)} \quad (11)$$

While the cathode is composed of steel with a catalyst coating activating its surface, the anode is typically composed of nickel or nickel-coated steel. In this configuration, the separator is essential since it needs to be both impermeable to gases and permeable to water ions. Previously, the separator was usually composed of a thick layer of asbestos, but the health risks and technical limitations (the operating temperature was only 80 °C) have led to research into safer and more effective substitutes, like ion exchange inorganic membranes. High pressure electrolyzers typically operate between 6 and 30 bar, though higher pressures have been shown at the laboratory scale. In contrast, atmospheric alkaline electrolyzers can produce hydrogen with a pressure between 1 and 6 bar. By passing the postproduction compression step, high pressure electrolyzers avoid the related expenses and EIs. The combined effect of high temperature and high pressure, however, has the disadvantage of compromising the separator's gas impermeability, which results in hydrogen with reduced purity [107].

The investment cost of alkaline electrolysis, a well-established and reasonably priced technology, is almost directly proportional to the installed capacity and, eventually, to the electrolyzer's total surface area. Alkaline electrolysis is therefore the most widely used commercial hydrogen production technology globally [107].

3.1.2.2. Polymer Electrolyte Membrane (PEM) Electrolyzers

Other names for polymer electrolyte membrane (PEM) electrolysis include "solid polymer electrolyte" (SPE) electrolysis and "proton exchange membrane" (PEM, as previously mentioned). PEM electrolyzers operate at temperatures between 50 and 100 °C, just like alkaline electrolyzers. However, rather than using a liquid electrolyte, PEM electrolyzers use a polymer electrolyte membrane. Equation (12) shows that water is oxidized at the anode, generating protons (H^+), electrons, and oxygen (gas). Equation (13) states that protons travel through the membrane to the cathode, where they are reduced, completing the circuit and producing hydrogen (gas) [107]

$$2H_2O \rightarrow O_2 + 4H^+ + 4e^- \text{ (anode)} \quad (12)$$

$$4H^+ + 4e^- \rightarrow 2H_2 \text{ (cathode)} \quad (13)$$

The term "membrane electrode assembly" (MEA) refers to the unit that consists of the anode, cathode, and membrane. Here, a very thin gas-tight polymer membrane, like Nafion (thickness: around 0.2 mm), takes the place of the thick separator typical of alkaline electrolyzers (thickness: around 5 mm). Noble metals like iridium and platinum are thickly coated on the electrodes. Even in the absence of any additional purification equipment, the hydrogen purity is usually very high, surpassing 99 to 99 vol percent. The ability of PEM electrolyzers to function with a variable power source is an additional benefit. This occurs because proton circulation in PEM electrolyzers quickly adjusts to power fluctuations, in contrast to ionic transportation in alkaline electrolyzers [107].

Compared to alkaline electrolyzers, PEM electrolyzers have a higher power density. However, they are only commercially available for production on a small scale. Furthermore, significant investment capital is still required for proton membranes and noble metal electrodes. A PEM electrolyzer and a PEM fuel cell, an electrochemical device that transforms hydrogen's chemical energy, back into electrical energy, are combined in an emerging technology. The large-scale version of this technology, known as the discrete regenerative fuel cell (DRFC), uses an electrolysis device to generate and store hydrogen, and an integrated fuel cell to return power from hydrogen when needed. This allows the DRFC to store excess energy that is intermittently produced by fluctuating renewable sources, such as wind and solar radiation. Additional benefits of this technology's small-scale variant, referred to as the unitized regenerative proton exchange membrane fuel cell (UR-PEMFC) or unitized regenerative fuel cell (URFC), include simpler architecture and a lower initial cost [108].

3.1.2.3. Solid Oxide Electrolyzers

A new technology called solid oxide electrolyzers, or SOEs for short, allows water, or more precisely, steam, to be electrolyzed at temperatures as high as 1000 °C. In theory, heat can provide around 40% of the energy needed for steam electrolysis, and compared to PEM and alkaline electrolysis, the amount of electricity needed can be significantly decreased. When a high-temperature heat source is available, such as with nuclear reactors or geothermal energy spots, this method is especially practical. According to Equation (14), steam is fed to the cathode in SOEs, where water molecules are reduced to produce hydrogen (gas). Recycled oxygen can be added to steam. Equation (15) states that the oxide anions generated at the cathode travel to the anode via the solid electrolyte, where they react to form oxygen (gas) and close the circuit. [107]

$$2H_2O + 4e^- \rightarrow 2H_2 + 2O_2^- \text{ (cathode)} \quad (14)$$

$$2O_2^- \rightarrow O_2 + 4e^- \text{ (anode)} \quad (15)$$

Cermet is the cathode (i.e. e. ceramic-metal composite) composed of yttrium-stabilized zirconia (YSZ) and nickel, with perovskite serving as the anode and YSZ serving as the solid electrolyte. Low EIs, particularly GHG emissions, are facilitated by SOEs' high efficiency in producing hydrogen while using comparatively little electricity. Nevertheless, because load variations lead to temperature swings that are likely to result in membrane cracking, SOEs are vulnerable to rapid degradation. The shortened lifespan of SOEs is impeding their broader commercial adoption [107]

The development of electrochemical technologies leads to the development of AEM, MECs, and bipolar membrane electrolysis. The benefits of alkaline electrolysis, which conducts OH- as the electrolyte, and PEM are combined in the AEM system. AEM is less expensive than PEM because it employs non-precious metal catalysts at lower temperatures. Using a Co/P dual-doped bifunctional catalyst (Co/PFe_3O_4@IF), AEM-based alkaline seawater electrolysis produced H_2/m^3 with a low energy expenditure of 4.38 KWh and a high current density of 500 mA/Al_2O_3 at 1.83 V without a chloride oxidation reaction. With a range of 95–97 percent retention rate and 80–800 mA/Al_2O_3 current density, the low-cost bifunctional nickel copper phosphide-nickel electrocatalyst demonstrated exceptional operational durability over 300 hours at 2 V and a performance of 30 mA/Al_2O_3 as a non-platinum group metal [88].

The MEC system uses organic feedstocks and electroactive microbes to produce H_2. According to its mechanism, microbes oxidize organic substrates to produce H+ and electrons at the anode, which then move via an ion exchange membrane and an external circuit to the cathode to form H_2. By enhancing the proton transport of membranes, MECs based on polyvinylidene fluoride membranes coated with polydopamine, polyethyleneimine, and silver nanoparticles have antifouling qualities and produce a high H_2 production rate of 2.65 $m^3/m^3/d$ [88].

Compared to raw food wastewater, MECs based on pre-fermentation effluents demonstrated a 34.4% higher H_2-producing potential of 911 mL/g of chemical O_2 demands (COD). In this case, a two-fold increase in Geobacter abundance at the anode in comparison to the control feed was linked to high H_2 production. There are several advantages to these electrochemical processes: (i) they produce high-purity H_2 that can be used directly in fuel cells; (ii) excess electricity from renewable sources, like solar and wind, can be converted to H_2; (iii) they can be scaled up based on the various applications; and (iv) they evolve H_2 without emitting greenhouse gases. To increase the yield of H_2 production, pilot-scale demonstration, and economy, electrochemical technologies are still being developed at different levels [88].

Easy H_2O dissociation and effective H_2 evolution are made possible by the bipolar junction of the composite membrane (anion/cation exchange layers) used in electrolysis in bipolar membranes. The bipolar membrane crosslinked with new bipyridine covalent triazine frameworks showed a

maximum current density of 1.29 A/Al_2O_3 at 2.5 V, with maximum ionic conductivity of 143 and 48.0 mS/cm for H^+ and OH-after dropping in H_2SO_4/NaOH at 80 ◦C. In order to split seawater into H_2 and O_2, the bipolar membrane, which is made up of cation and anion exchange layers integrated into a bipolar membrane H_2O electrolyzer, demonstrated current densities of 250 mA/°C. In contrast to PEM H_2O electrolyzers with acidic pH, which caused the PEM system to fail in seawater, it provides basic pH at the anode, which inhibits the generation of corrosive-free chloride. Although the electrochemical routes generally produce clean H_2, there is still room for improvement on a number of levels in terms of the system's cost-effectiveness and H_2 production efficiency. Research and development in these technologies, like PME and alkaline electrolysis, are ongoing and are thought to be the best ways to achieve sustainable and affordable results [88].

The electrolytic method of producing H_2 has a number of benefits, including the potential for low greenhouse gas emissions (since it is powered by renewable energy sources), the ease of scaling up to meet the increasing demand for H_2 across different industries, and the potential for energy storage by producing more H_2 with the excess electricity, which can then be stored and used later when energy demand is high or renewable energy sources are unavailable. However, in order to make the shift to a non-carbon-based economy, it is necessary to investigate recent advancements in H_2 production through the electrolytic route and comprehend the opportunities and challenges that come with them. Some noteworthy developments to date include: i) improvements in the fabrication of electrocatalytic materials, which lead to increased cost-effectiveness and efficiency; and ii) the creation of new synthesis techniques, which make it possible to produce innovative anodic and cathodic materials that are essential for H_2 electro generation [109].

3.1.3. Direct Solar Water-Splitting Routes

Light serves as the energy source for the photoelectrochemical (PEC) and photobiological processes that split H_2O into H_2 and O_2. Many of these processes are still in the early stages of research, but they currently hold long-term promises for sustainable H_2 generation with negligible environmental effects. PEC splits H_2O to produce H_2 using sunlight and specialized semiconductors called photoelectrochemical materials. Although PEC semiconductor materials are dipped in H_2O-based electrolytes (sunlight energizes the H_2O-splitting), they are similar to photovoltaic systems (solar electricity generation). A developed photoanode called WO_3/$BiVO_4$/Ni-PbS demonstrated a high current of 5–56 mA/Al_2O_3 in phosphate buffer saline and 0–5 M of Na_2SO_3 at an external potential of 1–23 V, along with 52–2 μmol of H_2/Al_2O_3 and the simultaneous removal of 99–9% of total organic carbon in the textile wastewater-integrated PEC system. In a different study, a vacancy-controlled MoSSe/MnSe heterostructure showed enhanced H_2 evolution reaction and high PEC activity of -7.15 mA/Al_2O_3 at 0V [88].

A study showed how the operating pressure affects the concentration overpotential, product gas crossover, bubble-induced optical losses, and bubble characteristics—all of which are critical for PEC H_2O-splitting. Additionally, the pressure range can be 6–8 bar to minimize losses and achieve effective PEC water-splitting. A high solar-to-H_2 efficiency of 12–5% was demonstrated by the dual spin-controlled chiral two-/three-dimensional perovskite-based PEC H_2O-splitting system. The R-TAP-Pd(II)@gC_3N_4 PEC system, a polymer carbon nitride (g-C_3N_4)-based photocatalyst, demonstrated a maximum H_2 generation rate of 1085 μmol/g/h in visible light, which was 278 times more advantageous than the control catalyst, g-C3N . Although PEC material cost, efficiency, and durability need to be improved to meet the desired market viability, PEC is a promising process that offers high conversion efficiency at low operating temperatures via particle semiconductor materials or cost-effective thin films in relation to the solar-to-H_2 pathway. The goals of ongoing research and development in this field are (i) efficiency and (ii) cost management of H_2 production through lower processing and material prices [88].

In photobiological processes, microorganisms like green microalgae and cyanobacteria split water into O_2 and H_2 ions when exposed to sunlight, converting water (and occasionally organic matter) into H_2. H_2 molecules are then created by the direct or indirect combination of the produced H_2 ions. In a bioreactor with a cathode and anode divided by an ion exchange membrane, bioelectrochemical systems (BES) generate H_2 using wastewater or biomass organic materials as substrates and electroactive microbes. By oxidizing substrates at the anode, the microbes produce electrons and H^+, which move towards the cathode via an ion exchange membrane and an external circuit, respectively, to form H_2 [110].

Extracellular electron transfer can contribute up to 76–3% of H_2 production in BES, while it only accounts for 18–7% in electric field-based systems, according to a comparison of bioelectrochemically and electric field-driven assisted dark fermentation reactors. Using industrial wastewater and non-limiting substrate concentrations, the nickel-foam-based cathode enhanced production to 19.1 L of H_2/°C /d at the pilot scale of 150 L. Following treatment, the H_2 production in BES increased from 41.4 to 642 mM/mol of total organic carbon. Overall, promising and clean H_2 production via photocatalytic routes can be provided by developments in materials science and photocatalyst reaction efficiency. Considering the future landscape, this developing region has the potential to be a crucial contributor to sustainable H_2 production. Low production rate released O_2 that may inhibit the H_2 production reaction and cause safety concerns when mixed with H_2 at certain concentrations, and low solar-to-H_2 efficiency are the three main obstacles to photobiological H_2 production. The following areas have been the focus of basic research to overcome these obstacles: (i) selecting desirable strains to increase the yield of H_2 production

through efficient utilization of sunlight; (ii) improving H_2-producing enzymes through protein engineering and metabolic pathway modulation; and (iii) designing and developing microbes and reactors for commercial H_2 production [88]

3.1.4. Biological Route

A viable substitute for the current processes of producing H_2 is the biological pathway. Through dark fermentation or photo-fermentation, these processes entail the microbial conversion of pure or biomass-derived sugars to H_2. Dark fermentation is the most promising and sustainable of these for producing H_2. Dark fermentative bacteria use this process to anaerobically ferment organic substrates, producing H_2 as a byproduct. A maximum output of 3–8 mol of H_2/mol of hexose was achieved using sugars or biowaste feed. Important culture studies on dark fermentative H_2 production have examined *Clostridium, Bacillus, Caldicellulosiruptor, Thermotoga, Citrobacter, Enterobacter*, and *Escherichia*. Under thermophilic conditions at 55 ◦C, the non-heat pretreatment sludge dominated by acetic acid-type fermentative *Thermoanaerobacterium* demonstrated high H_2 production of 3.68 mol/mol of hexose without regulating pH [88].

The goal of recent advancements in this field has been to increase the viability and efficiency of dark fermentative H_2 production through a variety of tactics, including genetically engineering bacteria, improving microbial consortia, investigating novel substrates (co-digestion), and optimizing reactor design and operating conditions. These developments have aided in the resolution of issues like low H_2 yield and scarce substrate supply. Dark fermentative H_2 production is therefore a feasible choice for the production of sustainable energy. Furthermore, there are more chances to optimize overall energy output and resource utilization when dark fermentative H_2 production is combined with other bioprocesses like organic waste management or wastewater treatment. However, in order to advance and commercialize this technology, issues such as optimizing reactor design and operating conditions, increasing the efficiency of microbial H_2 production, resolving substrate constraints, and enhancing process scalability must be resolved. Additionally, combining dark fermentative H_2 production with biofuel and other renewable energy technologies [111].

There is a great chance that recent advancements in dark fermentative H_2 production will help overcome obstacles and open up new avenues for the production of sustainable energy. A high purity of 83 percent and H_2 yields of 276 L/kg of volatile solids (VS) were obtained by co-digesting swine manure and food waste under carefully controlled operational dark fermentation conditions. The H_2 yields of 78.6 mmoL/g of COD were approximately four times higher in microbial consortia of Clostridium pasteurianum, Rhodopseudomonas palustris, and Syntrophomonas wolfei than in individual cultures. The greatest H_2 production from molasses, 910 mmol/L, was achieved by

bioprocessing and metabolically engineering Clostridium tyrobutyricum through endogenous hydrogenase overexpression [112]. Maximum H_2 production of up to 3–11 mol/mol of hexose was achieved by Enterobacter aerogenes through dark fermentative H_2 production using immobilization supports like ceramic balls, dead coral from the Persian Gulf, and ceramic saddles. The immobilized mixed culture demonstrated high H_2 and CH_4 production of 21.3 and 374 L/g vs. under a two-stage dark fermentation and AD process. 80 g of COD/L of f is a high feed loading [88].

A promising renewable energy technology is photo-fermentative H_2 production, which uses microalgae or photosynthetic bacteria to convert organic compounds to H_2 when exposed to light. Because it can use the limitless power of sunlight to create a clean and sustainable source of hydrogen gas, this technology has the potential to completely transform the way that clean energy is produced and stored. Among the many benefits of photofermentative H_2 production are its high energy conversion efficiency, low carbon footprint, and ability to use a variety of feedstocks. A maximum of 9.0 mol of H_2/mol of glucose was produced by R. capsulatus JP 91 under photofermentative conditions. Rhodobacter spp. were included in significant culture investigations on photofermentative H_2 production. (R. *Rhodopseudomonas* species, as well as sphaeroides and R. capsulatus. (R. R. *faecalis* and *palustris*. Nonetheless, there are still a number of obstacles to overcome and chances for advancement in this area. Low solar energy to chemical energy conversion rates, limitations in the biological systems used, and the requirement for optimal growth are some of the reasons behind the low efficiency of photo-fermentative H_2 production [88].

Numerous approaches have been tried to address these issues, including genetically modifying bacteria to increase their capacity to produce H_2, improving growth conditions and nutrient availability, adding nanoparticles to the production media, and creating innovative reactor designs to increase the efficiency of H_2 production. The cost-effectiveness and scalability of photo-fermentative H_2 production are other areas that require further development. Additionally, research is being done on novel photosynthetic bacterial strains or co-cultures with greater potential for H_2 production. By overcoming these obstacles, photo-fermentative H_2 production may be able to develop into a sustainable and profitable clean energy production process [88].

A study demonstrated that Rhodobacter pentothenatexigens KKU-SN1/1 under outdoor conditions had a significant 17-fold increase in H_2 production efficiency (493 mL/L) compared to traditional batch mode production. Light intensity has a significant impact on Rhodobacter sphaeroides KKU-PS1's capacity for growth and H_2 production. In this case, red light helped with high biomass accumulation, and green light doubled photo-H_2 productivity when compared to white light. In comparison to the base strain, R. sphaeroides' multi-dimension metabolic engineering demonstrated a 4-fold increase in photofermentative H_2 production to 17.6 L/L (3.0 mol/mol of acetate). Photofermentative H_2 production

is a promising renewable energy technology that can help create a cleaner and more sustainable future by allowing H_2 production and wastewater purification to occur simultaneously when integrated with current wastewater treatment systems. In theory, one mol of hexose would yield 12 mol of H_2 upon full conversion of sugars to H_2. Up to 4 and 2 moles of H_2 can be produced interm by the acetate and butyrate reaction under dark fermentation conditions [88].

Limited commercial production and pilot-scale research and development are underway for the biological H_2-producing pathways. Although the biological routes provide an environmentally friendly method of producing H_2, they are still limited in terms of production efficiency and the scalability of the bioprocess. In the near future, biotechnological developments in these pathways will be unlocked to produce H_2 efficiently and sustainably. In general, the following reactions are involved in the production of H_2 via dark and photo-fermentative pathways (Equations (16)–(20)) [88]:

$$\text{Sugar (hexose)} + 6H_2O\ (\text{Sunlight}) \rightarrow 12H_2 + 6CO_2 \quad (16)$$

$$\text{hexose} + 2H_2O \rightarrow 4H_2 + 2\ \text{acetate} + 2CO_2 \quad (17)$$

$$\text{hexose} \rightarrow 2H_2 + \text{butyrate} + 2CO_2 \quad (18)$$

$$\text{acetate} + 2H_2O\ (\text{light}) \rightarrow 4H_2 + 2CO_2 \quad (19)$$

$$\text{butyrate} + 6H_2O\ (\text{light}) \rightarrow 10H_2 + 4CO_2 \quad (20)$$

3.2 Hydrogen impacts on climate

3.2.1 Hydrogen's warming potency

The most well-known indicator for understanding the significance of a climate force as a contributor to climate change is its potential for global warming. The greenhouse gas potential of hydrogen has been documented for many years, but only in relation to its tropospheric effects and over a 100-year period, which includes many decades during which hydrogen does not affect the atmosphere [113]. Its impact has been undervalued as a result. According to recent studies, hydrogen's global warming potential (GWP) is twice as high as previously believed for the 100-year GWP and three times higher for the 20-year GWP than for the 100-year GWP, for both tropospheric and stratospheric effects, and for both 20- and 100-year timeframes [114]

The maximum GWP of hydrogen is approximately seven years after the first emission pulse, with a central estimate of 40 and a range of 25 to 60 depending on uncertainties. Compared to the most well-known GWP for hydrogen [113]. Since it takes several years for methane's atmospheric lifetime increase in response to less OH being available from the reaction with hydrogen, hydrogen's GWP first rises before falling once more. When comparing the warming effects of a pulse of emissions from a short-term forcer to those of a long-term forcer, it is expected that GWP will decrease for time horizons

of 10 to 100 years. This is because, 100 years later, H_2 is still in the atmosphere, while the effects of the short-term force have long since faded, indicating a decline in the relative potency of the short-term forcer. Hydrogen's GWP-20 (central estimate of 33) and GWP-100 (central estimate of 11) differ by a factor of 3, which is actually comparable to that of methane 80 and 30, respectively [115].

In **Figure11b**, the same GWP computation is employed, but instead of pulse emissions, it is taken into account a constant emission rate. When comparing the warming effects of hydrogen and carbon dioxide in situations where both are affecting the atmosphere over a given time horizon, the constant-emission-rate approach is more realistic in depicting hydrogen leakage in a hydrogen economy than a one-time pulse of emissions. It is also more logical. The potency of hydrogen in relation to carbon dioxide can be 50% greater when continuous equal emissions of both of these gases are taken into account rather than just one pulse at time D 0. This isn't consistent across all timescales, though. Actually, the pulse approach (GWP) produces higher potency values than the constant-emission-rate approach prior to ten years. This is because, for constant emissions, the carbon dioxide impact accumulates more quickly in the short term than the hydrogen impact, which takes years to fully manifest. In contrast to decaying impacts, continuous hydrogen emissions have a replenishing effect over time [11].

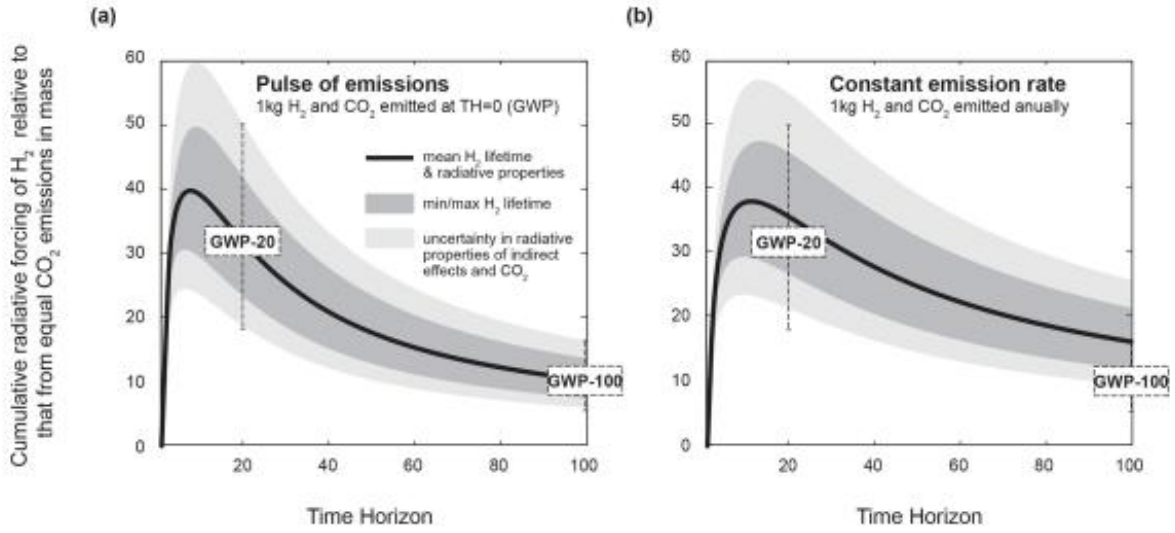

Figure 10 Warming potency of hydrogen relative to carbon dioxide using cumulative radiative forcing as a proxy for (a) a one-time pulse of equal emissions in mass (equals hydrogen's global warming potential) and (b) a constant emission rate of both hydrogen and carbon dioxide for equal emissions in mass. The solid lines represent the mean hydrogen lifetime and radiative effects, the dark shaded areas correspond to a minimum and maximum hydrogen lifetime based on soil sink uncertainty, and the light shaded areas represent 20 % uncertainty in the radiative effects of hydrogen from its indirect effects and uncertainties in carbon dioxide's radiative properties [11].

3.2.2 Warming impacts from replacing fossil fuel technologies with hydrogen alternatives

Figure 12 displays the findings of an analysis of the effects of methane and hydrogen emissions on the climate. Cumulative radiative forcing would change by -100 percent if there were no climate

forcing emissions from the hydrogen applications; additionally, if there was no replacement, the change would be 0 percent. A positive (negative) percentage change in cumulative radiative forcing would result from the climate forcing emissions from hydrogen alternatives producing more (less) warming over a specific time period than their fossil fuel counterparts [11].

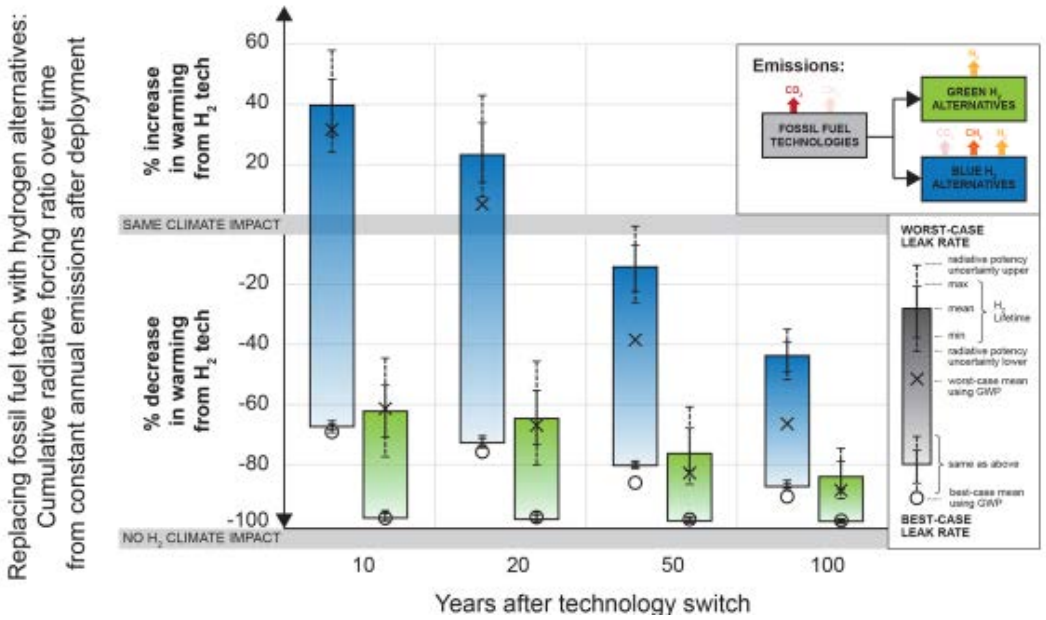

Figure 11 Impact on global warming over time of switching from fossil fuel technologies to green or blue hydrogen alternatives, for example. A ratio of cumulative radiative forcing for deploying 1 kg of H_2 per year vs. Relative warming impacts are measured using the annual avoided emissions from fossil fuels. For green hydrogen, the emissions are hydrogen; for blue hydrogen, they are hydrogen and methane. According to estimates from the Hydrogen Council (2017), carbon dioxide emissions from fossil fuel technologies are estimated to be 11 kg CO_2 avoided for every 1 kg H_2 deployed. The range of likely leak rates for methane and hydrogen emissions is from 1 percent (best case) to 3 percent (worst case) per unit H_2 deployed, and 1 percent (best case) to 10 percent (worst case) for hydrogen. The range of leakage is reflected in the height of each bar [11].

All things considered, any amount of hydrogen leakage will somewhat reduce the climate benefits of avoided carbon dioxide emissions; however, the results vary greatly, both positively and negatively, depending on the production process, total emissions, and time horizon. The worst scenario for blue hydrogen, for instance, could initially have a greater negative impact on the climate than CO_2 emissions from the corresponding fossil fuel technologies (10 percent hydrogen leakage and 3 percent methane leakage). This would result in up to 60 percent more warming during the first ten years and take about 50 years before the benefits of the technology switch are felt. However, compared to the CO_2 emissions from fossil fuels, the best scenario for green hydrogen—1% hydrogen leaks—could result in a nearly complete eradication of the climate impact. However, keep in mind that we do not account for greenhouse gas emissions related to the construction of the infrastructure required to meet the expanding demand for hydrogen and its uses counterparts [11].

The distinction between green (water-based renewable electricity) and blue (steam methane reforming with CCUS) in assessing the extent of climate benefits is evident. The cumulative radiative impact is still lower than that of fossil fuels, indicating a reduction in warming from the use of green hydrogen alternatives, even though hydrogen emissions can produce climate impacts for green hydrogen that are far from climate neutral over all timescales. However, depending on the leakage rate and time horizon, blue hydrogen may or may not be better for the climate. For instance, worst-case blue hydrogen emissions have the potential to increase the warming impact of fossil fuels by 40% over a ten-year period, while worst-case green hydrogen emissions have the potential to reduce warming by 60%. Green hydrogen could lessen the warming effect of fossil fuels by over 95% over the first ten years, while blue hydrogen could only lessen it by 65% for both at best-case leak rates. The situation is comparable over a 100-year period, with the worst-case leak rates resulting in a doubling of the climate impact of blue hydrogen relative to green hydrogen. Indeed, over all timescales, the worst-case benefits of green hydrogen are comparable to the best-case benefits of blue hydrogen (e.g., a 65 percent reduction in the warming impact of fossil fuel H_2 emissions over a 10-year period and an 85 percent reduction over a 100-year period). The warming effects of methane emissions from the natural gas supply chain are solely to blame for the discrepancy, since the hydrogen emissions in the blue and green scenarios are identical [11].

Emissions levels are just as important as the production process. For instance, the degree of leakage will have a significant impact on the long-term and short-term climate benefits of green hydrogen, which can range from over a 95% reduction in climate impacts from fossil fuel technologies to only 65% over the first ten years for total leakage rates of 1% and 10%, respectively. If there is significant leakage, green hydrogen may only reduce climate impacts by 85% over the long run (100 years). Blue hydrogen is another example of how leakage levels affect the climate. While high rates of both hydrogen and methane leakage could increase warming for decades compared to their fossil fuel counterparts, low rates of leakage could reduce climate impacts by more than half in ten years. Both the worst-case and best-case leak rates for blue hydrogen would probably result in less impact on the climate over a longer period of time (more than 100 years) [11].

However, the benefits vary in size, ranging from a 45 percent reduction to an 85 percent reduction. These findings highlight how crucial the emission rate is in assessing the potential advantages (and disadvantages) for the climate of switching from fossil fuel technologies to hydrogen alternatives. This analysis demonstrates how the picture changes when taking time horizons from 10 to 100 years into account, whereas the majority of evaluations of the climate benefits of alternative technologies naturally concentrate on the long-term effects because of the use of the GWP-100 metric. This is because the warming effects of hydrogen (and methane) are transient and do not

build up over time like those of carbon dioxide. As a result of preventing the accumulation of carbon dioxide in the atmosphere, the advantages of hydrogen applications increase over time. The results will not reflect the significantly greater relative climate impacts over shorter time horizons if only a long-term perspective is used when assessing hydrogen applications [11].

The worst-case scenario for green hydrogen, for instance, might only cut the warming effects of the fossil fuel applications it is replacing in half for the first few decades, but over a century, the warming effects might be cut in half. The combination of two short-term force emissions makes the temporal significance of blue hydrogen even more pronounced. For instance, the worst-case blue hydrogen alternatives would reduce the warming impact by almost half over a century, but they might increase warming in comparison to fossil fuel technologies for the first few decades. Consequently, one may obtain quite different insights into the climate benefits of hydrogen's decarbonization potential based on the time horizon taken into account in the analysis [11].

If the GWP metric is applied using a pulse approach rather than a constant emission rate, this becomes even more severe. The pulse approach undervalues the cumulative radiative forcing over time, even though it accurately depicts the short-term effects of hydrogen applications in comparison to those of fossil fuels. For instance, even after 100 years of replacing fossil fuel technologies, the worst-case blue hydrogen alternative might only result in a 45% reduction in warming, whereas GWP-100 predicts a 65% reduction. Furthermore, the near- and middle-term effects of hydrogen (and methane) leakage will be completely ignored if GWP-100 is used exclusively and taken to represent the impacts of hydrogen over any timescale, as is frequently the case. In some cases, this means assuming a benefit to the climate when it is actually a disbenefit for decades [11].

A general argument for preventing carbon dioxide emissions from fossil fuel technologies was discussed above. The amount of CO_2 avoided, which varies based on the technology replaced, will determine the perceived climate benefits of hydrogen alternatives. Therefore, researchers compare the relative climate impacts of the hydrogen applications over a 20-year time horizon (solid bars in **Fig.13**) and consider avoided emissions of 5, 10, and 15 kg per 1 kg of hydrogen deployed (compared with our central estimate of 11 kg) in order to test the sensitivity of our results to the amount of CO_2 avoided. While green hydrogen may only reduce warming by 20%, it is found that blue hydrogen could result in a more than 150 percent increase in warming over the first 20 years if CO2 emissions are avoided at the lower end and leak rates from hydrogen and methane are at the upper end. Nonetheless, both the worst-case blue and green hydrogen options would benefit the climate by lowering warming by 10% and 75%, respectively, if avoided CO_2 emissions are on the higher end [11].

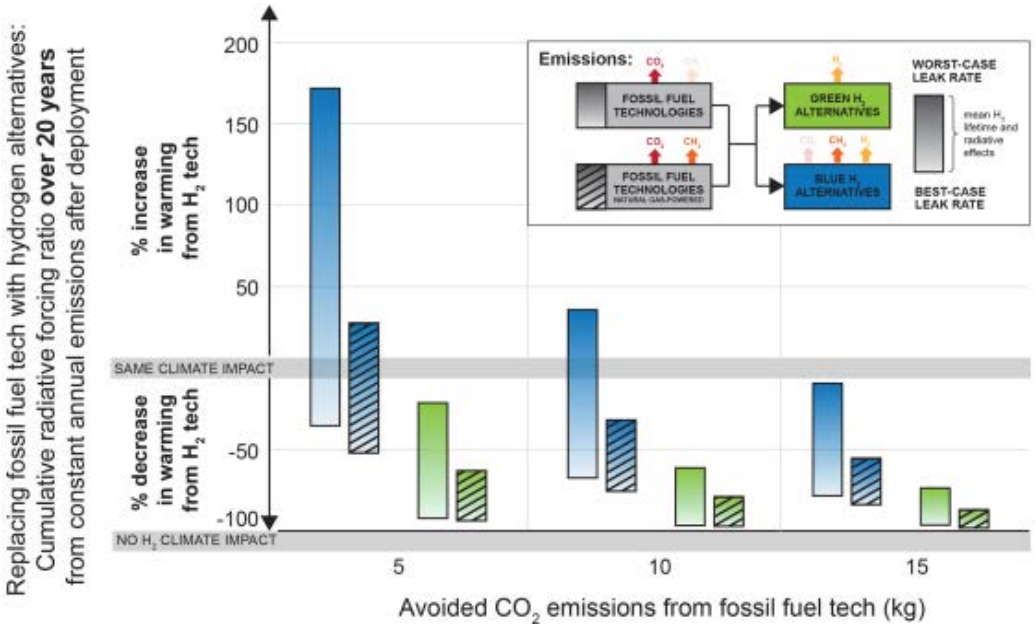

Figure 12. Relative warming impacts over time from replacing fossil fuel technologies with green or blue hydrogen alternatives for different levels of avoided carbon dioxide and methane emissions. A cumulative radiative forcing ratio for annually deploying 1 kg of H_2 vs. annually avoided fossil fuel emissions is used as a proxy for relative warming impacts. Emissions from hydrogen alternatives are hydrogen for green hydrogen and hydrogen and methane for blue hydrogen. Emissions from fossil fuel technologies are carbon dioxide and methane. Emissions of hydrogen and methane include a range of plausible leak rates from 1 % (best case) to 10 % (worst case) per unit H_2 deployed for hydrogen and from 1 % (best case) to 3 % (worst case) for methane. The height of each bar corresponds to the range of leakages. [11].

Since replacing fossil fuel technologies can also prevent methane emissions, we expanded the analysis to take into account a scenario in which natural gas was the fossil fuel burned to produce the CO_2 (hatched bars in **Fig. 13**), employing the same methane leak rates in the best and worst situations as in the hydrogen applications. Although there is a strong reliance on the corresponding CO_2 emissions that are avoided, we find that the avoided methane emissions may significantly increase the short-term benefits of hydrogen applications. For instance, the central estimate of avoided CO_2 would change from worse for the climate to better for the climate, even though the worst-case blue hydrogen alternative with the lower end avoided CO_2 values would still be worse for the climate over the first 20 years even when avoided methane is included. When accounting for avoided methane emissions, the climate benefits of the worst-case green hydrogen alternative would double for all levels of avoided CO_2. But since natural gas burns with less H_2 than coal, if methane emissions were higher, H_2 emissions would probably be lower as well, rather than both being on the higher end [11].

3.2.3 Absolute warming impacts due to hydrogen emissions

For all levels of hydrogen emissions, the current hydrogen demand (about 100 Tg) could result in warming of no more than 0.01 ◦C. According to five estimates based on various scenarios and sources, the average hydrogen demand for 2030 is 150 Tg. This could double the impact of 100 Tg

for uncertainties (0.02 ◦C) and upper-end leak rates (10 percent). According to 21 separate estimates, demand for 2050 is expected to range between 130 and 1370 Tg, with an average of 590 Tg. These demand levels may result in warming between 0.01 ◦C and 0.1 ± 0.05 ◦C for the worst-case hydrogen leak rates (10 percent). On the other hand, temperature responses could be less than 0.02 ◦C including uncertainties if total hydrogen emissions are kept to a minimum of 1%. For example, under a 2 ◦C scenario, a 590 Tg hydrogen demand could provide about 20% of the final global energy demand in 2050 [116] [117].

In 2050, using hydrogen to meet all of the final energy needs could result in warming of more than 0point 1 ◦C with a 5 percent leak rate and up to 0point 4 ◦C with a 10 percent leak rate and uncertainties in the radiative effects of hydrogen [11].

It is unrealistic to demand hydrogen at this level, though. Of the 2050 hydrogen demand projections that are currently available in literature, four places it is between 100 and 199 Tg, three between 200 and 499 Tg, eleven between 500 and 999 Tg, and three between 1000 and 1999 Tg. None predict hydrogen demands that are less than 100 or more than 2000. If leak rates and uncertainties are at the upper end, sustained hydrogen demands of 800 Tg or more, which could make up about 25% of the total energy demand in 2050, could contribute at least 0.1 ◦C to warming. For comparison, this amount of warming could counteract the 2050 warming that could have been prevented by using all economically viable strategies to reduce methane emissions worldwide over the ensuing ten years, which would have otherwise reduced global mean warming rates by as much as 15%, or the potential protection against warming that comes with the phase-out of hydrofluorocarbons [11] [118].

3.2.4 Hydrogen and Climate Change

Since hydrogen does not absorb infrared light, it is not regarded as a greenhouse gas in and of itself. It does, however, indirectly affect radiative forcing, a measure of the warming effect that greenhouse gases produce in the atmosphere. To put it another way, H_2 is an indirect greenhouse gas. Equation (21) states that hydrogen will probably react with OH groups once it is released into the atmosphere to form H_2O [107]:

$$H_2 + OH \rightarrow H_2O + H \qquad (21)$$

After that, H is probably going to recombine with O_2 to create HO_2, which is a component of reaction cycles that deplete the stratospheric ozone. On the other hand, a rise in the atmospheric concentration of hydrogen would raise the concentration of tropospheric ozone, presuming that all other emissions stay constant. In the meantime, the lifetime of CH_4, which is typically controlled by Equation (22), would also be extended due to the shortage of OH brought on by the reaction in Equation (21) [107].

$$CH_4 + OH \rightarrow CH_3 + H_2O \quad (22)$$

It has been estimated that for every 1 ppm increase in hydrogen concentration, the lifetime of CH_4 increases by roughly 1 year. Extending the lifetime of CH_4, the second-strongest GHG after H_2, would further increase its radiative forcing and, consequently, its GWP. It is also anticipated that variations in hydrogen concentration will impact atmospheric water vapor. Hydrological cycles govern the H_2O budget in the troposphere, the lowest part of the atmosphere that extends from the earth's surface to a height of roughly 6–10 km. However, increases in atmospheric hydrogen are likely to raise the amount of water vapor in the stratosphere, which is a part of the atmosphere that is above the troposphere and extends to a height of roughly 50 km above the earth's surface. In the context of the indirect climate impact of hydrogen, the radiative effects of stratospheric water vapor should also be taken into account [114].

In its gaseous state, hydrogen is much more likely to leak than methane because it is a much smaller molecule. As a point of comparison, the oil and gas supply chain leaks roughly 6.5 million metric tons of methane annually, or about 1% of total production. Ongoing surveys suggest that leaked volumes may eventually be much larger, but data is highly ambiguous. Hydrogen estimates vary from less than 1 percent to 20 percent, but because there is so little experimental data, any figures are essentially speculative. Since methane leaks compound hydrogen leaks, the effects of possible leaks along the supply chain become even more worrisome if hydrogen is produced via SMR [107].

To highlight the issue of emissions, Sun et al. In order to account for hydrogen being lost to the atmosphere along the production-to-end-use pathway, went back and reviewed the case studies that were first examined in the "Hydrogen decarbonization pathways" published by the Hydrogen Council in 2021. It was shown that the GWP of blue hydrogen in the short term (20 years) can be up to 14% worse than that of fossil fuel technologies, depending on the application, due to high methane (2.1%) and hydrogen (10%) emission rates. Because the short-term GWP was significantly worse than that of electric vehicles, with values ranging from 10 to 45 percent higher depending on the specific hydrogen and methane emission levels, it was predicted that the effects of methane and hydrogen emissions would be particularly detrimental in the application of light-duty vehicles. Similar to the ideal scenario of negligible hydrogen emissions, it was shown that high hydrogen emissions were harmful to the climate benefits of green hydrogen, which were decreased by up to 25 percent in the short term (20 years) and by up to 13 percent in the long term (100 years) [107].

Although the majority of climate change contributions only consider a century's worth of time, researchers imply that time is the true determinant of hydrogen's decarbonization effectiveness. Patel and colleagues conducted research on this subject. in their analysis of different methods for producing hydrogen. Both short-term and long-term estimates of the GWP were made, with

respective time horizons of 20 and 100 years. The GWP of all methane-derived hydrogen types (grey, blue, and turquoise) was found to be significantly higher in the short term than in the long term when taking into account potential methane leaks (but not hydrogen leaks). Depending on the specifics of the methane supply chain, the difference ranged from 12 to 25 percent. Because methane has a shorter lifetime than H_2, its GWP over 20 years (estimated at 81–83) is significantly higher than its GWP over 100 years (estimated at 27–30). This is the reason for the higher GWP at 20 years. On the other hand, Patel et al. 2024 determined that because green hydrogen is produced without the use of natural gas, its GWP stays constant over 20 and 100 years. Nevertheless, it was not taken into consideration the various lifetimes of gas species that may be connected to the indirect GWP of hydrogen since it implicitly assumes that hydrogen leaks are insignificant [107].

The fact that the GWP on a specific time scale, usually 100 years, is frequently computed as the impact of a single emission pulse presents another criticality in the life cycle assessment of hydrogen technologies. Nevertheless, [18] contended that this assumption might not be realistic as long as emissions from a functioning technology continue to occur continuously over time, which could be the cause of the atmosphere's GHG levels continuously replenishing. Consequently [18], proposed that the cumulative radiative forcing from continuous emissions over different time scales should be used to calculate the climate impact of hydrogen (similar to fossil fuels) in addition to GWP. Alvarez et al.'s "technology warming potential" (TWP) approach is used in this evaluation of climate impacts, which was created especially for comparing various fuel technologies over time [107].

Lastly, it should be mentioned that LCAs are frequently made ex-ante (prospective LCAs), which means that potential EIs of emerging technologies are computed as a function of expected future scenarios, particularly for research and development purposes. As previously stated, currently, only a small portion of (anthropogenic) hydrogen can be classified as "green," i.e. generated through electrolysis powered by renewable energy. Green hydrogen volumes are undoubtedly anticipated to rise in the future due to the increased accessibility and reduced cost of solar and wind-powered energy. The switch to renewable energy sources will also lessen the remaining green hydrogen EIs associated with the production and assembly of the electrolysis system as well as the possible use of backup power from the electrical grid. However, this shift will probably be gradual. In the meantime, the grid's decarbonization will also lower the greenhouse gas emissions linked to the life cycle of other forms of hydrogen, like methane pyrolysis (turquoise) hydrogen. In addition, increasing green hydrogen production to reach the 2050 net zero targets might compromise other impact categories. For instance, a shift in the burden from global warming to bio-geochemical flows might be anticipated. The use of essential materials, like platinum-group metals (for instance, in PEM electrolyzers), may turn into a technological and environmental hotspot, which calls for the

prompt identification of potential replacements and reprocessing techniques. The multifaceted issues brought on by large-scale production could eventually weaken green hydrogen's environmental advantage over other hydrogen technologies and alternate decarbonization strategies, necessitating a thorough evaluation that considers more than just climate change [107].

Chapter 4

Hydrogen storage

A key component of its use as a substitute energy source is H_2 storage. H_2 is stored in three different states—gaseous, liquid, and solid—using a variety of technologies. Generally speaking, there are two ways to store H_2: (i) physical-based, which includes compressed gas, cold/cryo compressed, and liquid H_2 storages; and (ii) materials-based, which includes chemical H_2 (NH_3BH_3), interstitial hydride (LaNi5H6), complex hydride ($NaAlH_4$), adsorbent (metal-organic framework, MOF-5), and liquid organic H_2 carriers (LOHCs). High-pressure tanks (350–700bar) and a cryogenic temperature of -253 ˚C are physically necessary for storing H_2 as gas. By adsorption or absorption, it can also be retained on surfaces or inside solids [88].

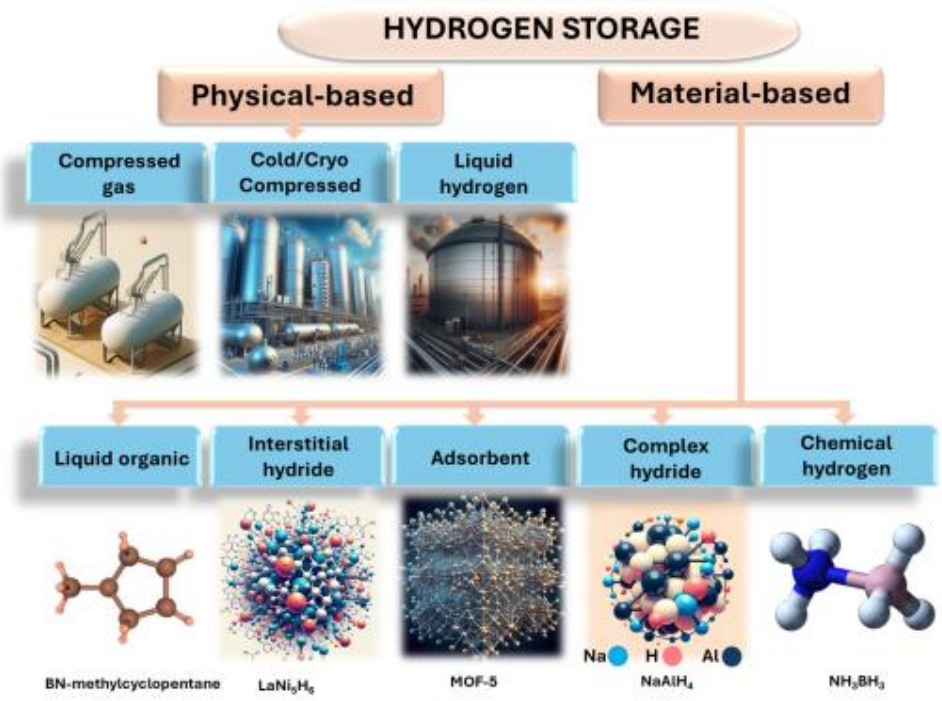

Figure 13 Illustration of H_2 storage processes [88].

4.1 Physical based hydrogen storage

4.1.1 Liquid H_2 (LH_2)

Hydrogen is a gas with a volumetric density of 70.8 gH_2/L, a system weight density of up to 90 wt, and a liquefaction point of -252 °C. $\%H_2$ is contingent upon the container. However, because of its unique characteristics (inverse Joule-Thomson effect), H_2 is not easily liquefied. In addition, liquid phase H_2 is stable at 99.8 percent in the para form, requiring the conversion from ortho to para. In contrast, gas

phase H_2 exists in two forms based on the nuclear spin alignment of its individual atoms (75 percent ortho) or not (25 percent para). Regretfully, this conversion is exothermal and slow (ΔH = 525 kJ/kg), which causes H_2 to inevitably evaporate (latent heat of vaporization = 476 kJ/kg), a process known as boil-off. A catalyst is frequently incorporated into the heat exchanger to aid in this gradual conversion during the cooling process. H_2 storage must be kept open to prevent catastrophic events because if this phenomenon is not taken into consideration, the pressure in a closed system could rise sharply. 90 Since existing systems lose about 1 to 5 weight, the question of effective thermal insulation is raised by open systems. percentH/day. The industrial liquefaction pla is the last one [119].

4.1.2 Underground H_2 storage

One possible large-scale, mid- to long-term stationary storage technology is underground H_2 storage (UHS). Pressurized pure H_2 or a mixture of gases containing H_2 can be stored in underground geological formations such as salt caverns, aquifers, and empty gas or oil reservoirs. Since H_2 can slowly react with the minerals that make up the UHS to form carbonates, a suitable UHS has a solid rock formation and an inert impermeable layer to stop H_2 leaks. To prevent H_2 leaks, UHS must also be able to tolerate an internal pressure between 30 and 80 percent of the lithostatic pressure. 95 There are currently only four artificial salt caverns in use worldwide [120].

Although they make up only 8% of the global capacity, salt caverns are the most effective UHS. Lastly, despite their great potential, UHS are particularly vulnerable to geological occurrences like earthquakes, difficult to design and monitor, restricted to particular geological conditions, and compete with other subterranean gas storage systems like CAES or H_2 storage.

4.1.3 Compressed Hydrogen Storage

The most popular method for storing and using hydrogen gas as a source of energy is hydrogen compression, which offers a number of exceptional benefits. First, the compression method is highly effective, resulting in high rates of hydrogen filling and release. Furthermore, energy is not needed for hydrogen release. For storing compressed hydrogen, hollow spheres are the most popular storage material. In addition to having a large surface area, hollow spheres contain pores that contain hydrogen. Furthermore, through binding sites on the surface or in the pores, the high surface area and porosity enable hybridization with other materials. As a result, the hollow spheres' absorption and catalytic activities can be greatly enhanced. Furthermore, hollow spheres are excellent hydrogen containers due to their low specific weight and high mechanical strength. The creation of hollow spheres with consistent sizes can be made easier by managing the various parameters, including reaction time, pH, temperature, and reactant ratio. Both atomic and molecular forms of hydrogen can be absorbed in hollow nanospheres [65].

A lot of research has been done on hollow spheres, which have average sizes between micrometers and nanometers. Numerous hollow spheres of various sizes and composed of various materials, such as metal, glass, carbon, and nonmetal, have been created.

4.1.3.1 Hollow Carbon Spheres (HCSs)

Hollow Carbon Spheres (HCSs) are primarily made using two techniques: hard templating and soft templating. Both techniques use various kinds of templates to produce a hollow sphere (HS). In order to create a hollow structure, the hard templating technique uses unique hard particles as a "core template.". After the core's surface develops a carbon shell, the core is extracted. Hard-templating processes frequently use silica, polymers, and hard metal particles as core templates. The self-assembly of carbon and other organic compounds directly creates a hollow structure in soft templating. Therefore, the "soft" precursor molecules that make up the core templates readily break down during the last pyrolysis.

HCSs are great materials for storing hydrogen. A high hydrogen capacity can be attained because of their mesoporous structure, which offers a high Brunauer–Emmett–Teller (BET) value as well as voids and hollow spaces that hydrogen can occupy. Nonetheless, the hydrogen storage capacity is significantly impacted by the HCS structure. Hydrogen diffusion in the substrate is significantly influenced by the size and form of the HCS. Hydrogen can readily occupy the active sites, which are highly dependent on the material's morphologies, when the adsorption energy is greater than the release energy. Furthermore, the HCS's thin walls and defects may facilitate the deposition of hydrogen into its pores, releasing the spaces between layers and boosting HCS’s hydrogen storage capacity [2].

Researchers created hollow carbon nanospheres (CNSs) with narrow pore distributions that resemble necklaces by employing reactants that contain pentagons. CNSs provided a capacity of 242 mAh/g at a current density of 200 mA/g, which translates to a hydrogen storage of 0–89 weight percent, according to the results of their electrochemical hydrogen storage experiments. This is significantly higher than the electrochemical capacities of solid chain carbon spheres and multiwalled carbon nanotubes. This demonstrates how carbon materials' morphology and structure have a significant impact on electrochemical hydrogen storage [2].

Hydrogen spillover is the process of doping hollow carbon materials with metals to store hydrogen. The binding energy between hydrogen and the pore walls can be raised by doping carbon materials with metals. Furthermore, doped metallic atoms and hydrogen molecules may bind together. Therefore, metal doping can improve a material's ability to store hydrogen. Palladium (Pd)-doped carbon materials have been found to improve the performance of hydrogen storage among the different metal-doped hollow carbons used to improve hydrogen storage. On the Pd surface, hydrogen molecules readily split apart, reducing storage efficiency. Therefore, tiny Pd particles

doped onto the material's porous surface in order to reduce the active surface area of Pd, improve its catalytic performance, and increase its hydrogen storage capacity [2].

Pd nanoparticles doped onto HCSs were synthesized and their hydrogen storage capabilities assessed by Zielinska et al. (2016). According to their findings, the hydrogen storage capacity was greatly impacted by the size and quantity of Pd nanoparticles, with size being more significant than quantity. The Pd nanoparticles' small size may increase their total surface area, which would increase the spillover effect. With an 11 nm diameter, the capacity achieved at 40 °C and 24 bar of pressure was 0.36 weight percent, which was twice as much as the storage capacity of pristine HCSs [2].

4.1.3.2. Hollow Glass Microspheres (HGMs)

The primary constituents of hollow glass microspheres (HGMs), sometimes referred to as microballoons or microbubbles, are soda lime silica and borosilicate. HGMs have pore sizes ranging from 100 to 500 nm, wall thicknesses ranging from 1 to 5 to 3 μm, and sizes ranging from 100 nm to 5 μm. The crush strength of HGMs is significantly influenced by their wall thickness, the higher the sphere density, the greater the crush strength. HGMs are regarded as high-potential hydrogen transport and storing materials because of their exceptional chemical stability, chemical resistance, strong mechanics, low density, high-temperature operation, high water resistance, noncombustibility, nonexplosibility, nontoxicity, and especially low production costs [2].

To improve hydrogen diffusion into HGMs, high pressure and high temperature must be used when operating them. This is due to the fact that temperature can alter gas diffusivity in addition to molecular size. To lower the diffusivity rate and keep the loaded hydrogen molecules in the pore cavities, the temperature must be lowered to room temperature after the hydrogen molecules have been absorbed in the HGMs. The HGMs must be heated to high temperatures in order to release hydrogen. Over 300 ◦C is the ideal temperature for both hydrogen desorption and absorption [2].

Both liquid-droplet and dry-gel methods can be used to create HGMs. In both techniques, the high-temperature furnace where the initial particles are created is crucial. To release the gas inside the dried gel or liquid, the blowing agent must first be broken down. Bubbles and hollow droplets are created as a result of the gaseous products' rapid growth. HGMs are then formed when the hollow droplets quickly cool from their liquid state. In relation to HGM synthesis, Wang et al. offered a fundamental formula for a novel kind of HGM that was based on interconnected businesses, conventional fabrication techniques, and knowledge of this material industry. They proposed that the weight percentages of the components of HGM were 27, 14.5, 15, 10, 3.5, 3, 0.5, and 26.5 percent, respectively, and included quartz sand, K_2CO_3, $Na_2B_8O_{13}.4H_2O$, Na_2CO_3, $Ca(OH)_2$,

$NaAlO_2$, and H_2O. Therefore, H_2 (68–75 percent), Na_2O (5–15 percent), CaO (8–15 percent), B_2O_3 (15–20 percent), and Al_2O_3 (2–3 percent) were the primary chemical constituents of HGM [2].

HGMs have a low capacity for storing hydrogen because of their poor thermal conductivity, which limits the loading of hydrogen molecules during the absorption and desorption processes. In comparison to conventional heating furnace methods, it has been found that the gas diffusion rate is significantly increased by light illumination when HGMs are doped with photoactive agents like Ti Cr, V, Fe, Zn, Mg, and Co. **Figure 15** shows how light absorption causes photo-induced outgassing in titanium (Ti) ion-doped HGMs. This study specifically examines how Ti doping affects HGMs' ability to retain gas and their photo-induced outgassing behavior. For the storage of hydrogen, HGMs' ability to retain gas is crucial. This study examined the gas retention characteristics of HGMs with varying Ti concentrations by assessing their deuterium (D2) permeability and pressure half-life (t1/2). The identification of photo-induced hydrogen diffusion via glass-shell HGMs loaded with photoactive metals opens the door to new and innovative techniques for hydrogen filling, storage, transportation, and release. [2].

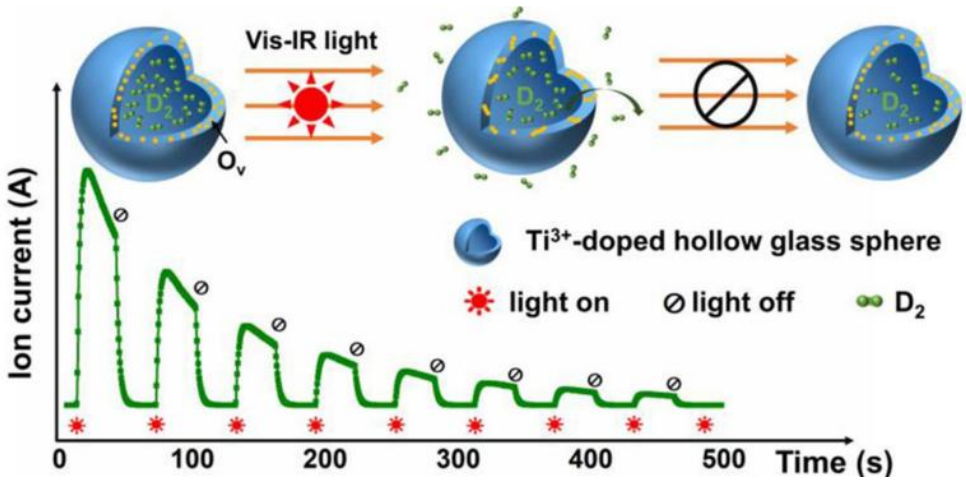

Figure 14 Photo-induced gas release in Ti^{3+}-doped hollow glass microsphere [121].

Changing the physical characteristics of hydrogen, like its temperature or pressure, raises its energy density, but doing so comes at a high energetic cost. If H_2 is to become a competitive energy vector, this energetic cost must be reduced (equivalent to more than 10% of the energy stored for 700 bar CGH_2 and between 40% and 45% for LH_2). Therefore, over the past few decades, research has been conducted to find new materials that can store H_2 by forming bonds ranging from weak Van der Walls interactions to covalent bonding. [2].

4.2 Chemical-based hydrogen storage

H_2's energy density can be increased by altering its physical characteristics, such as its temperature or pressure, but doing so comes at a high energetic cost in order to achieve effective storage. If H_2 is to become a competitive energy vector, this energetic cost must be reduced (equivalent to more than

10% of the energy stored for 700 bar CGH_2 and between 40% and 45% for LH_2). Therefore, over the past few decades, research has been conducted to find new materials that can store H_2 by forming bonds ranging from weak Van der Walls interactions to covalent bonding. Below is a review of the primary technologies used in chemical-based storage.

4.2.1 Adsorbents

4.2.1.1 Carbon-Based Materials

One of the most prevalent elements in both living and non-living things is carbon. Carbon materials have a tendency to interact with gas molecules and are readily prepared as high porosity powders. Consequently, carbon is a well-known gas-absorbing medium that has been employed as a purifier and detoxifier. Because of their many benefits, including high surface area, high porosity with a variety of pore structures, good chemical stability, low weight, and low cost, carbon-based materials have garnered a lot of interest as promising materials for hydrogen storage. Hydrogen is stored in a variety of carbon-based materials [2].

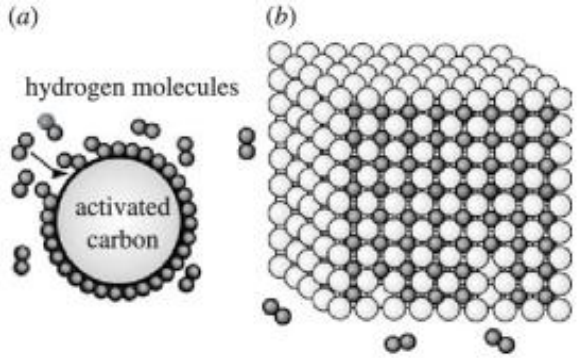

Figure 15 Schematic of hydrogen (a) physisorption and (b) chemisorption using activated carbon (AC) [122].

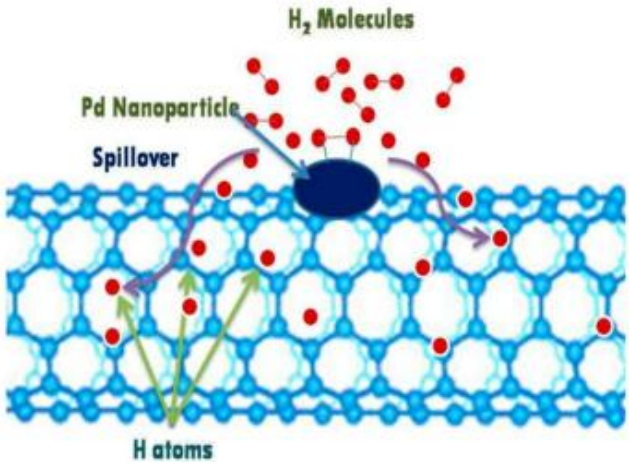

Figure 16 Carbon nanotube (CNT) mechanism for storing hydrogen [123].

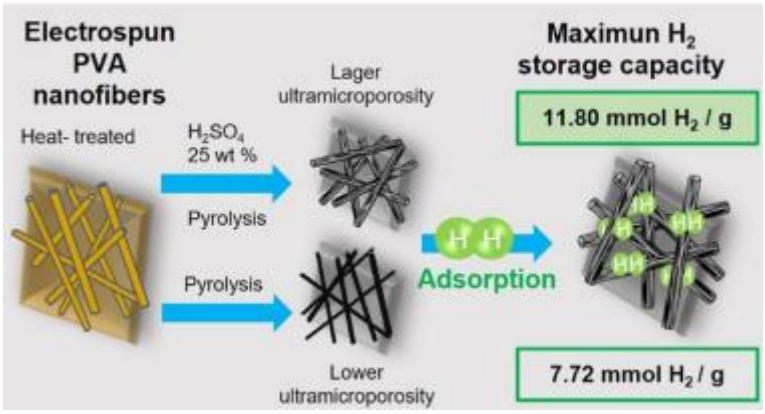

Figure 17 Ultramicroporous carbon nanofibrous mats for hydrogen storage [124].

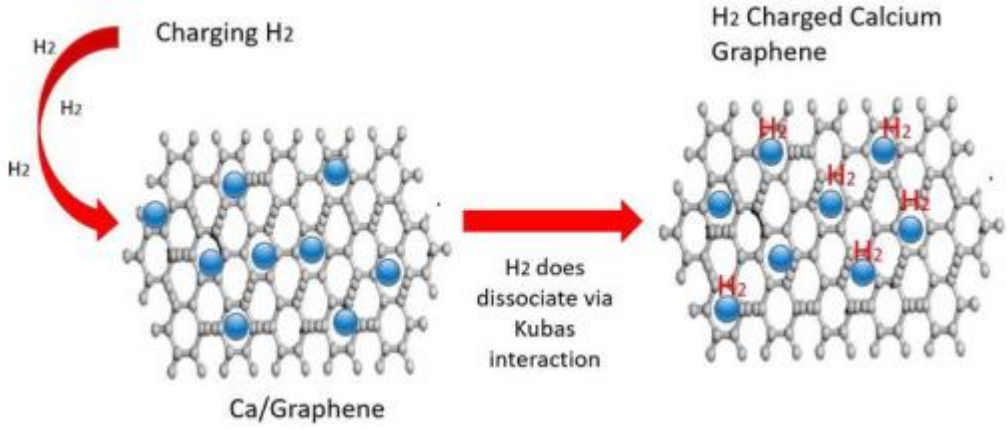

Figure 18 (D) Reaction mechanism of hydrogen charging Ca/Graphene nanocomposite [125].

4.2.1.2 Zeolites

Zeolites are highly crystalline, microporous, three-dimensional aluminosilicate substances. The tetrahedral framework structure of zeolites is characterized by the tetrahedral coordination of Si and Al atoms via shared oxygen atoms. Zeolites are well-known substances that have cages and channels that can hold water, cations, and tiny molecules. They are also very promising media for storing hydrogen due to their high thermal stabilities and good ion-exchange capacities. Zeolites fall into one of two categories: synthetic or natural. In a variety of settings, natural zeolites show enhanced resistivity and thermal stability. They cannot be used in industrial applications, though, because they contain impurities that vary in crystal size [126].

A variety of raw materials can be used to create zeolites. The raw materials must be easily accessible, reasonably pure, selective, and reasonably priced in order to satisfy the demands of economic efficiency. Zeolite is primarily made from raw materials like kaolin, rice husk ash, fly ash, paper sludge, blast furnace slag, lithium slag, and municipal solid waste. As previously

reported in studies, zeolites can be produced using a variety of techniques, such as solvothermal, hydrothermal, ionothermal, alkali fusion and leaching, microwave, and ultrasound energy methods. The hydrothermal process is the most popular of these methods, especially when it comes to creating zeolite membranes [126].

Zeolites are thought to be good hydrogen storage candidates because of their many synthetic processes and excellent properties. Dong and associates. examined the ability of various zeolites, such as Na-LEV, H-OFF, Na-MAZ, and Li-ABW, to store hydrogen. The findings demonstrated that the capacities of Na-LEV, H-OFF, Na-MAZ, and Li-ABW were 2.07, 1.75, 1.64, and 1.02 weight percent, respectively, at a temperature of 77 K and a pressure of 1.6 MPa. This finding demonstrates that increasing the zeolite capacity requires micropores with a larger volume and diameter that roughly correspond to the kinetic diameters of the hydrogen molecules. [126].

Researchers created Monte Carlo simulations to forecast hydrogen loading for MOFs, hypercrosslinked polymers, and zeolites at various pressure and temperature levels. Meta-learning made it possible to determine the ideal temperature for hydrogen storage with the highest working capacity in relation to the pressure value. The meta-learning system for predicting gas uptake is shown in **Figure 20**. This report states that at a temperature of 77 K and a pressure of 100 bar, the RWY-type and AWO-type zeolites show a hydrogen loading capacity of roughly 7 weight percent [60].

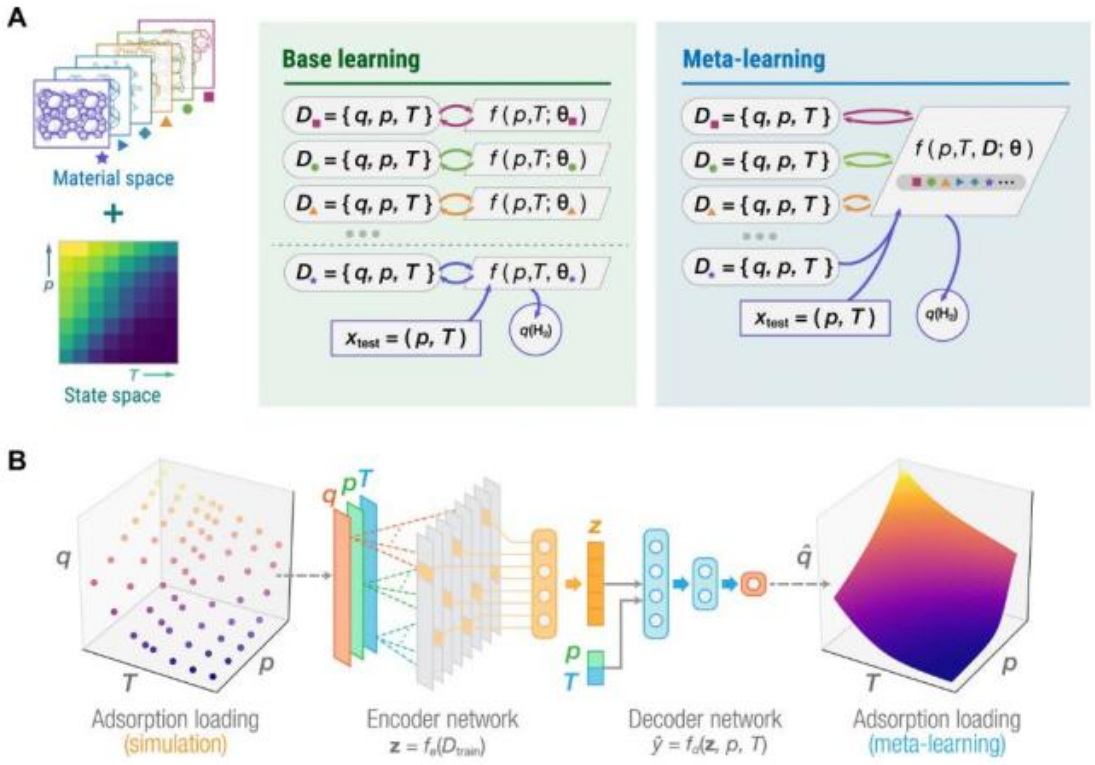

Figure 19. Predicting gas adsorption loading, q, in nanoporous materials using meta-learning. (A) Meta-learning problem setup. (B) A meta-learning framework for predicting gas adsorption [60].

4.2.1.3 MOFs

Metal ions, metal clusters, and organic linkers are all present in MOFs, a broad class of crystalline materials. Organic linkers include pyrrodiazole, 1,2,3-triazole, and azoles. dicarboxylates (such as malonic acid, succinic acid, oxalic acid, glutaric acid, etc.). Citric acid, trimesic acid, and other tricarboxylates are also included. are frequently employed in the production of MOFs. Strategies to produce MOFs with good pore structures and high-dimensional frameworks include adjusting the reaction temperature and altering the organic linker, in addition to regulating the metal/ligand ratio. These factors have a major impact on the hydrogen storage capacity. Like other porous materials like hollow spheres, carbon-based materials, or zeolites, MOFs store hydrogen primarily through the occupancy and retention of hydrogen molecules in their vacant spaces, or pores. **Figure 21** describes the schematic mechanism examples of MOFs.[2]

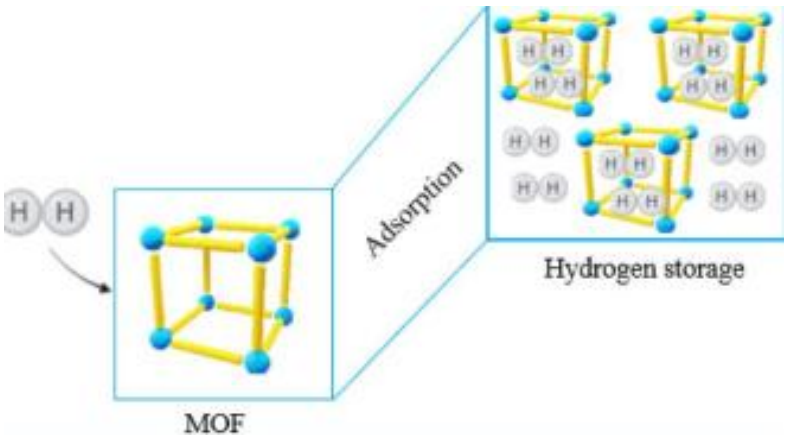

Figure 20 Diagram showing how MOFs use their adsorbent properties to capture hydrogen [2].

Because of their high crystallinity, large internal surface area (up to 6000 ˚C /g), and ultrahigh porosity (up to 90 percent free volume), MOFs materials are excellent candidates for potential clean energy applications, such as media for storing gases like hydrogen and methane. Furthermore, MOFs have good designability, tunable structures, and properties due to the diversity of metal and organic components in their structures. Nevertheless, MOFs have a low hydrogen uptake efficiency at room temperature and their production is highly complicated. Consequently, advancements in MOF fabrication technology are required [127] [128].

The MOF material that is produced after synthesis is usually offered as a powder. The use of MOFs in energy or gas storage applications may be hindered by the difficulty of incorporating powders into pertinent devices. For instance, MOFs may be easily blown off into the environment if they are added as loose powder to a tank with pipe fittings, making handling challenging and potentially contaminating the pipe fittings. Furthermore, the volumetric capacities of the pipe fittings may be jeopardized due to their low packing density. Using these methods, scientists have worked hard to shape MOFs. The fabrication strategy and anticipated textural characteristics of the MOF materials

determine which shaping technique is used. For improved hydrogen storage performance, shaped MOF materials with suitable mechanical strength, low flow resistance, intact or high secondary surface areas, and pore volumes are preferred. The polarizability of hydrogen molecules is low. Furthermore, most MOFs and hydrogen have comparatively weak interactions [111].

Storage at room temperature is still difficult, though. Researchers have been creating various strategies to improve the performance of MOF materials at higher temperatures in order to get around the restrictions on the driving ranges in fuel-cell vehicles when employing adsorption-based hydrogen storage technology. For instance, at room temperature, open metal sites within the framework can function as potent adsorption sites for hydrogen loading. The hydrogen adsorption capacity of 2.3 weight percent at 298 K and 100bar was demonstrated by the Be-BTB material with a high BET surface area of 4400 ˚C /g, which is significantly higher than that of the earlier investigations. Furthermore, adding carbon-based materials or doping with metal ions may cause a hydrogen spillover effect (HSPE), which can increase a material's room temperature hydrogen storage capacity [2].

A new approach to creating effective catalysts has been made possible by the discovery of HSPE. In particular, the HSPE has garnered a lot of interest as one of the most promising technologies for improving the ambient temperature hydrogen storage capabilities of porous materials, such as MOFs. Compared to pristine MOFs, the capacity of materials with induced hydrogen spillover was roughly five times greater. Researchers significantly improved the hydrogen storage performance by doping 10 weight percent Pt/AC catalysts into isoreticular MOF (IRMOF) materials to create a bridging spillover structure between hydrogen spillovers and carbon bridges. The IRMOF-1 and IRMOF-8 hydrogen storage capacities rose from 0point 4 to 3 weight percent and from 0point 5 to 4 weight percent at 298 K and 100 bar, respectively [2].

4.2.2 Metal hydrides/Interstitial hydrides

Because metals M can reversibly absorb H_2 at high temperatures in less than an hour, metal hydrides—solid-state materials—attracted early interest for individual transportation. The temperature, pressure, and presence of a catalyst regulate the kinetics of the dehydrogenation reaction, which yields the original metallic phase and H_2 on the same time scale. Additionally, because of the scaffolding effect of the composite, certain magnesium-based metal composite hydrides can be cycled up to 2000 times with good reversibility and minimal degradation. [129].

Hydrides are typically heavy substances with low volumetric and gravimetric densities. Additionally, because oxygen has a tendency to gradually evolve hydrogen to produce oxides, hydroxides, and carbon-oxygen compounds in the form of a surface passivation layer, they are

sensitive to both air and water (pyrophoricity). To improve the hydrogenation kinetics, this layer must be removed with H_2 at high temperatures. Common poisons are sulfur compounds as well. Lastly, these materials use a significant number of metals, and their solid state makes handling them more difficult from an industrial perspective. Depending on their composition and desorption temperature, metal hydrides can be classified as complex hydrides, high-temperature hydrides, or low-temperature hydrides [2].

Although low temperature metal hydrides, also referred to as intermetallic hydrides, have the ability to release H_2 at temperatures near room temperature and atmospheric pressure, this is both a benefit because virtually no energy is needed to capture H_2 and a disadvantage because of potential safety concerns in the event of unwanted heating. Ternary AxByHn materials are created by combining low affinity elements "B" such as Cr, Mn, Fe, Co, or Ni that function as dissociation promoters with high hydrogen affinity elements "A" such as Ca, Sc, Y, Ti, Zr, and other lanthanides. H_2 dissociates in surface H atoms during absorption and forms covalent bonds before migrating to the lattice's interstitial sites in the bulk of the material through atomic diffusion. Because the size of their interstitial sites varies with phase, the defined crystalline structures (AB5, AB2, A2B, …) are crucial to the H_2 adsorbing properties. Nevertheless, because of their mass, intermetallic hydrides typically have a maximum energy density of less than 2 weight percentH_2, well below the required 6 wt. %H_2 for mobility applications, as stated by the DOE. [130][131].

Desorption temperatures for high temperature metal hydrides must be higher than 200 °C in order to release the hydrogen atoms that are ionically bound. Because magnesium and its alloys are light, abundant, inexpensive, and have good reversibility, they are the basis for the majority of high temperature hydrides. With a high weight density of 7 wt, MgH_2 is the most researched. percentH_2. Unfortunately, because of its high stability, slow kinetics, and sensitivity to decrepitation, this material needs a temperature of at least 300 °C in order to harness H_2. By encouraging the dissociation and recombination of H_2, alloys of high temperature metal hydrides with transition metals such as Ti, V, Mn, Ni, and Fe have demonstrated enhanced thermodynamics, H_2 uptake/release kinetics, and stability [132].

4.2.3 Complex hydrides

Complex hydrides with only low molecular weight atoms have been extensively researched during the last 20 years. Their intermediate desorption temperature (100-200 °C) offers a good balance between safety and energy efficiency when compared to the desorption temperatures of low-temperature metal hydrides (room temperature to 100 °C) and high-temperature metal hydrides (200-300 °C). These desorption temperatures are attained by taking advantage of the hydrogen atom's dual role as an anion (H-dot) and cation (H^+). In fact, a combination of ionic and covalent

bonds stores H_2 in complex hydrides, which typically form tetrahedrons with hydrogen atoms at the corners and boron or aluminum at the center, with one or more spectator cations, such as Li or Na, balancing the charge. A pure metallic phase and a cation-hydride phase are usually formed during the dehydrogenation process, though this depends greatly on the metallic center [133].

Mechano-chemistry, such as ball milling, is typically used to synthesize complex hydrides, which restricts their industrialization. They also pose a significant chemical risk because they are extremely reactive when water is present and should only be used in anhydrous conditions. In addition, the absence of intermetallic compounds that lack hydrogen and the development of several phases throughout the dehydrogenation process may restrict reversibility. As a result, effective regeneration techniques are still being developed to advance this technology [133].

Depending on the metallic anion they contain, complex hydrides can be categorized. borohydrides such as $LiBH_4$ (18.5 wt.) and alanates such as $NaAlH_4$. The two essential atoms that make up B-N hydrogen carriers are nitrogen for protons and boron, which serve as a metallic center for hydrides. Initially, ammonia-borane (AB) was suggested as a substitute for borohydrides because of its high volumetric and gravimetric densities (19.4 wt. gH_2/L and percentH_2 respectively [134].

As the temperature rises, there are four more endothermic peaks in the hydrogen desorption from $LiBH_4$. Only about two peaks are released up to 275 °C, but they do occur, 1 weight percent of the 18-point 5 weight percent hydrogen theoretical maximum. The third peak at 400–680 °C (at ambient pressure) has the greatest desorption, with >9 weight percent. The final peak, which happens at temperatures too high for practical use, represents the breakdown of LiH. Consequently, the following is the total dehydrogenation reaction in the absence of LiH decomposition [135]

$$LiBH_4 \rightarrow LiH+B+32H_2 \qquad (23)$$

Similar conditions to the synthesis outlined by Friedrichs et al. are needed for the reabsorption of hydrogen. Therefore, the main drawbacks that must be eliminated or at the very least greatly reduced are the severe operating conditions and slow kinetics. Like the MH materials that were previously discussed, there are a number of ways to enhance those qualities. Three categories can be used to describe improvement techniques: using catalysts, reducing particle size to the nanoscale, and destabilizing $LiBH_4$ through metal doping. The dehydrogenation was found to be positively impacted by doping $LiBH_4$ with transitional metals (Fe, Co, Ni, Cu, Ti). Easy hydrogen desorption is made possible by the dopants' reduction of the hydrogen removal energy. Another way to destabilize the hydride and lower the desorption temperature is by partially substituting the Li+ cation or $LiZn2(BH_4)5$ $[BH_4]$ − anion (e.g. A. The $LiBH_3F$) [135]

Researchers looked into the effects of metal halides, such as ZnF_2, $TiCl_3$, and TiF_3 catalysts on $LiBH_4$'s reversibility and stability. The desorption temperature was considerably lowered from 300

°C to less than 100 °C by the listed halides, resulting in the release of 6–9 weight percent H_2. Only 3–6% of the weight could be absorbed at 500 °C and 70 bar during the subsequent re-absorption, indicating that the reversibility was still a problem. Because of the increased surface area, the kinetics were enhanced when the particle size was reduced to the nanoscale. This can be accomplished by nanoconfinement of the $LiBH_4$ particles in nanoporous scaffolds or by mechanical-force-driven physical vapor deposition (MFPVD). The reader is urged to consult Zhang et al.'s work for a more thorough summary of various enhancement techniques and resources. [135].

Ball milling NaH and Al powders and then exposing them to H_2 for one hour at 90 bar and 130 °C is a popular synthesis technique for $NaAlH_4$. This process can produce a high-purity product at a reasonable cost. High energy reactive ball milling can also be used to combine the two processes (ball milling and hydrogenation) into a one-step synthesis [135]

The following reaction occurs:

$$2NaH+2Al+3H_2 \rightleftarrows 2NaAlH_4 \qquad (24)$$

Researchers effectively illustrated how recycled Al-cans can be used to create $NaAlH_4$. NaH, a catalyst (TiF_3), and carbon nanotubes (a milling agent) were used to ball mill the recycled aluminum. According to the authors, the generated $NaAlH_4$ showed a reversible storage capacity of 3–7% weight percent at 150 °C and 100 bar H_2 pressure, which is comparable to capacities of $NaAlH_4$ made from high-purity starting materials. Although only 5 weight percent of $NaAlH_4$ has been reported in practice, the theoretical reversible gravimetric capacity is 5.5 weight percent. In order to desorb hydrogen, two reaction steps are needed, the first taking place at 30 °C and the second at 100 °C, both at 1 bar of pressure. In reality, faster kinetics are achieved by using higher operating temperatures (> 150 °C) and pressures (60–150 bar) [135].

$$3NaAlH_4 \rightleftarrows Na_3AlH_6+2Al+3H_2 \text{ (3.7 wt\%H2)} \qquad (25)$$

$$Na_3AlH_6+2Al+3H_2 \leftrightarrow 3NaH+3Al+4.5H_2 \text{ (1.8 wt\%H2)} \qquad (26)$$

Temperatures of up to 450 °C are needed for a third dehydrogenation step that further dissociates NaH, rendering it inappropriate for the majority of real-world uses. It is important to keep the materials away from water when handling them because they release flammable gases that can catch fire on their own. Additionally, the substance is poisonous and can result in severe burns to the skin. [135].

Using a Ti-catalyst ($TiCl_3$) to dope $NaAlH_4$, a study showed reversible functioning under noticeably kinder circumstances. A reversible operation at just above 100 °C and 100 bar was attained following additional research on Ti-doped systems. After the $TiCl_3$ demonstration it was successful. Only Sc was found to be promising among the trichlorides of other first-row transitional metals that

were examined. Indeed, under comparable circumstances, it was discovered that $ScCl_3$-doped $NaAlH_4$ had a higher storage capacity and a faster absorption rate (factor of 2) than $TiCl_3$-doped. The rates of desorption did not change. Sc's superiority over Ti is particularly noticeable when operating at lower pressures (10 times faster absorption rates at 50bar) [135].

Sc-doped samples, on the other hand, showed a memory effect in which a lower storage capacity was attained following a low-pressure absorption cycle than before. Additionally, the study found that Ce-doping could produce comparable absorption rates to Sc and improved cyclic stability. But in this instance, the storage capacity was smaller. Metal oxides (such as TiO_2 nanopowder and Nb_2O_5) are additional potential dopants. metal halides, such as $CeCl_3$, etc. Ti-incorporated MOF MIL-125(Ti), carbon-based materials (graphene, nanotubes, and activated carbon) and MOF-based additives. Ali et al. just released a thorough analysis of doped $NaAlH_4$ [135].

4.2.4 B-N H_2 carriers

The two essential atoms that make up B-N hydrogen carriers are nitrogen for protons and boron, which serve as a metallic center for hydrides. Initially, ammonia-borane (AB) was suggested as a substitute for borohydrides because of its high volumetric and gravimetric densities (19.4 wt. 144 gH_2/L and percentH_2 respectively). Because AB is a solid, it is dehydrogenated in the liquid phase using a protic solvent, such as methanol or water. However, oxidized dehydrogenated boron species are created as a result of this hydrolysis or alcoholysis, necessitating a rigorous regeneration process that involves the extensive use of strong hydrides or other intricate procedures. Thermolysis can be used to dehydrogenate solid AB. Depending on the reaction environment, AB can be dehydrogenated to linear, branched, or cyclic polyaminoborane species by heating it to up to 100 °C. Polymeric borazine (28) and boron nitride (29) can be formed by raising the temperature to 120–130 °C and 500 °C, respectively, producing two additional H_2 equivalents. [136].

$$nBH3 - NH3 \rightarrow [-BH2 - NH2 -]n + nH2 \quad (27)$$

$$[-BH2 - NH2 -]n \rightarrow [-BH2 = NH2 -]n + nH2 \quad (28)$$

$$[-BH2 = NH2 -]n \rightarrow [BN]n + nH2 \quad (29)$$

Due to boron nitride's high degree of stability, dehydrogenation is typically restricted to the first two stages in order to promote material regeneration, lowering the effective densities to 12.9 wt. gH_2/L and percentH_2. Furthermore, significant amounts (>20 wt) of byproducts such as ammonia and other gaseous products containing boron and nitrogen have been reported. percentage of the AB weight) as a result of AB breakdown. The mechanism of degradation is not yet completely understood, though, because it is highly reliant on the reaction conditions (solvent, solid-state, etc.). Since the solvent broke the intramolecular bond between the proton and the hydride and reduced the

carrier oxidation, AB solubilization in an aprotic solvent, such as ionic liquids, enhanced dehydrogenation. [136].

Likewise, the addition of a dopant improved the kinetics and selectivity of dehydrogenation while decreasing the induction period. Metal hydrides and AB nanoconfinement in a nanostructure behaved similarly. Lastly, heavier amidoboranes were produced by adding alkali, alkaline-earth, or metals (Al) to the AB structure. In these amidoboranes, the selectivity and dehydrogenation kinetics were improved by partially replacing the protons with a more electropositive element, but at the expense of some of the H_2 capacity. [136].

In the 1940s and 1950s, Schlesinger and Brown were two of the first to thoroughly investigate the synthesis of $LiBH_4$ and other borohydrides. One of the various synthesis pathways found is:

$$LiH+12B_2H_6 \rightarrow LiBH_4 \quad (30)$$

Brown et al. subsequently found a more useful technique by taking advantage of the cation exchange between commercial $NaBH_4$ and LiBr (or LiCl) in solvents such as tetrahydrofuran (THF) or ethyl ether (EE). After 48 hours at 25 °C in a magnetic stirrer, EE produced a 100% conversion. With THF, a complete conversion could be accomplished in 8 hours at 67°C in a mechanical stirrer. The reaction is as follows (NaBr needs to be separated after the reaction is finished) [135]:

$$NaBH_4+LiBr \rightarrow EE/THFLiBH_4+NaBr\ LiBH_4 \quad (31)$$

Friedrichs et al. have shown that Li (or LiH) and B can also be directly hydrogenated to produce $LiBH_4$. However, temperatures between 600 and 700 °C and hydrogen pressures between 70 and 350 bar are necessary because elemental B is inert. Large-scale production requires a more economical approach. The material must be handled carefully because there have been reports of flash fires when exposed to humid air [135].

As the temperature rises, there are four more endothermic peaks in the hydrogen desorption from $LiBH_4$. Only about two peaks are released up to 275 °C, but they do occur. 1 weight percent of the 18-point 5 weight percent hydrogen theoretical maximum. The third peak at 400–680 °C (at ambient pressure) has the greatest desorption, with >9 weight percent. The final peak, which happens at temperatures too high for practical use, represents the breakdown of LiH [135].

Similar conditions to the synthesis outlined are needed for the reabsorption of hydrogen. Therefore, the main drawbacks that must be eliminated or at the very least greatly reduced are the severe operating conditions and slow kinetics. Like the MH materials that were previously discussed, there are a number of ways to enhance those qualities. Three categories can be used to describe improvement techniques: using catalysts, reducing particle size to the nanoscale, and destabilizing $LiBH_4$ through metal doping [135].

A study found that doping $LiBH_4$ with transitional metals (Fe, Co, Ni, Cu, Ti) had a beneficial effect on dehydrogenation. The dopants facilitate hydrogen desorption by lowering the hydrogen removal energy. Partial substitution of the Li+ cation is another way to destabilize the hydride and lower the desorption temperature or the $[BH_4]$ −anion (e.g., $LiZn_2(BH4)5$. $LiBH_3F$). Researchers looked into the effects of metal halides, such as ZnF_2, $TiCl_3$, and TiF_3 catalysts on $LiBH_4$'s reversibility and stability. The desorption temperature was considerably lowered from 300 °C to less than 100 °C by the listed halides, resulting in the release of 6–9 weight percent H_2. Only 3–6% of the weight could be absorbed at 500 °C and 70 bar during the subsequent re-absorption, indicating that the reversibility was still a problem. Because of the increased surface area, the kinetics were enhanced when the particle size was reduced to the nanoscale. This can be accomplished by nanoconfinement of the $LiBH_4$ particles in nanoporous scaffolds or by mechanical-force-driven physical vapor deposition (MFPVD). [135]

4.2.5 Liquid organic hydrogen carrier (LOHC)

In order to store excess nuclear electricity through water electrolysis as an automotive fuel, the Liquid Organic Hydrogen Carrier (LOHC) technology was created back in the 1970s. This technology was promoted as a way to store large amounts of energy (GWh to TWh ranges) for a long period of time (seasonal) by recent advancements and environmental considerations. Similar to circular hydrogen carriers, the LOHC are liquid molecules that can load and unload H_2 at specific times and locations through catalytic hydrogenation and dehydrogenation reactions [136].

Compared to conventional physical systems, storing H_2 using covalent bonds on an organic liquid eliminates the need for bulky gas tanks and other cooling equipment while maintaining comparable volumetric densities and improving energy vector handling and safety. Another benefit of the liquid phase is that it allows the reaction to proceed without the H_2 carrier being diluted in a solvent. Furthermore, the majority of LOHCs are oil-like structures that, with minor systemic adjustments, can be readily transported by the existing oil and gas infrastructures, thereby lowering the technology's implementation costs. Because the carrier system is comparable to currently used fuels, social acceptance of the LOHC as a mobility option, is favorable. Various standards have been put forth to evaluate a LOHC's potential [136].

The dehydrogenation enthalpy value is frequently used to address energy efficiency. While the US Department of Energy (DOE) strives for 30-44 $kJ/molH_2$ so that the H_2 equilibrium pressure reaches 1 bar between -40 °C and 60 °C, classical LOHC systems have relatively high enthalpy values (between 50 and 75 $kJ/molH_2$). The volumetric and gravimetric energy densities demonstrate energy storage efficiency with ultimate targets of 6.5 wt, just like the other H_2 storage systems. $percentH_2$ and 50 gH_2/L, respectively, for an entire on-board system. To prevent the carrier from

being constantly replaced during cycling, the LOHC must also have exceptional stability (>99.9 percent). Lastly, the LOHC must also meet other requirements, including having a wide range of liquid temperatures, being readily available or simple to mass-produce from feedstock that is preferentially renewable, being expensive, having a high flow and quality of H_2 gas upon release (particularly for fuel cells), being toxic to carriers, and being biodegradable [136].

It is crucial to remember that the application and storage duration can significantly alter the LOHC's characteristics. For instance, stationary systems (off-grid systems) would be primarily motivated by the cost of the LOHC and its catalysts, whereas mobility applications for individual transportation vehicles would primarily require high gravimetric and volumetric densities, as well as a good cycling capacity and low dehydrogenation temperature. Finally, high densities and low system costs would be required for massive energy storage (seasonal storage). When compared to other technologies, the LOHC system has both advantages and disadvantages. The LOHC molecules' problematic toxicity, which is comparable to that of currently used fossil fuels, is one of the main bottlenecks. Furthermore, the development of bio-based structures would be preferred because the traditional LOHC systems are oil derivatives. Furthermore, platinum group metals (PGM) are rare and costly catalysts that are typically used in hydrogenation and dehydrogenation reactions [136].

Lastly, a significant worry is the stability of the LOHC structures, particularly following several cycles of hydrogenation and dehydrogenation. The development of the related heterogeneous catalytic systems, conditions for the hydrogenation and dehydrogenation reactions, and important molecules for the LOHC technology will be the subject of the following section of this literature review. To expand the understanding of LOHC structures, chemical functions that have the ability to store and release H_2 will also be examined. Furthermore, there is currently no standard method for comparing reactions carried out under various circumstances, such as reactor type, temperature, pressure, reaction atmosphere, catalytic loading and composition, and so forth. Consequently, it is frequently challenging to reach a readily generalized conclusion because the reaction's performance is heavily reliant on these parameters. Key points were summed up in the introduction and conclusion of each section whenever feasible [136].

4.2.5.1 Cycloalkanes

Because homocyclic structures are inexpensive and easily accessible due to their use in oil refining processes, cycloalkanes were the first structures investigated for the LOHC technology. Furthermore, the aromatization and specificity of C-H bond-breaking over C-C bond-breaking facilitates the dehydrogenation of homocyclic structures, enabling the development of selective catalytic systems since the 1910s. Most aromatic structures have dehydrogenation enthalpies between 50 and 80 kJ/ molH_2 from a thermodynamic perspective. Furthermore, conjugation reduces

the energy required for dehydrogenation in polyaromatic systems, except for anthracene-based systems, whose dehydrogenation enthalpy rises after three conjugated cycles as illustrated in **Figure 22** [137].

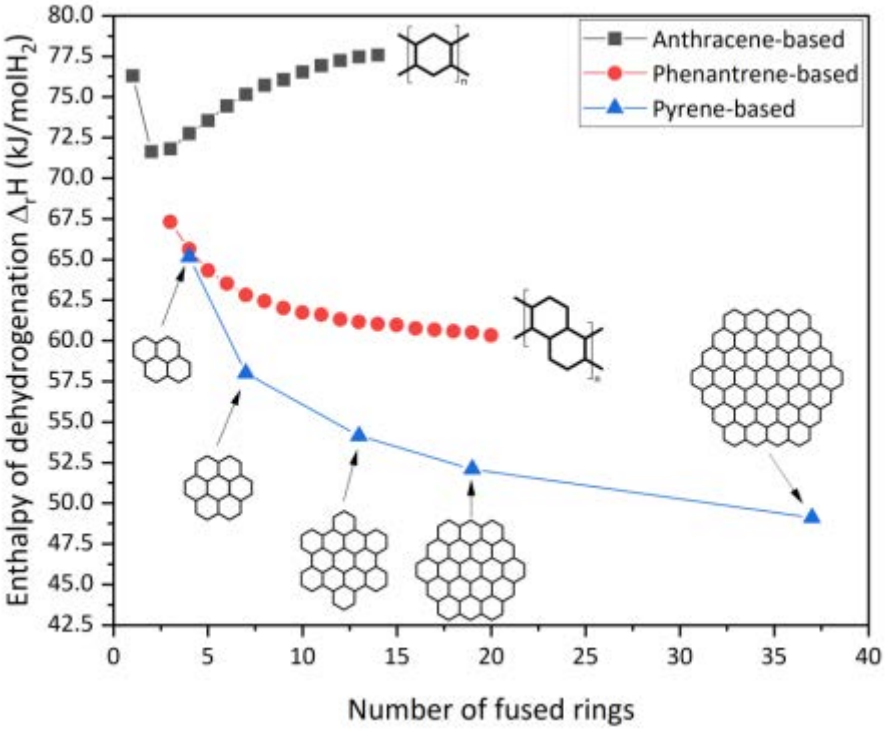

Figure 21. The PM semi-empirical method was used to calculate the dehydrogenation enthalpies as a function of the number of fused rings [137].

Intriguingly, graphene materials ought to possess the best thermodynamic characteristics of polybenzoic structures, with theoretical dehydrogenation enthalpies falling between 34 and 46 kJ/ molH$_2$. However, effective hydrogenation and dehydrogenation of such materials has not yet been accomplished because of their solid state, high fusion point, and low solubility. Furthermore, steric hindrance in fused ring systems hinders hydrogenation and dehydrogenation because it results in the formation of less reactive isomers and reactivity limitations at the ring nods due to poor accessibility. Hydrocarbons with linear bonds, on the other hand, were demonstrated to have higher kinetic activity [138].

4.2.5.1.1 Methylcyclohexane/Toluene (MCH/Tol)

Its high volumetric and gravimetric densities (resp. 6point 2 wt. MCH/Tol is frequently used as a model carrier for the LOHC technology because of its abundance, low cost (0.3 €/kg), reactive simplicity, lower toxicity compared to the cyclohexane/benzene LOHC couple, and lower computational cost compared to larger LOHC like Dibenzyltoluene [139].

Non-noble catalysts like Ni/Al_2O_3 were also able to hydrogenate Tol at atmospheric pressure with perfect selectivity at 170 °C. Because of the LOHC adsorption on the acidic sites of the surface,

hydrogenation with Pt/Al_2O_3 mixed/diluted with WO_3/Al_2O_3 and solid acids demonstrated better conversion than the pristine catalyst. This effect was also seen on a Ru/NiCo/Ni(OH)2–$Co(OH)^{2-}$ nanoislands supported on carbon catalyst, where the combination of the various sites had a ten-fold higher activity than the corresponding Ru/C catalyst and a 100% conversion in liquid phase at 60 °C in 1 hour [140].

Pt was the most active of a number of noble metal catalysts supported on nitrogen-doped carbon, with an activity order of Pt>Pd>Rh>Ir. A thorough investigation of Pt supported on perovskites and metal oxides revealed that 1 wt. Catalysts with a percentage higher than 3 weight were more effective percent catalysts, possibly as a result of the Pt nanoparticles' reduced size. By modifying the substrate by adding boron to a Pt/Al_2O_3 catalyst, strong acid sites could be tuned into weak acidic sites, reducing the formation of coke while maintaining the stability of the metal nanoparticles on the substrate. This method addressed the ineffectiveness of alkaline addition, which limited the dehydrogenation activity and indistinguishably covered all of the acidic sites. A Pt/Na-Y zeolite demonstrated that the dehydrogenation of methylcyclohexene results in hydrogenation or hydrogen transfer reactions, producing both MCH and Tol. As demonstrated by earlier contributions, toluene desorption is the step that determines the dehydrogenation rate [644].

Bimetallic catalyst synthesis is known to produce possible metal-to-metal synergistic effects. In contrast to Pt/Al_2O_3, Pt-Re/Al_2O_3 demonstrated a negligible effect of the H_2 partial pressure on the dehydrogenation rate, suggesting that the thermodynamic equilibrium had been alleviated. Single atom catalysts (SAC) have great potential to achieve high kinetics because the activity of a catalyst is typically increased by the reduction of the active metal nanoparticle. In contrast to 2.5 nm Pt NP on CeO_2 nanorods, a Pt SAC supported on CeO_2 nanorods was recently reported to catalyze both hydrogenation and dehydrogenation in continuous flow with activities 30 times higher. Liquid metal solutions such as $Ga52Pt/H_2$ could attain up to 84.5 percent selectivity to Tol by atomically dispersing Pt and optimizing the gas-liquid interface, much like Pt SAC [111].

4.2.5.1.2 Decalin/Naphtalene (Dec/Nap)

The polycyclic fused-rings molecule decalin is cheap (0.6 €/kg) and has high volumetric and gravimetric densities (7.4 wt. 66 gH_2/L and percent H_2 respectively). Naphtalene is a solid up to 80 °C, though, which suggests that the LOHC was either not fully converted or diluted in a solvent to maintain the system's liquid state according to a study. When compared to free-standing or unfused rings, multiple fused rings reduce the enthalpy of dehydrogenation. Moreover, the cycles fuse to form stereocenters, which enable the creation of cis- and transhydrogenated isomers. Remarkably, the trans-isomer has its conformation blocked and is the most stable isomer, whereas the cis isomer can experience a ring flip reaction [136].

Like the MCH/Tol couple, the ebullition temperatures of Naphtalene (218 °C) and Decalin (185 °C) are lower than the reaction temperatures for both hydrogenation and dehydrogenation, suggesting either thermodynamical limitations on the conversion in batch systems or gas-separation and/or purification.

Since nap is a homocyclic LOHC, noble metal catalysts like Ru, Pt, or Pd can typically hydrogenate it to Dec at temperatures above 200 °C. Nevertheless, the catalyst, reaction temperature, and pressure all affect which isomer forms preferentially. A series of Pt-Pd supported on $(Al_2O_3)(1-x)/(CeO_2)(x)$ (x from 0 to 0.5) catalysts used for the hydrogenation at 290 °C and 55 bar in a batch reactor demonstrated the impact of the support. The addition of CeO_2 increased the conversion to 99.5% in 3 hours, which was explained by the adsorption of Nap on acidic sites (Ce4+), changes to the acidic sites' redox characteristics, and further spillover reactions. Because the Zr, Al, or Ti dopants changed the Mo=O or Ni oxide active sites, non-noble catalysts like NiMo supported on Zr, Al, or Ti-hexagonal mesoporous silica (HMS) demonstrated selectivity to Dec, whereas the less active $NiMo/Al_2O_3$ changed Nap to the intermediate Tet [136] [4].

Because a high dehydrogenation temperature is required, Nap dehydrogenation occurs in the gas phase, just like MCH dehydrogenation. In order to get around that problem, liquid film state reactors were suggested because they prefer reactive distillation, which is known to make dehydrogenation easier than "suspended state" conditions because the dehydrogenated products are continuously removed. Either a spray pulse or a batch reaction in a large volume could produce these conditions. It should come as no surprise that Pt outperformed Pd as the metal that could catalyze the full dehydrogenation to Nap. Pt/C and Pd/C experimental dehydrogenation revealed that Pt was more active for Dec formation under the same conditions, whereas Tet formation was the opposite. DFT explained these findings, demonstrating that molecular alignment on the metallic surface was more significant than the metals' inherent activity [136].

Compared to catalysts supported on Al_2O_3, Pt supported on carbon materials demonstrated superior performance (85% conversion and 95% selectivity to Nap, 5% to Tet), possibly as a result of hydrogen spillover on the activated carbon support. 279 The dehydrogenation properties of Pt, as demonstrated in carbon nanofibers (CNF), were significantly influenced by the microstructure of the carbon support. A favorable effect was noted in the order platelet > fishbone > tube, where the platelet represents the edges of stacked graphene, and the tube represents basal graphene. DFT calculations supported these findings, demonstrating that Pt interacted more strongly with the CNF's edge planes than with the CNT's basal plane [136].

4.2.5.1.3 Perhydro-dibenzyltoluene/Dibenzyltoluene (18H-DBT/DBT)

In the 2010s, dibenzyltoluene (DBT) and its hydrogenated counterpart (18H-DBT) were suggested as a LOHC couple. Since then, the Wasserscheid group and their associates have accomplished a great deal. In terms of chemical risk, 18H-DBT and DBT are a safe couple to handle because they have a lower vapor pressure than Dec/Nap and significantly less toxicity and ecotoxicity than the MCH/Tol couple. On the other hand, the enthalpy of dehydrogenation is higher for the 18HDBT/DBT couple [141].

Lastly, because of its exceptional thermal stability, DBT is inexpensive (4 €/kg) and sold commercially as a heat-transfer oil under the brand name Marlotherm® SH. In 2017–2018, scale-up projects for the DBT technology began in both hydrogenation and dehydrogenation. A Ru/Al_2O_3 catalyst was the first to completely hydrogenate DBT in 4 hours at 150 °C and 50 bar [136].

Since K was demonstrated by DFT to favor heterolytic H_2 adsorption at low concentrations by charge transfer from Ru and the substrate, recent developments suggested a K-doped Ru supported on MgO catalyst. K and H_2 had direct interaction at higher concentrations, which reduced the catalyst activity. However, subsequent analysis of the reaction using 1H NMR and High Performance Liquid Chromatography (HPLC) also demonstrated that the hydrogenation took place on the side rings prior to the center ring [136].

Pt-based and Pd-based catalysts were initially used to dehydrogenate 18H-DBT; Pd-based catalysts were less active than their Pt-based counterparts. In comparison to Al_2O_3 and H_2, activated carbon produced the best results, demonstrating the primacy of support modification. Furthermore, the catalytic activity was further enhanced by the increased Pt surface dispersion brought about by the reduction in Pt loading. Last but not least, raising the temperature from 230 to 290 degrees Celsius improved the conversion from 16 to 92 percent in 3 to 5 hours, reaching an H_2 dehydrogenation rate on par with other cutting-edge LOHC NEthylcarbazole [136].

For modeling and designing LOHC systems with limited physical, chemical, and thermodynamical properties, the 18H-DBT/DBT couple has proven to be a great option. In order to support the process design, modeling, and engineering of the LOHC couple, thermophysical and chemical parameters of the DBT system were measured and computed. Although the hydrogenation and dehydrogenation reaction progress as a function of reaction temperature and pressure was traditionally evaluated using GC-FID and 13C NMR ex-situ follow-up techniques, machine learning was recently proposed to predict the influence of temperature, pressure, stirring speed, and relative quantities of catalyst and DBT on the H_2 storage. Using data from the literature, accuracy levels of up to 98 percent were attained [136].

4.2.5.2 N-heterocycles

Around the year 2000, a study revealed that conjugated 5-membered rings fused with 6-membered rings had a high potential for hydrogenation and dehydrogenation, and suggested N-heterocyclic from the carbazole family as LOHC because of their lower enthalpies when compared to homocyclic analogues. Clot and colleagues attributed the decrease in the enthalpy of dehydrogenation to the integration of N atoms, contingent on their quantity, location, and ring size (5 or 6) [142].

The enthalpy of dehydrogenation is significantly reduced when a N atom is added to a five-membered ring, resulting in aromaticity. Subsequent modeling revealed that the aromatic cycle was stabilized by adding electrodonating substituents, which reduced the enthalpy as a function of the Hammett parameter σ (para). Additionally, the destabilization of the αC-H bond caused by the N atom resulted in faster dehydrogenation kinetics for heterocycles than for the corresponding homocycles [136]

4.2.5.2.1 Perhydro-N-Ethylcarbazole /N-Ethylcarbazole (12H-NEC/NEC)

Carbazoles, indoles, or their derivatives are appealing for the LOHC technology because of the lower enthalpies that are favored by inductive and mesomeric donations, conjugation, and aromaticity. A study demonstrated the lower dehydrogenation enthalpy of this class of compounds compared to classic systems, as well as their ability to selectively store and unload H_2 [143].

The gravimetric densities of carbazole are high (6.7 wt. percentH_2), but its high fusion point (250 °C) is harmful because it needs to be diluted in a solvent or cannot exist as a liquid at temperatures close to room temperature. Although alkylated analogues, like N-Ethylcarbazole, have good gravimetric and volumetric densities (5.7 wt.), their much lower melting point (70 °C) makes them easier to use 63 gH_2/L and percentH_2 respectively) [137].

Additionally, the results of bimetallic catalysts such as Pd2Ru/SiCN were superior to the sum of their respective parts of Ir and the corresponding commercial Al_2O_3 or C supports. Additional research focused on lowering the amount of precious metal in the catalyst's composition. Therefore, TiO_2 with a primordial structure was used to synthesize Ru-Ni catalysts. While commercial Anatase/Rutile in a 1:4 mix produced better results than both pristine phases, Rutile was more active than Anatase but less selective. Because of a possible hydrogen spillover effect, the activity was marginally higher when Ni was added to Ru than when Ru was alone [136]

Bimetallic PdxCuy/rGO catalysts were also used to study Pd alloys containing non-noble metals. In 7 hours, Pd1.2Cu demonstrated 100% selectivity for NEC, lowering the Pd amount while being just as effective as Pd/rGO. The particle size and the amount of Cu were related to the catalytic activity:

the Pd binding energy did not change between 0 and 50% Cu replacement, suggesting catalytic activities comparable to those of pure Pd. However, above 50% Cu addition, catalytic activity decreased because of electronic transfers to Cu [136]

4.2.5.2.2 Perhydro-Phenanzine/Phenazine (12H-PHE/PHE)

Pez et al. studied polycyclic aromatic molecules with two or more N atoms in 6-membered rings up until 2012 [137]. Several structures were proposed, including phenantrolines, dipyridils, bipyrimidines, quinazoline, terpyridines, and naphtyridines.

With the exception of 4,7-phenantroline, for which Pd/C evolved more than 90% of the H_2 capacity in 8 hours at 250 °C, the majority of the systems under study were unreactive or unselective because of incomplete reactions and side-reactions like ring-opening. There was no follow-up research in the literature. A new LOHC couple, 12H-PHE/PHE, has high volumetric and gravimetric densities (7.2 wt. 69 gH_2/L and percentH_2) (II-22)). It costs 26 euros per kilogram, but it has been shown that it can be synthesized from lignin. PHE must then be diluted in solvents because it remains solid up to 172 °C [136].

The reaction requires solvent separation because Pd2Ru/SiCN fully catalyzed the hydrogenation in solvent conditions (dioxane/water) in 24 hours at 115 °C and 50 bar H_2 as well as the dehydrogenation in solvent conditions (diglyme) in 24 hours at 190 °C. Solvent-free conditions would be necessary for the 12H-PHE/PHE system to develop further, but no developments have been documented as of yet [136].

4.2.5.3 O-heterocycles

Because an O atom does not store hydrogen during hydrogenation, O-heterocycles are less advantageous than N-heterocycles. However, as demonstrated by the comparison of the dehydrogenation enthalpies carried out by [143], the addition of O atoms alters the thermodynamics of the aromatic rings in a manner comparable to that of the addition of N atoms.

While the thermodynamics gain is smaller for O-heterocycles than N-heterocycles, O-heterocycles still have lower dehydrogenation enthalpies than homocyclic LOHC and could prove useful to tune the physico-chemical properties of the LOHC and access bio-based structures. Dibenzofuran, the analogous structure of NEC, possesses high gravimetric and volumetric densities (6.7 wt.%H_2 and 67 gH_2/L). Early results presented its hydrogenation with a Ru/LiAl5O8 catalyst, yielding 90% of the hydrogenated carrier at 100 C and 60 bar H_2 and 10% of hydrogenolysized products. Here, the cleavage of the C-O bond by H_2 for O-heterocycles required the hydrogenation of the rings prior to the hydrogenolysis [137].

Furthermore, the hydrodeoxygenation of dibenzofuran using noble Pd/COK-12375 or non-noble $NiMo/Al_2O_3$ metal catalysts was documented in a number of publications. To specifically examine the metal activity for hydrogenation and hydrogenolysis, Pt, Pd, or Ru/H_2 catalysts were employed. Under the same conditions, Pt demonstrated a slower rate of hydrogenation activity but a higher selectivity to O-heterocycles, whereas Ru was the most active metal with a high hydrogenolysis capacity. The hydrogenolysis was confirmed to be caused by Ru or high H_2 pressure when dehydrogenation was carried out using a Pd/C catalyst at 225 °C and evolved 60% H_2 in 24 hours without hydrogenolysis [137].

Thus, O-heterocycles would exhibit poor cycling performances as LOHCs unless the hydrogenation is performed at low temperature and pressure using selective catalytic systems. Although no developments have been published to date, recent developments involving the selective hydrogenation (>99 percent) of eutectic mixtures containing diphenylether using a Pd/Al_2O_3 catalyst at 50 bar and 120 °C in 189 hours, and particularly a Rh/C catalyst at 20 bar H_2 and 60 °C in 18 hours, may pique interest in O-heterocycles [136].

4.2.5.4 Primary alcohol/Aldehydes-esters-carboxylic acids

Reversible hydrogenation/dehydrogenation of primary and secondary alcohols would be more suitable for the LOHC technology and open the way for readily bio-sourced LOHC structures, whereas the irreversible reforming decomposition of alcohols yields H_2. The various heterogeneous catalysts used to hydrogenate carbonyl compounds will be reviewed here, followed by a discussion of particular catalysts used to dehydrogenate ethanol (EtOH). EtOH was selected because of its chemical simplicity, which enables the study of its dehydrogenation into acetic acid (AcOH), ethyl acetate (EtOAc), and acetaldehyde (ACE) [136]

4.2.5.4.1 Hydrogenation of carbonyl compounds

Stoichiometric reduction using potent reducing agents such as LiAlH4 or boranes was the traditional method for hydrogenating carbonyl compounds to alcohol. Nevertheless, the development of stoichiometric by-products did not adhere to green chemistry guidelines, which encouraged the study of clean hydrogenation techniques. Using H_2 as a reducing agent, homogeneous catalysis was able to carry out the hydrogenation with a range of metals; however, this will not be covered in more detail [144].

It is well known that hydrogenation of aldehydes, esters, or carboxylic acids can be accomplished using heterogeneous catalytic systems based on platinum group metals (Pt, Pd, Ru, Rh, Ir, and Re). Pt/CeO_2-ZrO_2 recently catalyzed the full hydrogenation of carbonyl compounds in 2-4 hours at room temperature and 1 bar H_2. Similarly, the hydrogenation of carbonyl compounds to their

corresponding alcohols was catalyzed by noble metal-free catalysts based on Au, Cu, Ni, or Co. Since pure Cu catalysts were prone to deactivation by oxidation at high temperatures and pressures, different co-catalysts and catalysts, including B, Ce, La, Fe, In, Zn, Pd, Ag, or Au, were probed to adjust the electron density, catalyst stability, and dispersion of Cu. In particular, Cu demonstrated relevant activity for ester hydrogenation [136]

4.2.5.4.2 Primary alcohols/aldehydes

Acetaldehyde (ACE) is produced by intramolecular dehydrogenation of ethanol (EtOH) for poor gravimetric and volumetric densities of 4.3 wt.34 gH_2/L and percentH_2, respectively. Furthermore, because there is minimal stabilization of the dehydrogenated structure, the dehydrogenation enthalpy is comparable to that of homocyclic structures.

The development of Cu catalysts revealed that the support material (asbestos), the promoter (Co and Cr), and the copper salt precursor (copper nitrate) all affected the catalyst activity. 50 percent EtOH was converted to ACE with 85 percent selectivity under ideal conditions (275 °C), and 9–6% conversion to ethyl acetate and acetic acid was also noted. Furthermore, the catalyst gradually lost 14 percent of its activity after 28 hours, but H_2 allowed it to regenerate. Since then, several supporters have been tried to stabilize the active Cu NP and adjust the acidic/basic sites. Its affinity for well-dispersed Cu NP and the improved adsorption qualities encouraged by the nitrogen atoms allowed a Cu supported on N-rich carbon to achieve 98 percent selectivity to ACE [145].

Then, as the Si-OH groups encouraged the NP's dispersion, H_2/SiC and C/SiC supports were created. The enhanced desorption capabilities of the C/SiC support prevented side-reactions, which made it beneficial. When Cu/H_2/SiC and Cu/C/SiC were compared at 280 °C, the former had the best conversion rate (81 percent vs. 66 percent, respectively). but the latter was the most selective (94 percent versus 99 percent, respectively). The O-H EtOH bond breaking on support acidic sites was found to be the rate-determining step in the testing of metal oxides and HT structures as supports for Cu [146].

4.2.5.4.3 Primary alcohols/Carboxylic acids

The dehydrogenation of equimolar ethanol-water solutions yields acetic acid (AcOH), a potential LOHC with densities of 6point-3 wt. Rh/C in a closed vessel with 2.2 equivalents of base in H_2O at 100 °C under Ar produced the first example of heterogeneous acceptorless dehydrogenation, which yielded 100% conversion but limited selectivity (Rh>Pt>Ru/C). percentH_2 and 54 gH_2/L had lower dehydrogenation enthalpies than homocyclic and heterocyclic systems. The reactivity order NaOH>KOH>LiOH>Na_2CO_3>$NaHCO_3$>no base was also used to examine the impact of the base. To aid in the removal of H_2, the reaction was also carried out at 80 °C and lower pressure (0–8 bar). In six hours, quantitative yields were obtained from reactions on benzylic alcohols and aliphatics. [136]

Catalysts free of noble metals were also created. At 164 °C, ZnO and two equivalents of KOH catalyzed the conversion in 36 hours, producing 65–85% yields for the aliphatic product, and in 18 hours, comparable yields for the benzylic alcohols. The reaction pathway started with a zinc alkoxide species, which underwent a Tishchenko mechanism to further dehydrogenate into aldehydes and esters. Additionally, benzylic alcohol was cleanly converted to the corresponding carboxylic acids using 424 Co catalysts. In 24 hours at 100 °C, Co/N-doped CNT completely converted benzyl alcohol with 99 percent selectivity for the carboxylic acid. Aliphatic alcohol conversion was typically slower, but increasing the base amount and time produced good yields (>80%) [136]

4.2.5.4.4 Primary alcohols/Esters

Primary alcohols can be esterified through intramolecular reactions or intermolecular reactions involving homocoupling-A and heterocoupling -B variations. Cu/Cr_2O_3 catalyzed the formation of EtOAc with 95% selectivity at 200 °C, demonstrating the influence of Brønsted acid sites on selectivity, as did Cu-Cr catalysts that demonstrated high conversion and selectivity. In order to create a $CuCrO_4/CuO/Cu/BaCrO_4/Al_2O_3$ catalyst, additional catalytic development involved doping alumina with BaCrO4. This enhanced the EtOH conversion to 65–70 percent and the selectivity above 98 percent at 220 °C and 20 bar in flow conditions [136]

Dehydrogenative cross-esterification is a difficult and relatively new process. In fact, it was challenging to overcome homocoupling when combining two distinct primary alcohols, even though process techniques like drop-wise addition make it easier for a primary alcohol to cross-couple with a secondary or tertiary alcohol. A mixture of symmetrical and asymmetrical esters was produced despite attempts at direct cross-esterification using heterogeneous transition metal sulfides MoS2 and WS2 at 230 °C, which achieved a 52 percent conversion in 24 hours under 5 bar He pressure [136].

4.2.5.4.5 Secondary alcohols/Ketones

Due to their abundance in nature, ketones and secondary alcohols are of great interest for the production of LOHC from renewable feedstock. Additionally, the industrial production of acetone and isopropanol (IPA) amounts to over 8 million tons, demonstrating their accessibility. However, the volumetric and gravimetric densities of IPA are moderate (3.3 wt. as well as dehydrogenation enthalpy comparable to homocyclic systems, as well as percentH_2 and 26 gH_2/L). In addition, secondary alcohols are easier to store and recycle because they are less susceptible to overoxidation than primary alcohols. They are susceptible to aldolization in alkaline environments and can be highly reactive with peroxides [136].

When tested in the liquid film state, Ru and Ru-Pt supported on activated carbon demonstrated an enhanced conversion from 5 to over 85 percent in 2 hours at 100 °C because of a better

thermodynamic equilibrium displacement. A subsequent study described an enhanced configuration that used a Ni Raney catalyst to evolve up to 5 LH_2/h [136]

4.2.5.5 Alcohol and amine couplings

Various chemical motives, including amides, ureas, imides, or carbamides, can be produced by alcohol and amine couplings, allowing for the creative design of alternative structures for the LOHC technology. Amino acids may also serve as platform chemicals for the synthesis of bio-based, renewable O, NLOHC. Thanks to the amazing work of the Milstein group, amides, carbamides, and imides have already been successfully produced reversibly by the dehydrogenation/hydrogenation of alcohols and amines in homogeneous conditions, even though no heterogeneous catalyst has been reported to date [136]

A Ru PNN-pincer was the first catalyst to accomplish the dehydrogenative coupling of a primary amine and a primary alcohol to an amide, with up to 99 percent yield in 8 hours at 110 °C in toluene for both aromatic and aliphatic compounds. Applications for amide synthesis include polymer synthesis and bioengineering of polypeptides dot. The reaction of esters to amides by amine addition did not show any conversion. Ru-NHC, Ru-PNN, and Ru-PNP pincer-type catalysts were developed in subsequent articles to improve conversions and selectivity on a broad range of substrates. The amides were produced in yields ranging from 70 to 98 percent in 24 hours at 110 °C under diluted conditions, and the majority of Ru-pincer systems required a basic additive, frequently KOtBu or NaH. Carbamides are present in many natural chemicals, including urea. Subsequent research revealed a Ru PNP-pincer catalyst that could hydrogenate and dehydrogenate in solvent-free conditions with 76 percent and 60 percent yields, respectively 492. Further development also lowered the temperature of dehydrogenation to 35 to 55 °C. Ethylendiamine and methanol were acceptorlessly dehydrogenated with Ru PNPto accomplish their synthesis [136]

Imides, particularly aromatic imides, are highly prized in high-added value niche applications like electronics parts and are crucial intermediate synthesis for the creation of pigments. Although Pez et al. (2008) made an early attempt to hydrogenate cyclic imides. was shown to be ineffective at 170 °C using a heterogeneous Ru/LiAl5O8 catalyst. More recently, Mn and Ru PNN pincer catalysts were found to produce cyclic imides by dehydrogenating BDO with amines. According to preliminary findings, BDO was dehydrogenated with a range of amines in 60–99% yields in 40 hours at 110 °C using a Mn PNN-pincer catalyst and KH as an additive [147].

4.2.5.6 Amines/Nitriles

Pez et al. [143] suggested that the primary amine/nitrile function stores H_2. 220 and subsequently theorized 500 as a system that can store up to 13.3 weight of hydrogen. The best gravimetric

densities of traditional homocyclic LOHC are essentially doubled by percentH_2. Specifically, LOHC pairs such as 1,3-propanediamine/Malononitrile have the potential to achieve extraordinarily high volumetric and gravimetric densities (10.8 wt. 95 gH_2/L and percentH_2 respectively) at the expense of elevated toxicity and reaction enthalpy [143].

The less active Raney nickel and copper chromite are still used in industry because of their lower cost, even though many catalytic systems have been developed, including colloidal Pd, Ni Raney, Pt oxide, Raney Co, Cu2Cr2O5, supported platinum group metals metals, metal borides, and metal alloys. However, the development of non-noble transition metals Ni, Co, Cu, and Fe heterogeneous catalysts was aided by their problematic toxicity. Curiously, the majority of modern systems hydrogenated in the presence of ammonia to thermodynamically counteract the transamination reaction that yielded the dialkyl and trialkylamine compounds. Specifically, in 5 hours at 100 °C and 13 bar H_2 in ethanol, Ni/H_2 accomplished full conversion and 84 percent selectivity to the monoalkylamine [136].

Due to imine couplings, an early example of amine dehydrogenation using a Mo catalyst demonstrated amine dehydrogenation with disproportionation and achieved nitrile selectivity below 5%. Since then, no solvent-free selective heterogeneous catalyst has been documented for this reaction. Ru and Ir pincer catalysts were used in subsequent research to regulate the active center. When a base is present as a co-catalyst, the homogeneous catalysts have demonstrated great promise in catalyzing the reaction [136].

4.2.5.7 S-containing LOHC

Due to their high propensity to undergo hydrodesulphurization in the presence of H_2 and to significantly reduce the noble metal catalyst activity through irreversible binding, S-containing LOHC have frequently been disregarded. Toluene and naphtalene were hydrogenated with Pt-Pd/H_2-Al_2O_3 in the presence of dibenzothiophene in early attempts; however, no analysis was done on the products that were produced. Hydrogenation with Ru/C produced no dibenzothiophene conversion, and no subsequent study has documented it [136]

4.2.5.8 B, N-containing LOHC

The 1,2-Dihydro-1,2-azaborine/1,2-BN-Cylcohexane couple is the cutting edge of ammonia-borane and LOHC technologies, which theoretically have a 9.4 weight storage capacity. %H_2 in the event that the system is fully dehydrogenated from the perspective of ammonia-borane, 1,2-BN-cylcohexane can go through a trimerization process and intramolecular dehydrogenation on the B-N moiety. The analogous aromatic compound can be formed on the LOHC side by dehydrogenating the trimer's carbon atoms [136].

The monocyclic aromatized structure underwent two stages of hydrogenation. The carbon atoms were directly hydrogenated in 4 hours at 80 °C and 3 bar H_2, producing the hydrogenated cycle in 89 percent NMR yield and 99 percent GCMS yield. In order to obtain their hydrogenated form in quantitative yields, the B and N atoms underwent more complex hydrogenation processes that involved hydride (KH) and acid (HCl) treatments, respectively [136].

4.2.5.9 Si-containing LOHC

When silanes and alcohol are present, H_2 evolved, and an alkoxysilane is the byproduct. SiH4 with MeOH (5.0 wt) is the possible best monosilane system. SiH4 is a gas, but percentH_2 is not. The PhMe2SiH-Methanol couple, which has a pitiful gravimetric density of just 0.7 wt percentH_2, has been the basis for the majority of research to date. Tetrasilylmetane-Methanol could potentially reach a gravimetric density of 8.82 wt, and polysilanes have since been proposed as more effective storage systems. percentH_2 and 70 gH_2/L (based on methanol density) [136]

Analogous to alkoxy-boron, the high stability of alkoxy-silane makes their regeneration problematic. Although direct hydrogenation using heterogeneous catalysts has not yet been accomplished, there have been reported advancements. Originally, borane species were employed with sacrificial reagents like $NaBH_4$ and Ethylbromide, or traditional reducing agents like LiAlH4 546. The regeneration of silyl triflates with 4 bar H_2 and an Ir catalyst in the presence of a base, which achieved a 95 percent conversion at 60 °C in 48 hours, demonstrates how new processes are beginning to emerge [136].

In contrast, dehydrogenation is exothermic for LOHC couples. Using water as a proton source and a heterogeneous Ag/Hydroxyapatite catalyst, the first silane dehydrogenation examples were completed in 15 minutes. Nevertheless, it was challenging to regenerate the obtained Si-OH species using conventional techniques, and Si-O-Si species were also produced. Polysilanes and Methanol coupling under Bu4NF activation achieved an impressive 100 percent conversion at 25 °C in 10 s.. The reaction activity was linked to the steric hindrance of the alcohol, and diols could also be used on dihydrides silanes with yields superior to 90 percent at 60-90 °C. H_2 was also released in catalyst-free conditions using Silane and Sodium methoxide at room temperature in 15 s. Newer catalytic systems that could achieve superior conversion and stability on stream for one hour were based on Ru and Ircomplexes supported on rGO. In order to accomplish the full dehydrogenation of PhMe2SiH in 9 hours at 110 °C, a heterogeneous Cu-doped ZIF-8 zeolite was finally suggested [136]

4.2.6 Circular hydrogen carriers

Through chemical bonds with small gaseous molecules like N2 or H_2, circular hydrogen carriers store H_2 to create ammonia or methanol, respectively. Circular H_2 carriers' primary benefit is their practical transportation capabilities, which enable the production of H_2 at a convenient location

where the lean carrier can be captured prior to recycling. Furthermore, the hydrogenated carriers are valuable chemicals that can be utilized directly in chemical reactions; however, in that scenario, H_2 cannot be recovered. The primary concern is large-scale gas handling and the required gas separation and purification of the lean-carriers from H_2 during the dehydrogenation process [136]

4.2.6.1 Ammonia (NH_3)

For the production of fertilizers, ammonia (NH_3) is a valuable chemical that can serve as an energy vector and store H_2 in liquid form with good gravimetric (17.8 wt. percentH_2) and volumetric (107 gH_2/L) densities at room temperature under pressure of 8–6 bar. The Haber-Bosch process, which will generate about 185 million tons of NH_3 annually in 2020, ensures current production. With a low conversion of 15% per pass, NH_3 is created from N2 and H_2 under extreme temperature and pressure conditions, necessitating multiple reactant cycles to reach full conversion [136]:

$$N_2 + 3\ H_2 \rightarrow NH_3 \qquad (32)$$

Furthermore, fossil fuels provide the majority of the H_2 produced today. Consequently, this industrial process produces 3 equivalents of H_2 for every 8 equivalents of NH_3 and uses 1 to 2 percent of the world's annual energy production. However, since this process is nearly fully optimized, the only ways to mitigate H_2 are to develop low-carbon H_2 sources (water electrolysis rather than SMR) and to use CCS. To develop a better disrupting process, new ammonia production methods are also being researched. The current alternatives—which can be made directly from N_2 with water, in a two-step process where N_2 reacts with H_2 produced by electrolysis, or in a Li-mediated three-step cycle where the hydrolysis of Li3N facilitates the production of NH_3—require high electrical input and/or temperatures in order to produce ammonia via electrochemistry. These new procedures still require a lot of energy, and it is still unclear if they will be scalable.

Due to the endothermic nature of the process, ammonia decomposition has historically been accomplished at high temperatures (>400 °C) on Fe or Ru transition metal catalysts supported on alumina.

$$NH_3 \rightarrow N_2 + 3H_2\ ,\ \Delta H = 46\ kJ/mol \qquad (33)$$

The desorption of N2, which depends on the active metal, the support (basic and conductor like Al_2O_3, MgO, CNT, …), and promoters, determines the rate of decomposition. The NH_3-PEM incompatibilities (high decomposition temperature, membrane poisoning, catalyst cost, NH_3 toxicity, and corrosivity) limit the use of NH_3 as an H_2 carrier, despite its promising performance. Nevertheless, a SOE fuel cell can help to mitigate these NH_3-PEM incompatibilities. Lastly, massive energy transportation may be the most useful use of NH_3 [136].

4.2.6.2 Methanol (MeOH)

Since many important industrial processes depend on methanol to create high-value chemicals like formic acid, formaldehyde, esters, ethers, olefins, and others, it is one of the most produced chemicals in the world, with up to 164 million tons produced annually. In the so-called "Methanol Economy," MeOH has also been suggested as a fuel that is comparable to bioethanol. MeOH has good gravimetric and volumetric densities of 12.5 wt, which is important for H_2 storage. 99 gH_2/L and percentH_2. Furthermore, because it only contains one carbon, β-elimination is impossible, which reduces the number of possible side-reactions

Since the 1960s, there have been numerous reports and patents on the production of methanol from CO or H_2 using Cu-based catalysts at high temperatures (300–450 °C) [136]:

$$CO + 2\ H2 \rightarrow CH3OH;\ \Delta H = -90.8\ kJ/mol \quad (34)$$

$$CO2 + 3\ H2 \rightarrow CH3OH + H2O;\ \Delta H = -49.2\ kJ/mol \quad (35)$$

Nonetheless, the severe temperature conditions employed in these procedures advanced the study of procedures with softer settings. These days, new methods for producing MeOH from H_2 are appearing, such as gas-solid phase, amine/alkaline or acid-assisted H_2 reaction, biogenic synthesis, and formic acid disproportionation. However, the scalability of these methods has not yet been proven. Water is necessary for the multi-step process of MeOH non-oxidative dehydrogenation. Following the addition of water, two additional H_2 equivalents can be recovered to produce H_2. The first H_2 equivalent can be recovered by dehydrogenating to formaldehyde

$$CH_3OH \rightarrow CH_2O + H_2\ ;\ \Delta H = 85\ kJ/mol \quad (36)$$

$$H_2CO + H_2O \leftrightarrow CH_2\ (OH2\ ) \rightarrow HCOOH + H_2\ ;\ \Delta H = -21\ kJ/mol \quad (37)$$

$$HCOOH \rightarrow CO_2 + H2\ ;\ \Delta H = -31\ kJ/mol \quad (38)$$

At temperatures above 200 °C, Co, Ni, Cu, Pd, Ru, or Ir heterogeneously catalyze the dehydrogenation. However, PEM fuel cells may die as a result of CO by-production during the dehydrogenation process. Because of their slow kinetics and fuel permeation through the membrane, direct methanol fuel cells produce less energy. MeOH has a few obstacles to overcome despite its good biodegradability and compatibility with existing infrastructures. Its low point of ebullition (64point 7 °C) and potential flammability and toxicity make it too hazardous for general public use [136].

Chapter 5

Conclusions

H_2 has become a viable and sustainable alternative energy source with a wide range of uses in industries and transportation. By concentrating on effective and environmentally friendly techniques, significant advancements in H_2 production technologies have been made. One of these innovations is the electrolysis process, which produces H_2 using renewable energy sources like solar and wind power. The use of innovative catalysts and materials for increased H_2 production through a variety of pathways, including H_2O-splitting, biomass conversion, and microbial processes, are other recent developments. These developments in H_2 production help to lower GHG emissions and open the door to a more carbon-neutral and sustainable future. Numerous techniques and technologies are being investigated in the complicated and multidisciplinary field of H_2 storage. The field of H_2 storage is undergoing continuous research and development to increase its effectiveness, safety, and affordability.

Hydrogen emissions can significantly hinder the climate benefits of decarbonization strategies involving clean hydrogen, especially in the initial decades after implementation. Therefore, it's crucial to focus on understanding hydrogen's indirect climate effects and improving estimates of hydrogen emissions throughout the value chain. Reducing leakage is vital to ensuring hydrogen's effectiveness as a climate mitigation strategy. Additionally, preventing leakage is often easier when designing new systems rather than retrofitting existing ones, offering a unique chance to address this issue before widespread infrastructure deployment.

In order to minimize hydrogen's warming effects and enhance climate benefits in a future hydrogen economy have to be taken action as:

- Advance research on hydrogen's indirect radiative effects and temperature responses by incorporating interactive emissions, chemistry, and radiation parameterizations in further coupled chemistry climate models and simplified climate models.
- Use climate metrics and models that accurately reflect hydrogen's potential role in achieving net-zero goals within the desired timeframes, potentially adopting a dual GWP-20/GWP-100 approach rather than relying solely on GWP-100.
- Improve the measurement of hydrogen leakage rates by developing field-deployable technologies capable of detecting hydrogen emissions at low thresholds (ppb level).

- Consider the likelihood of hydrogen leakage and its impacts when making decisions about hydrogen deployment, such as co-locating production and end-use applications.
- Identify leakage mitigation measures and best practices before developing infrastructure.

To tackle the climate challenge effectively, it's essential to examine each decarbonization pathway using robust and appropriate metrics and data. The near- and medium-term warming impacts of hydrogen emissions are greater than commonly perceived. These impacts should be explicitly and quantitatively addressed to maximize the climate benefits of transitioning from fossil fuels to hydrogen. By taking a proactive, scientific approach to understanding and addressing hydrogen leakage, we can help ensure that the global shift to hydrogen delivers its promised climate benefits over all timescales.

References

1. Osman, A.I., Mehta, N., Elgarahy, A.M. *et al.* Hydrogen production, storage, utilisation and environmental impacts: a review. *Environ Chem Lett* **20**, 153–188 (2022). https://doi.org/10.1007/s10311-021-01322-8

2. Le, T.H.; Kim, M.P.; Park, C.H.; Tran, Q.N. Recent Developments in Materials for Physical Hydrogen Storage: A Review. Materials 2024**,** 17**,** 666. https://doi.org/10.3390/ma17030666

3. Mulky, L., Srivastava, S., Lakshmi, T., Sandadi, E. R., Gour, S., Thomas, N. A., Priya, S. S., & Sudhakar, K. (2024). An overview of hydrogen storage technologies – Key challenges and opportunities. *Materials Chemistry and Physics*, *325*, 129710. https://doi.org/10.1016/j.matchemphys.2024.129710

4. Q Xu, G Qian, S Yin, C Yu, W Chen, T Yu, L Luo, Y Xia, P Tsiakaras, Design and synthesis of highly performing bifunctional Ni-NiO-MoNi hybrid catalysts for enhanced urea oxidation and hydrogen evolution reactions, ACS Sustainable Chemistry & Engineering 8 (18), 7174-7181, 2020

5. Hirscher, M., Yartys, V. A., Baricco, M., Von Colbe, J. B., Blanchard, D., Bowman, R. C., Broom, D. P., Buckley, C. E., Chang, F., Chen, P., Cho, Y. W., Crivello, J., Cuevas, F., David, W. I., De Jongh, P. E., Denys, R. V., Dornheim, M., Felderhoff, M., Filinchuk, Y., . . . Zlotea, C. (2019). Materials for hydrogen-based energy storage – past, recent progress and future outlook. *Journal of Alloys and Compounds*, *827*, 153548. https://doi.org/10.1016/j.jallcom.2019.153548

6. Suárez S. H., D. Chabane, A. N'Diaye, Y. Ait-Amirat and A. Djerdir, "Feasibility of efficiency improvement in a fuel cell system powered by a metal hydride tank," *IECON 2022 – 48th Annual Conference of the IEEE Industrial Electronics Society*, Brussels, Belgium, 2022, pp. 1-6, doi: 10.1109/IECON49645.2022.9968539.

7. Roy, Poulomo, and S. K. Srivastava. *Nanomaterials for Electrochemical Energy Storage Devices*. Cambridge, MA: Hoboken, NJ: Scrivener Publishing; Wiley, 2019

8. D Medvedev, V Maragou, E Pikalova, A Demin, P Tsiakaras, Novel composite solid state electrolytes on the base of BaCeO3 and CeO2 for intermediate temperature electrochemical devices, Journal of power sources 221, 217-227, 2013

9. J Lyagaeva, D Medvedev, A Demin, P Tsiakaras, Insights on thermal and transport features of BaCe0. 8− xZrxY0. 2O3− δ proton-conducting materials, Journal of Power Sources 278, 436-444, 2015

10. L.A Dunyushkina, A.A Pankratov, V.P. Gorelov, A, Brouzgou, P. Tsiakaras, Deposition and Characterization of Y-doped $CaZrO_3$ Electrolyte Film on a Porous $SrTi_{0.8}Fe_{0.2}O_{3-\delta}$ Substrate, Electrochimica Acta, 202, 39-46, 2016.

11. Ocko Ilissa B. and Steven P. (2022) Hamburg Climate consequences of hydrogen emissions, *Atmos. Chem. Phys*., 22, 9349–9368

12. S Song, V Maragou, P Tsiakaras, How far are direct alcohol fuel cells from our energy future?, J. Fuel Cell Sci. Technol. 4(2): 203-209, 2007

13. Gan, B., Li, Y., & Wu, Y. (2023). A comparison study between the lithium sulphur battery and fuel cell in new energy vehicle applications. *Journal of Physics Conference Series*, *2649*(1), 012063. https://doi.org/10.1088/1742-6596/2649/1/012063

14. FA Coutelieris, S Douvartzides, P Tsiakaras, The importance of the fuel choice on the efficiency of a solid oxide fuel cell system, Journal of Power Sources 123 (2), 200-205, 2003

15. GM Andreadis, AKM Podias, PE Tsiakaras, The effect of the parasitic current on the direct ethanol PEM fuel cell operation, Journal of Power Sources 181 (2), 214-227, 2008

16. CG Vayenas, S Bebelis, IV Yentekakis, P Tsiakaras, H Karasali, Non-faradaic electrochemical modification of catalytic activity reversible promotion of platinum metals catalysts, Platinum Metals Rev 34 (3), 122, 1990

17. C Molochas, P Tsiakaras, Carbon Monoxide Tolerant Pt-Based Electrocatalysts for H2-PEMFC Applications: Current Progress and Challenges, Catalysts 11 (9), 1127, 2021

18. P Tsiakaras, CG Vayenas, Oxidative coupling of CH4 on Ag catalyst-electrodes deposited on ZrO2 (8 mol% Y2O3), Journal of Catalysis 144 (1), 333-347, 1993

19. E Gorbova, V Maragou, D Medvedev, A Demin, P Tsiakaras, Influence of sintering additives of transition metals on the properties of gadolinium-doped barium cerate, Solid State Ionics 179 (21-26), 887-890, 2008

20. Tsiakaras P., C. Athanasiou, G. Marnellos, M. Stoukides, J.E. ten Elshof. Methane activation on aLa0.6Sr0.4Co0.8Fe0.2O3 perovskite: Catalytic and electrocatalytic results. *Applied catalysis A:General 169 (2)*, 249-261, 1998.

21. A Tan, Y Wang, Z Fu, P Tsiakaras, Z Liang, Highly effective oxygen reduction reaction electrocatalysis: Nitrogen-doped hierarchically mesoporous carbon derived from interpenetrated nonporous metal-organic frameworks, Applied Catalysis B: Environmental 218, 260-266, 2017

22. R Wu, P Tsiakaras, PK Shen, Facile synthesis of bimetallic Pt-Pd symmetry-broken concave nanocubes and their enhanced activity toward oxygen reduction reaction, Applied Catalysis B: Environmental 251, 49-56, 2019

23. SL Douvartzides, FA Coutelieris, PE Tsiakaras, On the systematic optimization of ethanol fed SOFC-based electricity generating systems in terms of energy and exergy, Journal of Power Sources 114 (2), 203-212, 2003

24. Y Wang, C He, A Brouzgou, Y Liang, R Fu, D Wu, P Tsiakaras, S Song, A facile soft-template synthesis of ordered mesoporous carbon/tungsten carbide composites with high surface area for methanol electrooxidation, Journal of power sources 200, 8-13, 2012

25. K Wang, Y Wang, Z Liang, Y Liang, D Wu, S Song, P Tsiakaras, Ordered mesoporous tungsten carbide/carbon composites promoted Pt catalyst with high activity and stability for methanol electrooxidation, Applied Catalysis B: Environmental 147, 518-525, 2014

26. D Liu, A Barbar, T Najam, MS Javed, J Shen, P Tsiakaras, X Cai, Single noble metal atoms doped 2D materials for catalysis, Applied Catalysis B: Environmental 297, 120389, 2021

27. GM Andreadis, AKM Podias, PE Tsiakaras, The effect of the parasitic current on the direct ethanol PEM fuel cell operation, Journal of Power Sources 181 (2), 214-227, 2008

28. G Andreadis, S Song, P Tsiakaras, Direct ethanol fuel cell anode simulation model, Journal of Power Sources 157 (2), 657-665, 2006

29. A Brouzgou, S Song, P Tsiakaras, Carbon-supported PdSn and Pd3Sn2 anodes for glucose electrooxidation in alkaline media, Applied Catalysis B: Environmental 158, 209-216, 2014

30. A. Kalyakin, G. Fadeyev, A. Demin, E. Gorbova, A. Brouzgou, A. Volkov, P Tsiakaras, Application of Solid oxide proton-conducting electrolytes for amperometric analysis of hydrogen in H_2+N_2+H_2O gas mixtures, Electrochimica Acta 141, 120-125, 2014.

31. Luo, C., Xie, H., Wang, Q., Luo, G., & Liu, C. (2015). A review of the application and performance of carbon nanotubes in fuel cells. Journal of Nanomaterials, 2015,44. https://doi.org/10.1155/2015/560392

32. Murata, S., Imanishi, M., Hasegawa, S., & Namba, R. (2014). Vertically aligned carbon nanotube electrodes for high current density operating proton exchange membrane fuel cells. Journal of Power Sources, 253, 104–113. https://doi.org/10.1016/j.jpowsour.2013.

33. Huang, L., Wei, M., Qi, R., Dong, C. L., Dang, D., Yang, C. C., Xia, C., Chen, C., Zaman, S., Li, F., You, B., & Xia, B. Y. (2022). An integrated platinum-nanocarbon electrocatalyst for efficient oxygen reduction. Nature Communications, 13(1), 6703. https://doi.org/10.1038/s41467-022-34444-w

34. Amin, R., Kumar, P. R., & Belharouak, I. (2020). Carbon nanotubes: Applications to energy storage devices. Carbon Nanotubes-Redefning the World of Electronics, 10**,** 5772–94155. https://doi.org/10.5772/intechopen.94155

35. Agrawal, P., Ebrahim, S., & Ponnamma, D. (2024). Advancements in nanocarbon-based catalysts for enhanced fuel cell performance: a comprehensive review. *International Journal of Energy and Water Resources*. https://doi.org/10.1007/s42108-024-00324-w

36. Verma, S., Sinha-Ray, S., & Sinha-Ray, S. (2020). Electrospun CNF supported ceramics as electrochemical catalysts for water splitting and fuel cell: A review. Polymers, 12(1), 238. https://doi.org/10.3390/polym12010238

37. Shen, A., Zou, Y., Wang, Q., Dryfe, R. A., Huang, X., Dou, S., Dai, L., & Wang, S. (2014). Oxygen reduction reaction in a droplet on graphite: Direct evidence that the edge is more active than the basal plane. Angewandte Chemie, 126(40), 10980–10984. https://doi.org/10.1002/anie.201406695

38. Hu, C., & Dai, L. (2019). Doping of carbon materials for metal-free electrocatalysis. Advanced Materials, 31(7), 1804672. https://doi.org/10.1002/adma.201804672

39. Tao, L., Wang, Q., Dou, S., Ma, Z., Huo, J., Wang, S., & Dai, L. (2016). Edge-rich and dopant-free graphene as a highly efcient metalfree electrocatalyst for the oxygen reduction reaction. Chemical Communications, 52(13), 2764–2767. https://doi.org/10.1039/C5CC09173J

40. Valenzuela-Muñiz, A. M., Alonso-Nuñez, G., Botte, G. G., MikiYoshida, M., & Verde-Gomez, Y. (2014). Infuence of nickel on the electrochemical activity of PtRu/multiwalled carbon nanotubes electrocatalysts for direct methanol fuel cells. Journal ofApplied Electrochemistry, 44**,** 695–700. https://doi.org/10.1007/
s10800-014-0679-x

41. Vengrenovich, R. D., Ivanskii, B. V., Panko, I. I., Yarema, S. V., Kryvetskyi, V. I., & Stasyk, M. O. (2014). Ostwald ripening of the platinum nanoparticles in the framework of the modifed LSW theory. Journal of Nanomaterials, 2014, 138–138. https://doi.org/10.1155/2014/821584

42. Kumar, D., Abraham, J. E., Varghese, M., George, J., Balachandran, M., & Cherusseri, J. (2024). Nanocarbon assisted green hydrogen production: Development and recent trends. International Journal of Hydrogen Energy, 50, 118–141. https://doi.org/10.1016/j.ijhydene.2023.07.257

43. Timofeeva, E. V., Segre, C. U., Pour, G. S., Vazquez, M., & Patawah, B. L. (2023). Aqueous air cathodes and catalysts for metal–air batteries. *Current Opinion in Electrochemistry*, *38*, 101246. https://doi.org/10.1016/j.coelec.2023.101246

44. Pavlov, D. (2017) Lead-Acid Batteries: Science and Technology. 2nd Edition, Elsevier, Amsterdam

45. Otto, J. Lead Acid Type Storage Battery. Google Patents US3257237A, 1966

46. Beaudin, M.; Zareipour, H.; Schellenberglabe, A.; Rosehart, W. Energy storage for mitigating the variability of renewable electricity sources: An updated review. Energy Sustain. Dev. 14, 302- 314, 2010

47. McKeon, B.B.; Furukawa, J.; Fenstermacher, S. Advanced Lead-Acid Batteries and the Development of Grid-Scale Energy Storage Systems. Proc. IEEE. 102, 951-963, 2014

48. Hage, D.S. Reference Module in Chemistry, Molecular Sciences and Chemical Engineering; Elsevier Inc.: Amsterdam, The Netherlands, 2013.

49. Zelinsky, M.; Fetcenko, M.; Kusay, J.; Koch, J. Storage-integrated PV systems using advanced NiMH battery technology. In Proceedings of the Fifth International Renewable Energy Storage Conference (IRES 2010), Berlin, Germany, 2010

50. Poullikkas, A. A comparative overview of large-scale battery systems for electricity storage. Renew. Sustain. Energy Rev. 27, 778-788, 2013.

51. Avril, S.; Arnaud, G.; Florentin, A.; Vinard, M.Multi-objective optimization of batteries and hydrogen storage technologies for remote photovoltaic systems. Energy. 35, 5300-5308, 2010

52. Moeller, K.-C. Overview of battery systems. In Lithium-Ion Batteries: Basics and Applications; Springer Science and Business Media LLC: Berlin/Heidelberg, Germany. pp. 3-10, 2018

53. Dehghani-Sanij, A., Tharumalingam, E., Dusseault, M., & Fraser, R. (2019). Study of energy storage systems and environmental challenges of batteries. *Renewable and Sustainable Energy Reviews*, *104*, 192–208. https://doi.org/10.1016/j.rser.2019.01.023

54. Noga, M.; Juda, Z. The application of nimh batteries in a light-duty electric vehicle. Czas. Tech. 1, 197-222, 2019

55. El Kharbachi, A.; Zavorotynska, O.; Latroche, M.; Cuevas, F.; Yartys, V.; Fichtner, M. Exploits, advances and challenges benefiting beyond Li-ion battery technologies. J. Alloys Compd. 817, 153261, 2020

56. Hu, C., Xiao, Y., Zou, Y., & Dai, L. (2018). Carbon-Based Metal-Free electrocatalysis for energy conversion, energy storage, and environmental protection. *Electrochemical Energy Reviews*, *1*(1), 84–112. https://doi.org/10.1007/s41918-018-0003-2

57. Li, B., Geng, D., Lee, X.S., et al.: Eggplant-derived microporous carbon sheets: towards mass production of efficient bifunctional oxygen electrocatalysts at low cost for rechargeable Zn-air batteries. Chem. Commun. **51**, 8841–8844 (2015a)

58. Yang, H., Miao, J., Hung, S., et al.: Identifcation of catalytic sites for oxygen reduction and oxygen evolution in N-doped grapheme materials: development of highly efcient metal-free bifunctional electrocatalyst. Sci. Adv. **2**, e1501122 (2016)

59. Qu, L., Liu, Y., Baek, J., et al.: Nitrogen-doped graphene as efficient metal-free electrocatalyst for oxygen reduction in fuel cells. ACS Nano **4**, 1321–1326 (2010)

60. Sun, Y.; DeJaco, R.F.; Li, Z.; Tang, D.; Glante, S.; Sholl, D.S.; Colina, C.M.; Snurr, R.Q.; Thommes, M.; Hartmann, M. Fingerprinting Diverse Nanoporous Materials for Optimal Hydrogen Storage Conditions Using Meta-Learning. *Sci. Adv.* 2021, *7*, eabg3983

61. Y Wang, C He, A Brouzgou, Y Liang, R Fu, D Wu, P Tsiakaras, S Song, A facile soft-template synthesis of ordered mesoporous carbon/tungsten carbide composites with high surface area for methanol electrooxidation, Journal of Power Sources 200, 8-13, 2012

62. Li, Y., Wang, J., Li, X., Geng, D., Banis, M.N., Li, R., Sun, X., *Electrochem. Commun.*, 18, 12–15, 2012

63. Ren, X., Zhu, J., Du, F., et al.: B-doped graphene as catalyst to improve charge rate of lithium-air battery. J. Phys. Chem. C **118**, 22412–22418 (2014)

64. Wang, J.; Liu, H.; Fan, S.; Wang, S.; Xu, G.; Guo, A.; Wang, Z. Dehydrogenation of Cycloalkanes over N-Doped Carbon-Supported Catalysts: The Effects of Active Component and Molecular Structure of the Substrate. Nanomaterials 2021, 11 (11), 2846. https://doi.org/10.3390/nano11112846

65. Zhang, F.; Zhao, P.; Niu, M.; Maddy, J. The Survey of Key Technologies in Hydrogen Energy Storage. Int. J. Hydrog. Energy 2016**,** 41**,** 14535–14552

66. Zhi, M., Yang, F., Meng, F., Li, M., Manivannan, A., Wu, N., Effects of Pore Structure on Performance of An Activated-Carbon Supercapacitor Electrode Recycled from Scrap Waste Tires. *ACS Sustain. Chem. Eng.*, 2, 1592–1598, 2014.

67. Inal IIG, Aktas Z. Enhancing the performance of activated carbon based scalable supercapacitors by heat treatment. Appl Surf Sci. 2020;514:145895

68. Ahmed S, Ahmed A, Rafat M. Nitrogen doped activated carbon from pea skin for high performance supercapacitor. Mater Res Express. 2018;5:045508

69. Jana, M., Saha, S., Khanra, P., Samanta, P., Koo, H., Murmu, N.C., Kuila, T., Non-covalent functionalization of reduced graphene oxide using sulfanilic acid azocromotrop and its application as a supercapacitor electrode material. *J. Mater. Chem. A*, 3, 732–7331, 2015

70. Han, J., Zhang, L.L., Lee, S., Oh, J., Lee, K., Potts, J.R., Ji, J., Zhao, X., Ruoff, R.S., Park, S., Generation of BDoped Graphene Nanoplatelets Using a Solution Process and Teir Supercapacitor Applications. *ACS Nano*, 7, 19–26, 2013

71. Wu, G., Tan, P., Wang, D., Li, Z., Peng, L., Hu, Y., Wang, C., Zhu, W., Chen, S., Chen, W., High-performance Supercapacitors Based on ElectrochemicalInduced Vertical-aligned Carbon Nanotubes and Polyaniline Nanocomposite Electrodes. *Sci. Rep.*, 7, 43676, 2017.

72. Saha, S., Kumar, J.S., Murmu, N.C., Samanta, P., Kuila, T., Controlled electrodeposition of iron oxide/nickel oxide@Ni for the investigation of the effects of stoichiometry and particle size on energy storage and water splitting applications. *J. Mater. Chem. A*, 6, 9657–9664, 2018.

73. E Gorbova, F Tzorbatzoglou, C Molochas, D Chloros, A Demin, P Tsiakaras,Fundamentals and Principles of Solid-State Electrochemical Sensors for High Temperature Gas Detection, Catalysts 12 (1), 1, 2022

74. G Balkourani, T Damartzis, A Brouzgou, P Tsiakaras, Cost effective synthesis of graphene nanomaterials for non-enzymatic electrochemical sensors for glucose: a comprehensive review, Sensors 22 (1), 355, 2022

75. G Balkourani, A Brouzgou, M Archonti, N Papandrianos, S Song, P Tsiakaras, Emerging materials for the electrochemical detection of COVID-19Journal of Electroanalytical Chemistry 893, 115289, 2021.

76. X Yuan, D Yuan, F Zeng, W Zou, F Tzorbatzoglou, P Tsiakaras, Y Wang, Preparation of graphitic mesoporous carbon for the simultaneous detection of hydroquinone and catechol, Applied Catalysis B: Environmental 129, 367-374, 2013

77. A Brouzgou, E Gorbova, Y Wang, S Jing, A Seretis, Z Liang, P Tsiakaras, Nitrogen-doped 3D hierarchical ordered mesoporous carbon supported palladium electrocatalyst for the simultaneous detection of ascorbic acid, dopamine, and glucose, Ionics 25 (12), 6061-6070, 2019.

78. G Fadeyev, A Kalakin, A Demin, A Volkov, A Brouzgou, P Tsiakaras, Electrodes for solid electrolyte sensors for the measurement of CO and H2 content in air, International journal of hydrogen energy 38 (30), 13484-13490, 2013.

79. A Demin, E Gorbova, A Brouzgou, A Volkov, P Tsiakaras, Sensors based on solid oxide electrolytes, Solid Oxide-Based Electrochemical Devices, 167-215, 2020

80. G. Fadeyev, A. Kalyakin, A. Demin, A. Volkov, A. Brouzgou, P. Tsiakaras, Electrodes for solid electrolyte sensors for the measurement of CO and H_2 content in air, International Journal of Hydrogen Energy, 38(30), 13484-13490, 2013.

81. A Kalyakin, A Demin, E Gorbova, A Volkov, P Tsiakaras, Combined amperometric-potentiometric oxygen sensor, Sensors and Actuators B: Chemical 313, 127999, 2020.

82. A Kalyakin, A Volkov, J Lyagaeva, D Medvedev, A Demin, P Tsiakaras, Combined amperometric and potentiometric hydrogen sensors based on BaCe0. 7Zr0. 1Y0. 2O3− δ proton-conducting ceramic, Sensors and Actuators B: Chemical 231, 175-182, 2016.

83. A Kalyakin, J Lyagaeva, D Medvedev, A Volkov, A Demin, P Tsiakaras, Characterization of proton-conducting electrolyte based on La0. 9Sr0. 1YO3–δ and its application in a hydrogen amperometric sensor, Sensors and Actuators B: Chemical 225, 446-452, 2016.

84. A Kalyakin, A Volkov, A Demin, E Gorbova, P Tsiakaras, Determination of nitrous oxide concentration using a solid-electrolyte amperometric sensor, Sensors and Actuators B: Chemical 297, 126750, 2019.

85. A Volkov, E Gorbova, A Vylkov, D Medvedev, A Demin, P Tsiakaras, Design and applications of potentiometric sensors based on proton-conducting ceramic materials. A brief review, Sensors and Actuators B: Chemical 244, 1004-1015, 2017.

86. G Fadeyev, A Kalyakin, E Gorbova, A Brouzgou, A Demin, A Volkov, P Tsiakaras, A simple and low-cost amperometric sensor for measuring H2, CO, and CH4Sensors and Actuators B: Chemical 221, 879-883, 2015.

87. Qureshi, F.; Yusuf, M.; Ibrahim, H.; Kamyab, H.; Chelliapan, S.; Pham, C.Q.; Vo, D.-V.N. Contemporary avenues of the Hydrogen industry: Opportunities and challenges in the eco-friendly approach. Environm. Res. 2023, 229**,** 115963

88. Patel, S.K.S.; Gupta, R.K.; Rohit, M.V.; Lee, J.-K. Recent Developments in Hydrogen Production, Storage, and Transportation: Challenges, Opportunities, and Perspectives. Fire 2024, **7**, 233. https://doi.org/10.3390/fre7070233

89. Li, F.; Liu, D.; Sun, K.; Yang, S.; Peng, F.; Zhang, K.; Guo, G.; Si, Y. Towards a future hydrogen supply chain: A review of technologies and challenges. Sustainability 2024a, **16**, 189

90. Marcantonio, V.; Di Paola, L.; De Falco, M.; Capocelli, M. Modeling of biomass gasification: From thermodynamics to process simulations. Energies 2023, **16**, 7042.

91. Zabed, H.M.; Akter, S.; Yun, J.; Zhang, G.; Zhang, Y.; Qi, X. Biogas from microalgae: Technologies, challenges and opportunities. *Renew. Sustain. Energy Rev.* 2020, *117*, 10950

92. Saha, S., Kumar, J.S., Murmu, N.C., Samanta, P., Kuila, T., Controlled electrodeposition of iron oxide/nickel oxide@Ni for the investigation of the effects of stoichiometry and particle size on energy storage and water splitting applications. *J. Mater. Chem. A*, 6, 9657–9664, 2018.

93. MA Goula, SK Kontou, PE Tsiakaras, Hydrogen production by ethanol steam reforming over a commercial Pd/γ-Al2O3 catalyst, Applied Catalysis B: Environmental 49 (2), 135-144, 2004

94. G Long, K Wan, M Liu, Z Liang, J Piao, P Tsiakaras, Active sites and mechanism on nitrogen-doped carbon catalyst for hydrogen evolution reaction, Journal of Catalysis 348, 151-159, 2017

95. C Yu, J Lu, L Luo, F Xu, PK Shen, P Tsiakaras, S Yin, Bifunctional catalysts for overall water splitting: CoNi oxyhydroxide nanosheets electrodeposited on titanium sheets, Electrochimica Acta 301, 449-45, 2019

96. L Yan, B Zhang, J Zhu, Y Li, P Tsiakaras, PK Shen, Electronic modulation of cobalt phosphide nanosheet arrays via copper doping for highly efficient neutral-pH overall water splitting, Applied Catalysis B: Environmental 265, 118555, 2020

97. C Yu, F Xu, L Luo, HS Abbo, SJJ Titinchi, PK Shen, P Tsiakaras, S Yin, Bimetallic Ni–Co phosphide nanosheets self-supported on nickel foam as high-performance electrocatalyst for hydrogen evolution reaction, Electrochimica Acta 317, 191-198, 2019

98. B Zhang, J Shan, W Wang, P Tsiakaras, Y Li,, Oxygen Vacancy and Core–Shell Heterojunction Engineering of Anemone-Like CoP@ CoOOH Bifunctional Electrocatalyst for Efficient Overall Water Splitting, Small, 2106012, 2022

99. A Saad, Y Gao, KA Owusu, W Liu, Y Wu, A Ramiere, H Guo, P Tsiakaras, Ternary Mo2NiB2 as a Superior Bifunctional Electrocatalyst for Overall Water Splitting, Small 18 (6), 2104303, 2022

100. L Yan, B Zhang, J Zhu, Y Li, P Tsiakaras, PK Shen, Electronic modulation of cobalt phosphide nanosheet arrays via copper doping for highly efficient neutral-pH overall water splitting, Applied Catalysis B: Environmental 265, 11855, 2020

101. L Yan, B Zhang, J Zhu, Y Li, P Tsiakaras, PK Shen, Electronic modulation of cobalt phosphide nanosheet arrays via copper doping for highly efficient neutral-pH overall water splitting, Applied Catalysis B: Environmental 265, 118555, 2020

102. B Long, H Yang, M Li, MS Balogun, W Mai, G Ouyang, Y Tong, Panagiotis Tsiakaras, Shuqin Song, Interface charges redistribution enhanced monolithic etched copper foam-based Cu2O layer/TiO2 nanodots heterojunction with high hydrogen evolution electrocatalytic activity, Applied Catalysis B: Environmental 243, 365-372, 2019

103. J Lu, Z Tang, L Luo, S Yin, PK Shen, P Tsiakaras, Worm-like S-doped RhNi alloys as highly efficient electrocatalysts for hydrogen evolution reaction, Applied Catalysis B: Environmental 255, 117737, 2019

104. S Jing, D Wang, S Yin, J Lu, PK Shen, P Tsiakaras, P-doped CNTs encapsulated nickel hybrids with flower-like structure as efficient catalysts for hydrogen evolution reaction, Electrochimica acta 298, 142-149, 201

105. P Xu, L Qiu, L Wei, Y Liu, D Yuan, Y Wang, P Tsiakaras, Efficient overall water splitting over Mn doped Ni2P microflowers grown on nickel foam, Catalysis Today 355, 815-821, 2020

106. L Zhang, J Lu, S Yin, L Luo, S Jing, A Brouzgou, J Chen, PK Shen, P. Tsiakaras, One-pot synthesized boron-doped RhFe alloy with enhanced catalytic performance for hydrogen evolution reaction, Applied Catalysis B: Environmental 230, 58-64, 2018

107. Sola, A., Rosa, R., & Ferrari, A. M. (2024). Green Hydrogen and its supply chain. A Critical assessment of the environmental impacts. *Advanced Sustainable Systems*. https://doi.org/10.1002/adsu.202400708

108. T.M. Gulotta, R. Salomone, F. Lanuzza, G. Saija, G. Mondello, G. Ioppolo Life Cycle Assessment and Life Cycle Costing of unitized regenerative fuel cell: a systematic review Environ Impact Assess Rev, 92 (2022), Article 106698, 10.1016/j.eiar.2021.106698

109. Esfandiari, N.; Aliofkhazraei, M.; Colli, A.N.; Walsh, F.C.; Cherevko, S.; Kibler, L.A.; Elnagar, M.M.; Lund, P.D.; Zhang, D.; Omanovic, S.; et al. Metal-based cathodes for hydrogen production by alkaline water electrolysis: Review of materials, degradation mechanism, and durability tests. Process Mater. Sci. 2024

110. Eikeng, E.; Makhsoos, A.; Pollet, B.G. Critical and strategic raw materials for electrolysers, fuel cells, metal hydrides and hydrogen separation technologies. Int. J. Hydrogen Energy 2024**,** 71, 433–464

111. Chen, Z.; Kirlikovali, K.O.; Idrees, K.B.; Wasson, M.C.; Farha, O.K. Porous Materials for Hydrogen Storage. Chem 2022**,** 8, 693–716

112. Fu, H.; Yang, D.; Li, X.; Guo, X.; Mo, Y.; Wang, S.; Wang, J. Metabolic and process engineering of *Clostridium tyrobutyricum* for efficient hydrogen production from sugarcane molasses. *Fuel* 2024, ***371*, 132075**

113. Derwent, R. G., Stevenson, D. S., Utembe, S. R., Jenkin, M. E., Khan, A. H., and Shallcross, D. E.: Global modelling studies of hydrogen and its isotopomers using STOCHEMCRI: Likely radiative forcing consequences of a future hydrogen economy, Int. J. Hydrogen Energ., 45, 9211–9221, https://doi.org/10.1016/j.ijhydene.2020.01.125, 2020

114. Warwick, N., Griffiths, P., Keeble, J., Archibald, A., Pyle, J., and Shine, K.: Atmospheric implications of increased Hydrogen use, Department for Business, Energy and Industrial Strategy, 75 pp., https://www.gov.uk/government/publications/ atmospheric-implications-of-increased-hydrogen-use (last access: 15 April 2022), 2022

115. Forster, P., Storelvmo, T., Armour, K., Collins, W., Dufresne, J. L., Frame, D., Lunt, D. J., Mauritsen, T., Palmer, M. D., Watanabe, M.,Wild, M., and Zhang, H.: The Earth's energy budget, climate feedbacks, and climate sensitivity, in: Climate Change 2021: The Physical Science Basis, Contribution of Working Group I to the Sixth Assessment Report of the Intergovernmental Panel on Climate Change, edited by: Masson-Delmotte, V., Zhai, P., Pirant, A., Connors, S. L., Pean, C., Berger, S., Caud, C., Chen, Y., Goldfarb, L., Gomis, M. I., Huang, M., Leitzell, K., Lonnoy, E., Matthews, L. B. R., Maycock, T. K., Waterfield, T., Yelekci, O., Yu, R., and Zhou, B., Cambridge University Press, 923–1054, https://www.ipcc.ch/report/ar6/wg1/downloads/report/IPCC_AR6_WGI_Chapter07.pdf

116. Hydrogen Council: Hydrogen scaling up A sustainable pathway for the global energy transition, 78 pp., https://hydrogencouncil. com/en/study-hydrogen-scaling-up/, 2017

117. BloombergNEF: Hydrogen Economy Outlook Key messages, Bloomberg Finance L. P., 14 pp., https://assets.bbhub.io/professional/sites/24/ BNEF-Hydrogen-Economy-Outlook-Key-Messages-30-Mar-2020. pdf (last access: 26 April 2022) 2020

118. Xu, Y., Zaelke, D., Velders, G. J. M., and Ramanathan, V.: The role of HFCs in mitigating 21st century climate change, Atmos. Chem. Phys., 13, 6083–6089, https://doi.org/10.5194/acp- 13-6083-2013, 2013

119. Aasadnia, M.; Mehrpooya, M. Large-Scale Liquid Hydrogen Production Methods and Approaches: A Review. Applied Energy 2018, 212, 57–83. https://doi.org/10.1016/j.apenergy.2017.12.033

120. Zivar, D.; Kumar, S.; Foroozesh, J. Underground Hydrogen Storage: A Comprehensive Review. International Journal of Hydrogen Energy 2021, 46 (45), 23436–23462. https://doi.org/10.1016/j.ijhydene.2020.08.138.

121. Li, F.; Zhou, Y.; Li, B.; Zhang, Z. Permeation and Photo-Induced Outgassing of Deuterium in Hollow Glass Microspheres Doped with Titanium**.** Int. J. Hydrog. Energy 2024b, **49**, 303–313

122. Edwards, P.; Kuznetsov, V.; David, B. Hydrogen Energy. Philos. Trans. A Math. Phys. Eng. Sci. 2007**,** 365**,** 1043–1056

123. Lyu, J.; Kudiiarov, V.; Lider, A. An Overview of the Recent Progress in Modifications of Carbon Nanotubes for Hydrogen Adsorption. *Nanomaterials* 2020, *10*, 255

124. Vergara-Rubio, A.; Ribba, L.; Picón Borregales, D.E.; Sapag, K.; Candal, R.; Goyanes, S. Ultramicroporous Carbon Nanofibrous Mats for Hydrogen Storage. *ACS Appl. Nano Mater.* **2022**, *5*, 15353–15361

125. A. Ngqalakwezi and D. Bevon Nkazi, 'Hydrogen Storage: Materials, Kinetics and Thermodynamics', Advanced Applications of Hydrogen and Engineering Systems in the Automotive Industry. IntechOpen, Apr. 28, 2021. doi: 10.5772/intechopen.94300.

126. Khaleque, A.; Alam, M.M.; Hoque, M.; Mondal, S.; Haider, J.B.; Xu, B.; Johir, M.A.H.; Karmakar, A.K.; Zhou, J.L.; Ahmed, M.B.; et al. Zeolite Synthesis from Low-Cost Materials and Environmental Applications: A Review. *Environ. Adv.* **2020**, *2*, 100019.

127. Zhou, H.C.; Long, J.R.; Yaghi, O.M. Introduction to Metal–Organic Frameworks. Chem. Rev. 2012, 112, 673–674

128. A Tan, Y Wang, Z Fu, P Tsiakaras, Z Liang, Highly effective oxygen reduction reaction electrocatalysis: Nitrogen-doped hierarchically mesoporous carbon derived from interpenetrated nonporous metal-organic frameworks, Applied Catalysis B: Environmental 218, 260-266, 2017

129. Dehouche, Z.; Djaozandry, R.; Huot, J.; Boily, S.; Goyette, J.; Bose, T. K.; Schulz, R. Influence of Cycling on the Thermodynamic and Structure Properties of Nanocrystalline Magnesium Based Hydride. Journal of Alloys and Compounds 2000, 305 (1), 264–271. https://doi.org/10.1016/S0925-8388(00)00718-0.

130. Okada, M.; Kuriiwa, T.; Kamegawa, A.; Takamura, H. Role of Intermetallics in Hydrogen Storage Materials. Materials Science and Engineering: A 2002, 329–331, 305–312. https://doi.org/10.1016/S0921-5093(01)01580-5

131. Tarasov, B. P.; Fursikov, P. V.; Volodin, A. A.; Bocharnikov, M. S.; Shimkus, Y. Y.; Kashin, A. M.; Yartys, V. A.; Chidziva, S.; Pasupathi, S.; Lototskyy, M. V. Metal Hydride Hydrogen Storage and Compression Systems for Energy Storage Technologies. International Journal of Hydrogen Energy 2021, 46 (25), 13647–13657. https://doi.org/10.1016/j.ijhydene.2020.07.085.

132. Jain, I. P.; Lal, C.; Jain, A. Hydrogen Storage in Mg: A Most Promising Material. International Journal of Hydrogen Energy 2010, 35 (10), 5133–5144. https://doi.org/10.1016/j.ijhydene.2009.08.088.

133. He, T.; Cao, H.; Chen, P. Complex Hydrides for Energy Storage, Conversion, and Utilization. Advanced Materials 2019, 31 (50), 1902757. https://doi.org/10.1002/adma.201902757.

134. Urgnani, J.; Torres, F. J.; Palumbo, M.; Baricco, M. Hydrogen Release from Solid State $NaBH_4$. International Journal of Hydrogen Energy 2008, 33 (12), 3111–3115. https://doi.org/10.1016/j.ijhydene.2008.03.031.

135. Klopčič, N., Grimmer, I., Winkler, F., Sartory, M., & Trattner, A. (2023). A review on metal hydride materials for hydrogen storage. *Journal of Energy Storage*, *72*, Article 108456. https://doi.org/10.1016/j.est.2023.108456

136. d'Ambra Florian. Evaluation of the hydrogen storage system liquid organic hydrogen carrier (LOHC). Chemical engineering. Université Grenoble Alpes [2020-..], 2023. English. ffNNT : 2023GRALI029ff. fftel-04563684

137. Cooper. Alan C. Design and Development of New Carbon-Based Sorbent Systems for an Effective Containment of Hydrogen; 86-377-P, 1039432; 2012; pp 86-377-P, 1039432. https://doi.org/10.2172/1039432.

138. Kalenchuk, A.; Bogdan, V.; Dunaev, S.; Kustov, L. Influence of Steric Factors on Reversible Reactions of Hydrogenation-Dehydrogenation of Polycyclic Aromatic Hydrocarbons on a Pt/C Catalyst in Hydrogen Storage Systems. Fuel 2020, 280, 118625. https://doi.org/10.1016/j.fuel.2020.118625

139. Niermann, M.; Beckendorff, A.; Kaltschmitt, M.; Bonhoff, K. Liquid Organic Hydrogen Carrier (LOHC) – Assessment Based on Chemical and Economic Properties. International Journal of Hydrogen Energy 2019, 44 (13), 6631–6654. https://doi.org/10.1016/j.ijhydene.2019.01.199.

140. Zhu, L.; Zhang, H.; Hu, W.; Zheng, J.; Zhang, N.; Yu, C.; Ye, H.; Yang, Z.; Chen, B. H. Nickel Hydroxide– Cobalt Hydroxide Nanoparticle Supported Ruthenium–Nickel–Cobalt Islands as an Efficient Nanocatalyst for the Hydrogenation Reaction. ChemCatChem 2018, 10 (9), 1998–2002. https://doi.org/10.1002/cctc.201701847.

141. Brückner, N.; Obesser, K.; Bösmann, A.; Teichmann, D.; Arlt, W.; Dungs, J.; Wasserscheid, P. Evaluation of Industrially Applied Heat-Transfer Fluids as Liquid Organic Hydrogen Carrier Systems. ChemSusChem 2014, 7 (1), 229–235. https://doi.org/10.1002/cssc.201300426.

142. Clot, E.; Eisenstein, O.; H. Crabtree, R. Computational Structure–Activity Relationships in H 2 Storage: How Placement of N Atoms Affects Release Temperatures in Organic Liquid Storage Materials. Chemical Communications 2007, 0 (22), 2231–2233. https://doi.org/10.1039/B705037B.

143. Pez, G. P.; Scott, A. R.; Cooper, A. C.; Cheng, H.; Wilhelm, F. C.; Abdourazak, A. H. Hydrogen Storage by Reversible Hydrogenation of Pi-Conjugated Substrates. US7351395B1, April 1, 2008. https://patents.google.com/patent/US7351395B1/en

144. Taniguchi, T.; Curran, D. P. Silica Gel Promotes Reductions of Aldehydes and Ketones by N-Heterocyclic Carbene Boranes. Org. Lett. 2012, 14 (17), 4540–4543. https://doi.org/10.1021/ol302010f

145. Zhang, P.; Wang, Q.-N.; Yang, X.; Wang, D.; Li, W.-C.; Zheng, Y.; Chen, M.; Lu, A.-H. A Highly Porous Carbon Support Rich in Graphitic-N Stabilizes Copper Nanocatalysts for Efficient Ethanol Dehydrogenation. ChemCatChem 2017, 9 (3), 505–510. https://doi.org/10.1002/cctc.20160137

146. Li, M.-Y.; Lu, W.-D.; He, L.; Schüth, F.; Lu, A.-H. Tailoring the Surface Structure of Silicon Carbide Support for Copper Catalyzed Ethanol Dehydrogenation. ChemCatChem 2019, 11 (1), 481–487. https://doi.org/10.1002/cctc.201801742

147. Kumar, A.; Janes, T.; Espinosa-Jalapa, N. A.; Milstein, D. Selective Hydrogenation of Cyclic Imides to Diols and Amines and Its Application in the Development of a Liquid Organic Hydrogen Carrier. J. Am. Chem. Soc. 2018, 140 (24), 7453–7457. https://doi.org/10.1021/jacs.8b04581